Wideband Linear and Circularly Polarised Transmitarray Antennas

Magid Khalifa Milad Alzidani

Thesis

In the Department

of

Electrical and Computer Engineering

Presented in Partial Fulfillment of the Requirements

For the Degree of

Doctor of Philosophy (Electrical and Computer Engineering) at

Concordia University

Montréal, Québec, Canada

September; 2022

CONCORDIA UNIVERSITY

School of Graduate Studies

This is to certify that the thesis prepared

By: **Magid Khalifa Milad Alzidani**

Entitled: **Wideband Linear and Circularly Polarised Transmitarray Antennas**

and submitted in partial fulfillment of the requirements for the degree of

Doctor of Philosophy (Electrical and Computer Engineering)

complies with the regulations of the University and meets the accepted standards with respect to originality and quality.

Signed by the final examining committee:

Dr. Zhibin Ye	Chair
Dr. Carlos Saavedra	External Examiner
Dr. Rajamohan Ganesan	External to Program
Dr. Ahmed A. Kishk	Examiner
Dr. Christopher W. Trueman	Examiner
Dr. Abdel Razik Sebak	Thesis Supervisor

Approved by:

Dr. Jun Cai, Graduate Program Director

September 22, 2022

Dr. Mourad Debbabi, Acting Dean,
Gina Cody Schoool of Engineering & Computer Science

Abstract

Wideband Linear and Circularly Polarised Transmitarray Antennas

Magid Khalifa Milad Alzidani, Ph.D.

Concordia University

The millimetre-wave (mm-wave) band is expected to be one of the solutions for future wireless communication systems, as it provides wide bandwidth, enhancing the data transmission rate. Therefore, high-directive antennas, which are principal elements for mm-wave wireless communications, are used since they can overcome the negative effects of high path losses. These high-gain antennas can be used in various applications, including point-to-point communication, automotive radar, and imaging.

The main goal of this project is to design a transmit-array (TA) antenna that operates at the mm-wave band (around 28 GHz) with high aperture efficiency, high gain, wide bandwidth, and a low-profile TA surface. Basically, the aperture efficiency of the TA antenna depends on the unit cell (UC) characteristics and the feed antenna radiation pattern. The UC characteristics, including the transmission coefficient, bandwidth, and phase range, all play an essential role in designing efficient TA antennas. Therefore, the unit cells of the TA surface are designed to have a wide bandwidth with a stable broadside radiation pattern and a full phase range (0°-360°). Such unit cells are designed using two techniques: 1) Capacitive feeding to extend bandwidth and 2) differential feeding to minimize cross-polarization and enforce a broadside radiation pattern that; enhances the antenna gain.

Simulated results show that the unit cells have achieved a 360° phase range and a maximum element loss of 0.5 dB. In addition to the design's high-performance UC, a wideband feeder antenna is required to illuminate the TA surface. Thus, a wideband patch antenna which is a part of the UC is used to illuminate the TA surface. Also, a hybrid antenna with a high data rate has been designed and fabricated to excite the TA aperture. The designed hybrid antenna has a 14.5 dBi maximum realized gain at 30 GHz, and its return loss bandwidth is 34.48%. Results show that the TA's aperture efficiency depends on the illuminating source's radiation pattern, such as its amplitude and phase distribution over the TA surface.

Experiments show efficient illumination of TA surface requires a specific radiation pattern; therefore, a circular horn antenna has been designed with high acceptable amplitude tapering, uniform phase distribution, symmetric radiation pattern, and low sidelobe level. This utilized horn antenna has a particular radiation magnitude distribution, and the radiation pattern model is sec θ, which makes it capable of dealing with the relative difference in path loss and resulting in a good tapering efficiency. The TA antenna's surface and the feeding antenna have been designed, fabricated and measured. The TA antenna measured results show a maximum gain of 31.15 dBi, with a 1-dB gain bandwidth of 12.7%, while the 3-dB gain bandwidth is 21%, around 28 GHz. On the frequency range from 25 to 31.5 GHz, the aperture efficiency is better than 50%, and the cross-polarization level is less than -37 dB. Furthermore, factors that affect the TA antenna's performance are studied and summarized in this work. These factors are mutual coupling, phase errors in TA design, quantization error, phase range error, feed antenna, TA antenna shape, and incident angle approximation.

Circular polarization antennas have advantages over linear polarization antennas because rapid alignment is not required between transmitter and receiver antennas, reducing polarization mismatching error. The Faraday rotation effect also harms the linear polarized waves. Moreover, circularly polarized wave energy is on both planes, suppressing interference. A circular polarizer is used to convert the LP incident signal to CP signals, in which the incident electric field is resolved to its orthogonal components, introducing a 90° phase shift. The proposed polarizer contains two layers of the Jerusalem cross (JC). The JC UC simulated results show equal orthogonal retransmitted electric fields with 90° phases. The designed CP array results show a maximum realized gain of 30.5 dBi, with an AR bandwidth of 23%. Finally, a general TA antenna design methodology is also provided.

All praise and thanks to Allah for my success in completing this thesis. I would like to thank my parents for giving me this life and presenting me with the opportunity to achieve this mile stone on my journey towards my PhD. I would also like to pay this forward to my parents legacy. They have been with me every step of the way through out my life and have encouraged me to go outside of my comfort zone.

Acknowledgments

I would like to express my utmost gratitude to my supervisor, Dr Abdel Razik Sebak, for providing me with extensive professional guidance and for his patience and invaluable comments. Thanks are also due to my Dissertation Committee (Dr. Ahmed Kishk, Dr. Christopher W. Trueman, Dr. Carlos Saavedra, Dr. Zhibin Ye and Dr. Rajamohan Ganesan) for the professional, scientific research guidance they provided while serving on my examining committee. I would also like to thank the Concordia University technical staff, especially Mr Vincent Mooney-Chopin, for the technical assistance in presenting this work. I wish to thank my loving and supportive wife and my wonderful children, who provide me with invaluable emotional support. Finally, I would like to thank the Libyan Cultural Affairs and Scholarships Sector for giving me this PhD scholarship at Concordia University.

Contribution of Authors

Multiple publications have come to be as a result of this thesis. The authors' contributions that have been jointly published in two journals related to this thesis are presented as follows. In addition, my supervisor, Professor Abdel Razik Sebak, attests to the accuracy of this statement. The contributions of this thesis are divided into three major parts: 1) the design and specification of linear and circular TA antenna components for the proposed frequency band; 2) integrating the components of the LP transmit-array and CP transmit-array antennas; and 3) the fabrication and implementation of the proposed wideband TA antennas. The contributions of the reported work include information from Chapter 3, covering the design of a wideband capacitive differential feeding antenna used to excite pyramidal structures. This work has been published in the IEEE Access journal bhe contribution of the authors can be summarized as follows:

- I have studied the topic, designing, simulating, and measuring all of the capacitive feeding, differential feeding, and the hybrid antenna, followed by writing the paper;
- Dr Islam Afifi has helped me with the fabrication and measurement processes, as well as the revision of the paper;
- Dr Muftah. Asaadi helped me write the article, and
- as the research supervisor, Professor Abdel Razik Sebak provided guidance and direction on all aspects of the topic.

In Chapter 4, the design of the TA antenna using the true time delay (TTD) technique is presented. There is a journal publication based on this part [j2]. The contributions of the authors can be summarized as follows:

- I have researched and studied the TA antennas, designed and simulated the antenna, and written the paper;
- Dr Islam Afifi has helped in writing a MATLAB code, taking measurements, revising the paper; and
- as the research supervisor, Professor Abdel Razik Sebak provided guidance and direction on all aspects of the topic.

Chapter 5 presents the design of the linear-to-circular polarization converter. The polarizer combined with the LP TA antenna produces a CPTA antenna. There is another paper in the process step. The contributions of the authors can be summarized as follows:

- I have researched and studied the topic, as well as designed and simulated the antenna;
- Dr Islam Afifi has helped in writing the paper; and
- as the research supervisor, Professor Abdel Razik Sebak provided guidance and direction on all aspects of the topic.

Contents

List of Figures

List of Tables

List of Abbreviations

1D	One-Dimension
2D	Two-Dimension
3D	Three-Dimension
3G	Third-generation communication
4G	Forth-generation communication
5G	Fifth generation communication
Kbps	Kilo bit per second communication
Mbps	Mega bit per second communication
Gbps	Giga bit per second communication
AF	Array factor
Hz	Hertz
BW	Bandwidth
CSTMWS	Computer Simulation Technology Microwave Studio
MMW	Millimeter Wave
MS	Microstrip
PCB	Printed Circuit Board
PEC	Perfect Electric Conductor
TA	Transmit-array
RA	Reflect-array
Rx	Receiver
SIW	Substrate Integrated Waveguide
SNR	Signal-to-Noise Ratio
Tx	Transmitter
Rx	Reciever
UC	Unit Cell
EM	Electromagnatic
LP	Linear Polarization
CP	Circular Polarization
EHF	Extreme High Frequency
FSS	Frequency Selective Surface
R T	Receive Transmit
SLL	Sidelobe Level
Co-pol	Co-polarization
X-pol	Cross-polarization
RHCP	Right Hand Circular Polarization
LHCP	Lift Hand Circular Polarization
LCPC	Linear Circular Polarizer Converter

List of Symbols

C	Capacitance
f	Frequency
L	Inductance
R	Resastance
Z	Impedance
n_i	Material Index
θ_i	Incident Signal Angle
θ_t	Transmit Single Angle
k	Quantization Step
N	Number of Bits
D	Antenna Directivity
A	Aperture Area
λ	Signal Wavelength
G	Antenna Gain
A_e	Antenna Effective Area
η_a	Aperture Efficiency
η_s	Spillover Efficiency
η_i	Illumination Efficiency
η_r	Radiation Efficiency
E	Electric Field
H	Magnatic Field
AR	Axial Ratio

Chapter 1

Introduction

1.1 Introduction

Current wireless communication systems suffer from capacity issues due to the significant increase in the number of mobile users, the limited frequency spectrum, and the increased demand for higher data rates, which raised from a range of 25 kbps to 2 Mbps in the third generation of cellular systems (3G) to 100 Mbps to 1 Gbps in the fourth generation of cellular systems (4G) [4]. Accordingly, both manufacturers and operators must find ways to resolve capacity issues and accommodate user demands either by improving the existing wireless channel capacity or by operating at very high frequencies with much wider bandwidths [5,6].

Some traditional ways to resolve such capacity issues in the current cellular systems include adding microcells and microsites or decreasing the site-to-site distance [5, 6]. However, the latter approach increases the channel's capacity at the cost of network management complexity, handover, and an increase in channel interference. To overcome these challenges, a solution is proposed to move up to the licensed frequency spectrum at the mm-wave bands, which can increase the wireless capacity by tens to hundreds of times more than that of the 4G system [7,8]. In addition, the wavelength of the mm-wave spectrum allows for the use of mm-wave antenna arrays within relatively small physical dimensions, resulting in higher gain characteristics that are vital for the reliability of future cellular implementations.

Several practical studies have been performed to analyze the behaviour of the mm-waves at both 28 and 38 GHz in cellular applications [7,8]. This new mm-wave cellular technology has also encouraged antenna designers to develop new antennas that can serve their applications. Dish antennas and phased array antennas have been used for wideband applications and high gain for a long time. Recently, antenna designers have been using RA and TA antennas as alternatives to phase array and parabolic antennas because of the disadvantages of the latter two antennas; such drawbacks include feeding the network loss of phased array antennas (especially at high frequency) and dish antenna size limitations. TA antennas are preferred over RA antennas because of feed blockage issues. Moreover, TA antennas have features such as being lightweight and having a low profile, high gain, and wide frequency band [9].

1.2 Problem Statement and Motivation

High data rates of up to 1 Gbps are required to overcome the high increase in data traffic for point-to-point communication [5]. The millimetre-wave spectrum has garnered high interest from service providers because it can be the optimal solution for the trade-off between high channel capacity demand and currently available bandwidth. Additionally, the mm-wave spectrum can be used to provide high data rates; in fact, the mm-wave frequency band can deliver multiple gigabits per second, which can address wireless data congestion at lower frequencies. However, researchers and engineers can not use this mm-wave frequency band due to some challenges, such as high atmospheric attenuation losses, scattering in rain conditions, penetration losses, and the negative impact of the wireless transmission medium on the mm-wave signal behaviour. Despite these challenges, atmospheric absorption minimumal at short distances, especially at 28 and 38 GHz, when high-gain antennas are used. High-gain and wideband antennas support users by providing wider bandwidth for dealing with huge transmission rate demands.

A high-gain wideband antenna is required to exploit the mm-wave spectrum band, so researchers have implemented reflectors, lenses, and phased-array, reflect-array (RA), and transmit-array (TA) antennas.

Transmit-array antennas are used as alternatives to reflectors, reflect-arrays, and lens antennas due to their ability to eliminate feed blockage and reduce fabrication complexity as opposed to the curved surface. Transmit-array antennas are also lightweight, low in profile, inexpensive, and easy to fabricate, providing high gain and operating at wide frequency bands. Moreover, the proposed transmit-array antenna promises to be the initial solution because it can be integrated with different antennas, such as horn or printed antennas. Figure1.1 shows the TA antenna configuration. Basically, a TA antenna consists of a feed antenna and re-transmits a flat surface. The feed antenna (horn antenna) is placed at the focal point to illuminate the TA surface. The TA surface operates as a discrete lens; this surface contains several unit cells (UCs) to convert the incident non-plane wave to an outgoing plane wave. In other words, the primary duty of the UC is to compensate for the different path phase delays.

The TA aperture efficiency depends on the UC characteristics, such as high directivity, wide bandwidth, quantization steps, and phase range. Therefore, TA antenna designers' main challenge is to design the UC with high performance, which includes the UC phase range, reflection coefficients, and UC radiation pattern characteristics. Unfortunately, as shown in the reported designs in [10–13], a 360° phase shift has not been achieved. In addition, the insertion losses are higher than 0.5 dB. Accordingly, the quantization phase, and the aperture's effectiveness are limited. Furthermore, previous works suffer from moderate cross-polarization, so, for the first time, differential feeding is used as a technique to reduce the cross-polarization for UC.

The aim here is to design a TA antenna that operates at an mm-wave region in which it can be used in many applications like imaging and point-to-point communication. Receive-transmit (R/T) technology will be used to design the proposed UC. The proposed UC has eight quantization steps and a 360° phase range. The UC is considered an

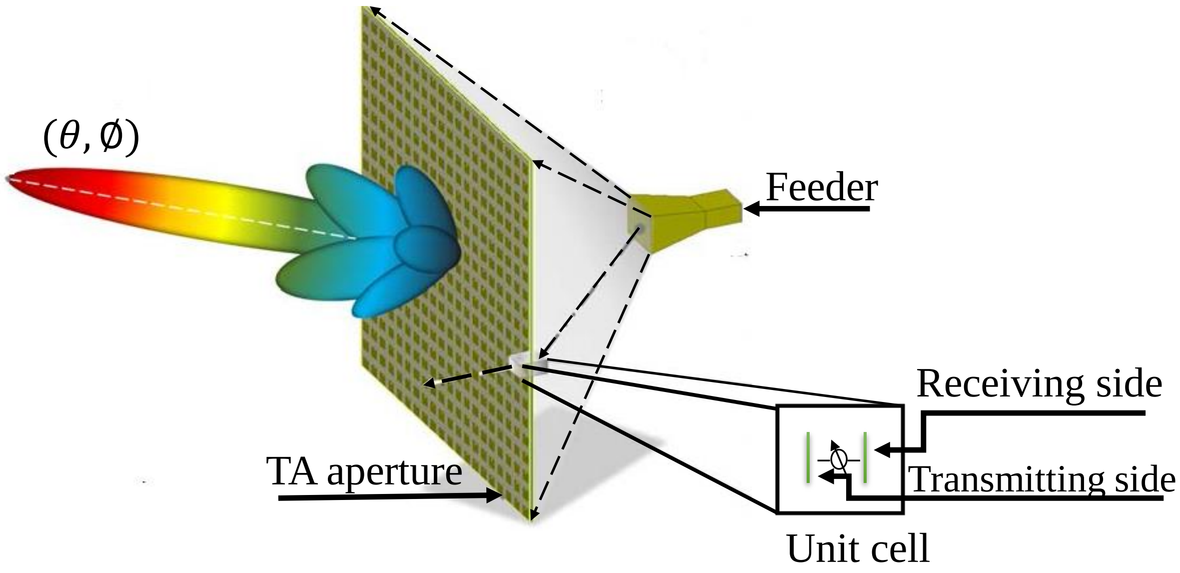

Figure 1.1: Transmit-array antenna configuration

antenna in which both differential feeding and capacitive feeding are used. These features increase both the level of the retransmitted signal power and the UC bandwidth, suppressing both the side loop and the cross-polarization level. In addition, using electromagnetic (EM) wave polarization properties increase the quality and capacity of communication links and extract the required information from noise. The second goal of this work is to create a technique increasing the capability to use the same TA antenna in different EM wave polarizations. However, the requirement of an ultra-wideband circular polarized antenna is met through a polarization converter, which changes the incoming signal polarization, re-radiating the output as a wave with circular polarization characteristics. A printed CP transmit-array antenna at the millimetre-wave band is designed by employing an LP transmit-array antenna with a CP converter. It is found that the TA antenna features (such as gain and bandwidth) are not affected, and a CP wave has been created. The measured results of the designed CPTA antenna are as follows: the realized gain is 30.6 dBi; and the AR bandwidth is 23%.

1.3 Objectives

This work aims to design a transmit-array (TA) antenna operating at 28 GHz. The proposed transmit-array antenna can provide a high gain and wider bandwidth than the reported designs. It also has advantages such as low cross-polarization and low sidelobe level. The main building block of TA antennas is the UCs, which can minimize the cross-polarization and force the radiation pattern to be broadside, enhancing antenna gain. The whole TA antenna performance will be addressed and investigated, including factors affecting the antenna's aperture efficiency (i.e., phase range, feeding antenna, quantization error, and mutual coupling). The following aspects are proposed as part of the research activities:

- Design broadband, low cross-polarization antennas as part of the unit cell and feeding antenna that uses capacitive and differential feeding techniques.
- Design broadband LP transmit-array antenna.
- Analysis and design of new UC operating at 28 GHz using R/T and the true time delay mechanism.
- Analysis and design of a feeder antenna to excite the TA antenna. The designed feeder's radiation pattern enhances the designed TA antenna aperture efficiency.

Circularly polarized waves could reduce mm-wave sensitivity interms of rain, atmospheric absorption, and interference. Also, CP waves overcome misalignment problems between transmitting and receiving antennas that cause polarization mismatching error. Therefore, the second aim is to design CP transmit-array antenna, in which the LP unit cell is used and two layers are added to convert the LP incident signal to CP out-going signal. The following aspects are proposed as part of the research activities:

- Design broadband high gain wide band CP transmit-array antenna.

- Apply polarization converter layers to the designed LP unit cell.

1.4 Research Methodology

After researching suitable candidates of antennas that can operate at the mm-wave band, the research concluded by selecting planar high-gain antennas as suitable antenna candidates. The idea is to enhance the antenna's gain and bandwidth to satisfy mm-wave antenna requirements. Lens antennas have become a research subject because of their features and principles studied. Another survey has been conducted to evaluate the work done on the transmit-array antenna for mm-wave applications. A recent paper [14] has been chosen to duplicate the results. The simulated results are promising and have encouraged me to continue my research upon seeing the bigger picture of the current work on the mm-wave antenna. The authors made their design by combining existing principles, designs, and ideas to satisfy the mm-wave application requirements while providing better results surpassing those already published.

Since a TA antenna can be considered a discrete lens antenna and it gathers phased array antennas and lenses, understanding aperture antennas and phased array antennas is an essential step. Also, understanding reflect-array (RA) antennas make TA antennas easier to understand because both RA and TA antennas have similar principles. The proposed planar TA antenna work started with choosing a specific type of TA antenna. After that, the design started with the use of fundamental equations of phased array antennas and reflector antennas to determine the phase distribution of the feed over the aperture area. Then, the initial system configuration was calculated in terms of aperture shape, aperture dimensions, and feed antenna coordinates. A feeding methodology must also be considered during the design process. The TA aperture is illuminated using different feeding sources, so the feeding source effect on the TA efficiency is understood. Horn antennas with specific radiation patterns have been designed and simulated as the feed antenna for this work. The unit cell (UC), a single element, is designed to compensate for the phase difference through high performance in terms of gain, cross-polarization, bandwidth, phase range, and radiation pattern before assembling an array out of this single element. The CST simulator was used to optimize the final version of the UC. The next step includes the design of the TA antenna, including the feeding source; the simulation is used to evaluate the antenna's performance in terms of the far-field, radiation patterns, and aperture efficiency. Upon the simulation results, a decision about the suitability of the proposed antenna can be evaluated. One attractive feature of the simulation program is its ability to optimize the proposed antenna results. Henceforth, optimization techniques might be needed for the final design, as in the previous step. Due to a massive number of required UCs for building the TA aperture, a MATLAB code is written to calculate the phase distribution over the TA aperture, to create the UCs on the CST software, and, finally, to place the individual UC in the proper position according to the phase distribution calculation. Creating a 27×27 array would be time-consuming and open to errors without this MATLAB code. In the last step, the comparison between the simulated results, surveys, and published results should occur to determine the design's worthiness. In case this design performance is acceptable, the eight-step designing methodology takes place, proving the design validity by fabricating the optimized antenna version. Figure 1.2 shows a block diagram of the research methodology.

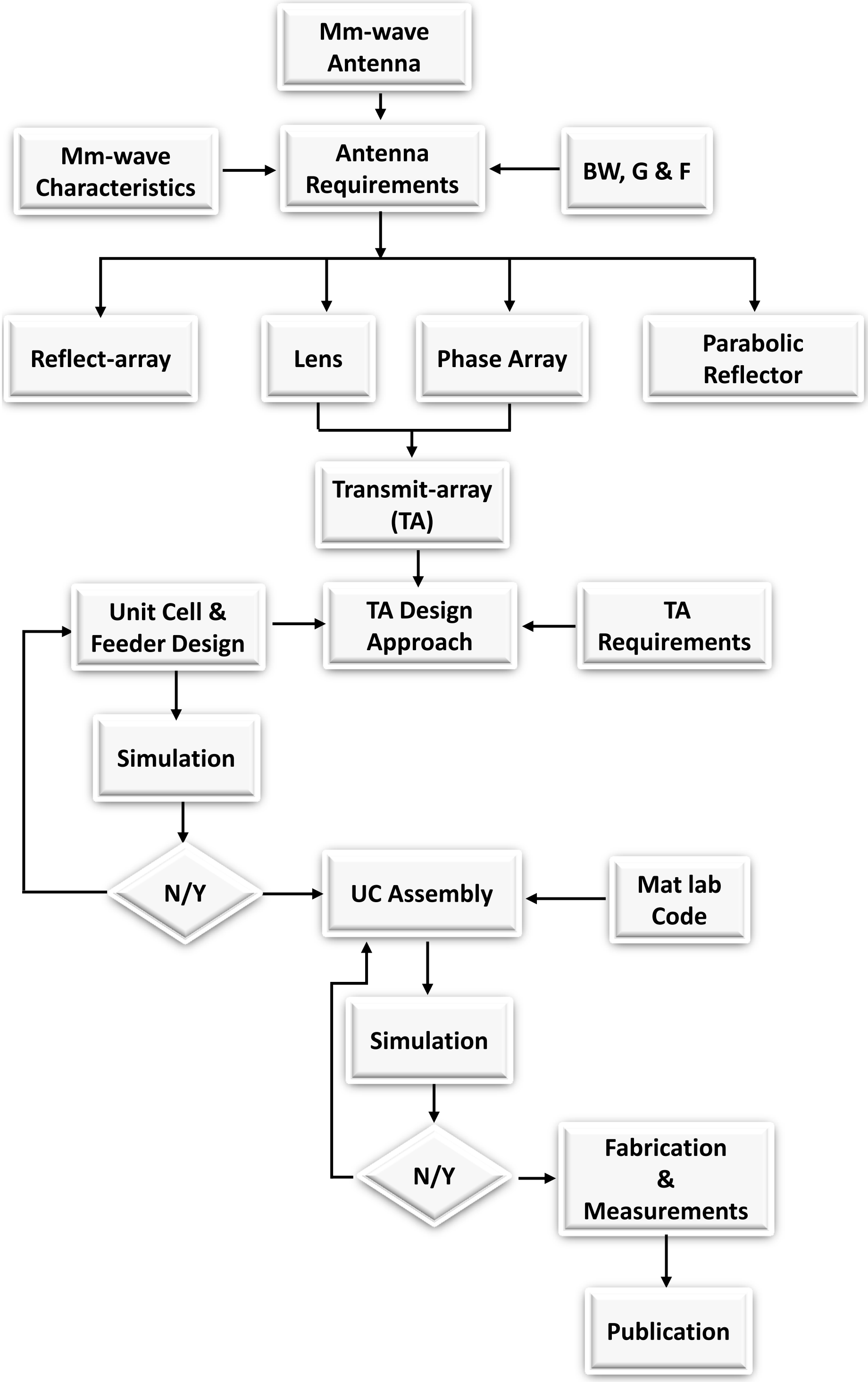

Figure 1.2: Transmit-array antenna design methodology

1.5 Contributions

The contributions of this thesis are divided into three major parts: 1) the design and specification of linear and circular TA antenna components for the proposed frequency band; 2) the integration of the components with antennas to form LP transmit-array and CP transmit-array antennas; and 3) the fabrication and implementation of the proposed wideband TA antennas. The contributions of the reported work are:

Illuminating the TA surface efficiently is the goal for enhancing TA antenna aperture efficiency; therefore, wideband hybrid horn antennas and conical horn antennas are designed. Moreover, a study of the feeding antenna radiation pattern on the TA aperture efficiency is included.

Designing a wideband hybrid horn antenna, in which the patch antenna is used to excite pyramidal structure [j1]. The designed antenna is suitable to be the feeder of the TA antenna. It has a fractional bandwidth of 59.22% at 28 GHz. The design process can be divided into:

- Designing a wideband, low cross-polarization patch antenna. A capacitive coupling technique enhances the antenna bandwidth, while a differential feeding technique minimizes cross-polarization and ensure a stable broadside radiation pattern. The designed antenna’s simulated matching bandwidth is 56.8% at 30 GHz.
- Designing a wideband rat-race coupler and probe stripline transition using PCB technology for differential feeding purposes.
- The transition circuit is shielded using vias around the probe and the stripline to prevent leakage. The rat-race coupler divides the power into two equal portions with a 180° phase difference, and the isolation level is better than 15 dB.
- The final stage combines the design of a capacitive differential feeding antenna with a horn antenna to overcome path loss at an mm-wave frequency band. The designed antenna shows a wideband and a good radiation pattern.

A circular horn antenna is designed with high performance. The designed antenna has a unique amplitude radiation pattern, that enhances the TA aperture efficiency.

- The antenna's radiation pattern's mathematical model is $(\sec\theta)$ with a particular magnitude distribution, 10 dB gain, and a beamwidth of 35°.
- The antenna's radiation makes it capable of dealing with the relative difference in path loss, resulting in a good tapering efficiency.
- The radiation pattern is also symmetric and has a uniform phase distribution within the required beamwidth, facilitating the distribution of the unit cells on the TA surface.

Designing a wideband linear polarized transmit-array antenna operates at the mm-wave band (around 28 GHz). The TA antenna should have high aperture efficiency, wide bandwidth, and low profile. Essentially, the aperture efficiency of the TA antenna depends on the unit cell (UC) characteristics [j2]. The TA antenna's design process involves the following:

- One of the keys to enhance TA aperture efficiency is depending on the design of a UC with high performance. The designed UC is based on the receive/transmit true-time delay technique.
- The UC structure contains dual capacitive coupling differential feeding; these features increase the UC bandwidth and suppress the cross-polarization level. The techniques used to design the proposed UC significantly affect the TA antenna's performance in terms of gain and bandwidth.
- The designed UC performances have a complete phase range of 360°, a transmission bandwidth of 24%, and an insertion loss of better than 0.5 dB. Moreover, the designed UC can rotate the polarization of a linearly polarized electromagnetic wave to its orthogonal direction with high efficiency; a polarization conversion ratio higher than 0.9 is achieved over the operating frequency band.

- The TA antenna is designed based on a 3-bit quantization phase; therefore, the required phases are 0°, 45°, 90°, 135°, 180°, 225° 270°, and 235°.
- A wideband and high-gain TA antenna was assembled using a 27×27 2D array. The TA antenna's surface and the feeding antenna have been designed, simulated, and measured, where the maximum gain is 31.15 dBi. The 1-dB gain bandwidth is 12.7%, while the 3-dB gain bandwidth is 21%, around 28 GHz. The aperture efficiency is better than 50%, and the cross-polarization level is less than -37 dB in the frequency range from 25 to 31.5 GHz.
- Furthermore, factors that affect the TA antenna's performance have been studied and summarized. These factors are mutual coupling, phase error on TA design, quantization error, phase range error, feeding antenna, and incident angle approximation.

Finally, as known CP waves are less sensitive to rain, the atmospheric effect in compression to LP waves is also a factor. Designing a wideband circular polarized transmitarray antenna with high gain and wideband takes place. The procedures for designing the CPTA antenna are as follows.

- The conventional way to create CP waves is by extracting CP waves from the LP components. However, the challenge faced is maintaining the characteristics of the previous design while converting the LP outgoing waves to CP waves. Designing a CP polarizer UC with high performance, including phase shift and the equal amplitude of the orthogonal electric fields is crucial.
- The designed JC UC could provide the CP converter with a 90° phase shift and create equal amplitude portions of electric fields for wide bandwidth, resulting in a high-quality CP wave. The CP surface is assembled, placed, and excited using an LPTA antenna. The CPTA antenna results show a maximum gain of 28.9dBi, an AR bandwidth of 24%, and a cross-polarization level of less than -37 dB.

1.6 Organization of The Thesis

This Thesis is organized into five chapters: A literature review and background introduction to millimetre-wave characteristics and antenna requirements are presented in chapter two. First, there is an introduction to mm-wave characteristics and the reasons behind choosing 28 GHz for wireless communication applications. Also, the antenna's performance that can be used in this band is discussed. Then, in the next section, a theory background is discussed; wave propagation, Snell's law, reflector, and lens these subsections are considered potential knowledge for the transmit-array antenna. The TA antenna is in a specific section, in which a literature review and operating concepts are presented. Also, an introduction to how transmit-array antenna aperture efficiency is maximized. The effect of factors such as the quantization phase, feed antenna, and aperture area are also introduced. The proposed research here is to introduce and discuss the proposed TA antenna. Since the unit cell is considered an antenna, this chapter reviews some techniques for increasing antenna bandwidth. A new section contains a summary of the circular polarization wave creation and CP antenna review; the circular polarizer review and operating mechanism also take an entire section.

Chapter three conclude the discussion about the proposed feeding antennas. The first feeding antenna design includes three stages. First, we will introduce the design and the preliminary results of A 28 GHz rectangular capacitive coupled patch with a wide bandwidth, and then the patch will be fed differentially. A TA antenna feeding source comes from the UC, in which a wideband patch antenna is used to excite the TA antenna. Then the patch antenna is used to fabricate a hybrid horn antenna, which is used to illuminate the TA antenna. Finally, a discussion of the critical consequence of feeding the antenna differentially takes place and the code results. The second feeding antenna design includes the design of a conical horn antenna, which positively impacts the TA antenna efficiency. Chapter four includes the LP UC design, which satisfies the mm-wave requirements. Then, a novel design of the transmit-array antenna structure operates at 28 GHz; the simulated and measured results are presented.

Next, the TA antenna has experimented with various feeding techniques, including a patch antenna, hybrid horn antenna, and conical horn antenna. Finally, this chapter is concluded with a summary of the designed feeding antennas' effect on the TA antenna gain. The design of CP UC and the CPTA antenna is introduced in chapter five. Next the UC structure, the frequency response, the simulated and measured results are presented. Finally, the conclusion and a future research plan of action and expected milestones are introduced in chapter six.

Chapter 2

Literature Review and Background

2.1 Introduction

This chapter includes literature about the advantages and disadvantages of using the mm-wave for wireless communications and the required antenna performances. Then new section presents the TA antenna operating mechanism; and a literature review of the previous works for TA antennas. Also, this chapter includes how antenna designers enhanced patch antenna bandwidth and minimized cross-polarization levels.The final section includes circular polarized antenna review, a circular polarizer converter review and the polarizer operating techniques.

2.2 Millimeter Wave Characteristics and Antenna Requirements

Designers and researchers encountered obstacles to using wireless communication systems in mm-wave bands because they suffered substantial propagation losses. These losses include high atmospheric attenuation loss, oxygen absorption, scattering in rainy conditions, and penetration loss. While low-frequency signal travels long-distance with low transmission loss and penetrate buildings more efficiently. Users of this frequency band must consider the propagation characteristics of radio signals. Designers require knowledge of different kinds of losses at the operating frequency at a particular location to design a reliable communication link. Figure 2.1(a) shows atmospheric absorption characteristics of mm-wave propagation, and Figure 2.1(b) shows the rain attenuation per kilometre as a function of rain rate [15].

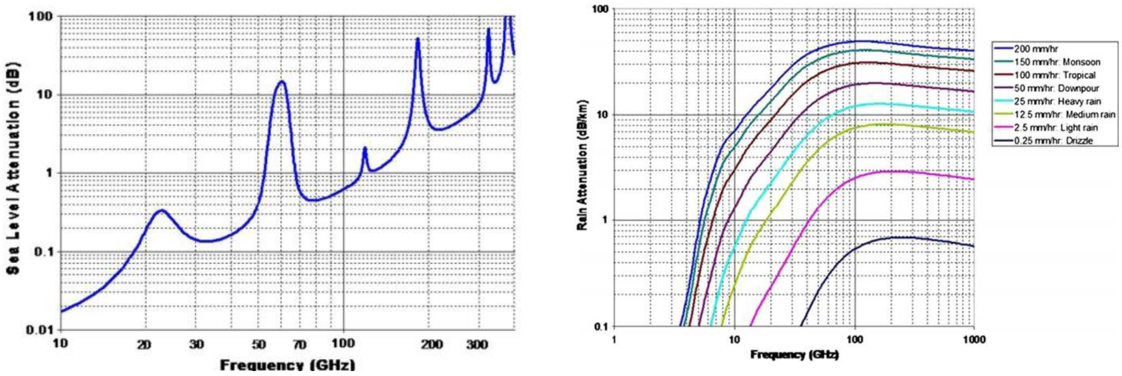

(a) (b)

Figure 2.1: (a) Atmospheric absorption effect (b) Rain attenuation on mm wave propagation. (Q. Zhao et al [11], ©2006 IEEE.)

Millimetre-wave communications depend on the Line of sight (LOS) transmission rate to maximize transmitted data because it contains the most transmitted energy. In general, high attenuation affects the transmitted power through non-line of sight (NLOS) channels, so mm-wave suffers from a few numbers of NLOS paths. According to previous studies, the millimetre-wave band is an excellent candidate for using directive antenna beams in an outdoor short-range. Low-frequency signals can travel as ground waves. It penetrates buildings and natural obstacles easier than extremely high frequencies (EHF), which have difficulty penetrating the solid surface. Due to weak diffraction ability, mm-wave communications are sensitive to blockage from obstacles such as humans and objects. The channel blockage from human mobility (1-5 people) is about 1-2% [16], while the attenuation level depends on the object's material surface [6]. In brief terms, the mm-wave at both 28 GHz and 38 GHz bands has the ability to deliver a high data rate for short-distance if the high-gain wideband antenna is used. The transmission medium and the surrounding environments have a particular effect on mm-wave signal behaviour. Accordingly, the proposed antenna must have specific characteristics to overcome free space negative impacts. It is clear that Atmospheric absorption causes signal attenuation and reduces the signal's penetration ability. Therefore, a high-gain antenna is needed to ensure point-to-point communication with less attenuation.

Millimeter-wave communications depend on the Line of sight (LOS) transmission rate to maximize transmitted data because it contains most of the transmitted energy . In general, high attenuation affects the transmitted power through non-line of sight (NLOS) channels, so mm-wave suffers from a few numbers of NLOS paths. According to previous studies, the millimeter-wave band considered an excellent candidate to use in an outdoor short-range by using directive antenna beams. Low-frequency signals can travel as ground waves. It penetrates buildings and natural obstacles easier than extremely high frequencies (EHF), which have difficulty penetrating the solid surface. Due to weak diffraction ability, millimeter-wave communications are sensitive to blockage from obstacles such as humans and objects.The channel blockage from human mobility (1-5 people) is about 1-2% [16], while the attenuation level depends on the object's material surface [6]. In brief terms the mm-wave at both 28 and 38 GHz bands can deliver a high data rate for short-distance if the high-gain wideband antenna is used.

The transmission medium and the surrounding environments have a particular effect on mm-wave signal behaviour. Accordingly, the proposed antenna must have specific characteristics to overcome free space negative impacts. It is clear that Atmospheric absorption causes signal attenuation and reduces the signal's penetration ability. To ensure point -to- point communication with less attenuation high-gain antenna is needed.

Several antenna design techniques have been adapted to serve the promising 5G technology. Since obtaining optimum 5G antenna structures is still the beginning, the research stream opens a range for new and improved design ideas and concepts. Antennas designed specifically for 5G applications need to satisfy the essential requirements of new technology. As previously stated, the large number of elements is one of the most valuable tools to obtain high antenna characteristics for utilizing the positive feature of small mm-wavelengths. Also, circular polarization waves (CP) with narrow beamwidth radiation have less path loss when compared with a linear signal [15].

Generally, wireless networks are designed to provide service to fixed and mobile users. The circularly polarized signal is better than the linear one in connectivity terms. However, the receiver antenna orientation is random, leading to an out-of-phase signal with energy in which all planes are preferred to overcome this problem. The reflected linear polarized signal, which is not on the same plane, might lose the signal strength, but the energy is in all planes in the circularly polarised signal. In linear polarization signals, the reflected signal weakens the propagated signal, especially in the opposite phase. The out of phase radio signals can result in dead spots, but in CP reflected signal has the opposite orientation. Moreover, CP signal energy is absorbed differently, so it is highly likely to be delivered. The proposed antenna should utilize the broad spectrum offered by the mm-wave to satisfy the demands of the channel's bandwidth. Depending on the application, a small and integrated antenna might be required.

2.3 Wave Propagation Concepts

Propagation and refraction theory illustrates the main concepts of electromagnetic propagation phenomena. The propagation of light waves was demonstrated in 1678 by Huygens, and his principle provides a convenient way to visualize a propagating wave of light at any moment. He stated that the signal wavefront is considered the sum of the radiated points at the different medium boundaries at the prior moment. These points on an envelope of spherical shape serve as new radiation sources; it radiates just forward and at the same speed as the light source. Each new radiation source generates a half-circle of radiation. Combining those wavelets is considered the propagated wave at a particular time.

As illustrated in Figure 2.2 the new wavefront is the tangent line for all of these wavelets. Consequently, the origin point can be compensated by the new radiated points [17]. Then Fermat described the signal reflection and diffraction of light rays. Fermat's principle gave a degree of freedom to control wavefront direction by introducing a phase shift along the boundary wavefront. The suitable interface between two mediums establishes the required phase shift over the optical path. The material properties and angle of incidence are considered the main factors controlling the new signal direction. Snell's law is used to design optical lenses. This law describes the relationship between the incident angle and the transmit angle of the same signal when it travels at the boundary of different material properties. Figure2.5, Figure2.3(b), and Figure2.3(c) shows Snell's law principle, the dielectric lens and the parabolic reflector.

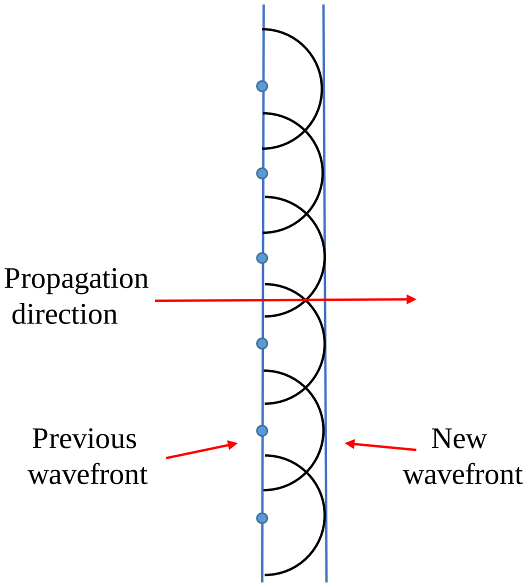

Figure 2.2: Huygens propagating and refraction phenomena.

$$n_i \sin\theta_i = n_t \sin\theta_t \tag{2.1}$$

Where: n_i material index, θ_i incident signal angle, and θ_t transmitted signal angle

Let's assume that the wavefront crosses the boundary surface between two mediums, in which the second medium has a lower speed of light (high-index material). As a result, the wave direction becomes toward the orthogonal plane. Since different materials differ in phase velocities, designing a lens with suitable materials directs incident signals to the focal point. Each incidence signal takes a different path delay inside the lens, resulting in re-transmitted singles that become in phase, as shown in Figure 2.3(b). On the other hand,

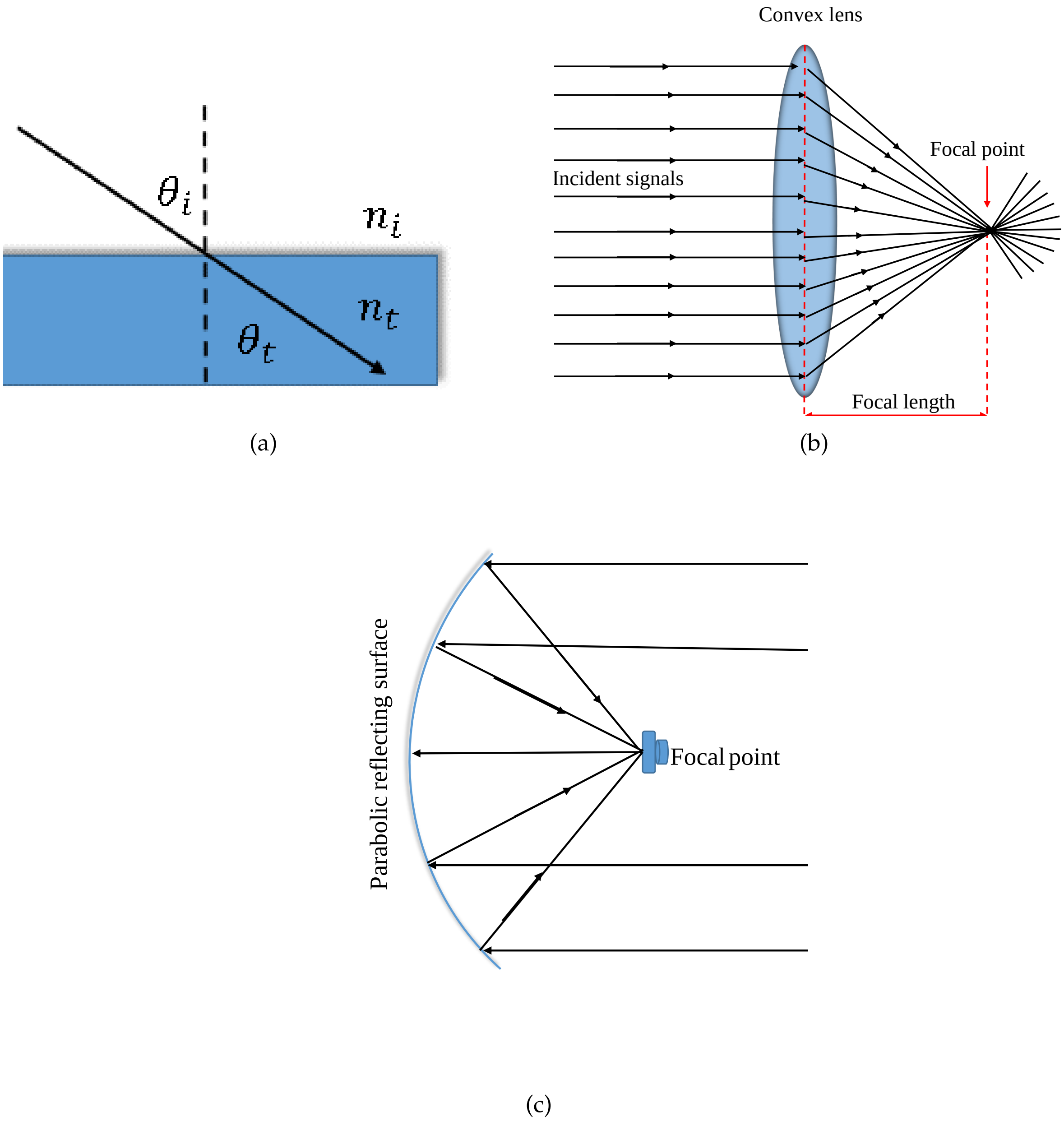

Figure 2.3: (a) Snell's law (b) Dielectric lens (c) Parabolic reflector

Figure 2.3(c) shows the operating mechanism of a parabolic reflector, in which the sum of the incidence and reflected paths for different rays are equal on a planar surface parallel to the parabolic surface [18]. Due to the shape of the parabola, all the ray paths end up with the same length, so the reflected signals are in the same phase. In parabolic/lens, the structure curvature controls the signal phase.

Both TA and RA antennas designers use the same idea, in which the plane surface with discrete elements is used to compensate for the phase difference between the centre point and other points on the aperture surface. This method is called the guided-wave approach. A comprehension of some of the previous assessments is presented in the next section.

2.4 Transmit-array Antenna Concepts

Transmit-array antenna is considered a discrete planar lens because it combines the advantages of the lens antenna from the optical theory and the phased array antenna [3, 10, 19]. Moreover, the transmit-array antenna has features such as lightweight, low profile, low cost, high-gain, easy fabrication, and wide frequency band [20]. Transmit-array antenna is classified into two classes: the frequency selective surface (FSS) and the receive re-transmit (R/T) antennas. The FSS or the active type uses the UC dimensions to control the transmission coefficient phase. In the other kind, the receive re-transmit or the passive type, the receiving layer is used to receive the incident signals, and the re-transmitting layer is used to re-transmit the corrected phase signals [21]. Figure1.1 shows the general overview of the TA antenna. The transmit-array antennas have a thin surface and a feeding source in the aperture's focal point. The TA surface consists of several unit cells (UC) to convert the spherical incident wave into a plane wave; hence, a high-gain can be achieved. Figure 2.4 shows the operating principle of the TA antenna. The working mechanism of the TA antenna is the same as the RA antenna, but there are two critical differences between them. RA elements reflect the incident signal with a specific phase within the designed bandwidth, and the groundsheet reflects incident signals between

UCs with 180° phase shifts. On the other hand, the UC of the TA antenna is responsible for re-transmitting the incident signals with the required phase shift within the operating bandwidth. However, the TA antenna is considered a band-pass filter because it reflects the incident signals above or below the TA antenna bandwidth.

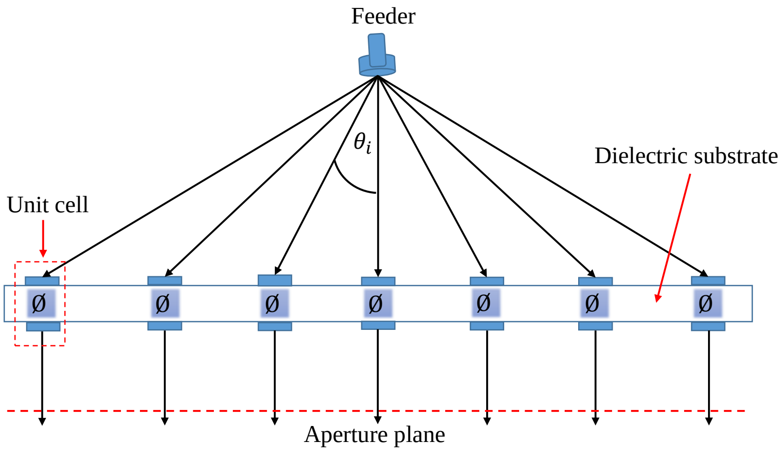

Figure 2.4: Transmit-array antenna principle schematic.

2.4.1 Transmit-array Antenna Literature Review

It is beneficial for designers and researchers to know how others enhance the directivity and bandwidth of the TA antenna. The core issue of TA design is the design of a unit cell with a high amplitude transmission coefficient and can provide a 360°phase range. Figure 2.5 represents some used unit cells to enforce re-radiated signals in phase. Ahmed. H. et al. [22], reported a transmit-array antenna that operates at 11.5 GHz in which the UC contains three layers of spiral dipoles. Their antenna achieved 28.9 dB gain, 9% of 1-dB gain bandwidth and 19.4% of 3-dB bandwidth. In [3], the authors introduced the cross-slot element UC with three layers and a smaller aperture diameter. The operating frequency is 11.3 GHz. This antenna achieved a gain of 23.76 dB for the oblique incident, 1-dB gain bandwidth of 4.2%, and 3-dB gain bandwidth of 9.4%. A linear-polarised transmit-array unit cell is operating at 10 GHz, as reported in [2]. The UC comprises three layers of three slots in cascade form. Although the antenna achieved 1-dB gain bandwidth of 15.5%, 55% aperture efficiency, and less than -29 dB cross-polarization, the unit cells provided 320° phase response which affected the antenna's gain by 24.8 dB. Wideband low-loss linear and circular polarized transmit arrays are designed by H. Kaouach, et al; that antennas operate at V-band as stated in [23]. The antenna design is based on two patch antennas separated by ground plane and connected through via. It has a 2-bits quantization phase where the upper patch rotation is used to have a 180° phase shift. The results were 7% of 1-dB gain bandwidth, 27 dBi of directivity, and 17% of aperture efficiency. Later, they proposed circularly polarized discrete lens antennas in 60 GHz Band [1], consisting of two patch antennas separated by common ground and connected via drilled through the substrate. The upper patch is rotated to achieve different electric field orientations. The proposed lens provided a 1-dB gain bandwidth of 12%, a gain of 20.85 dB, and maximum aperture efficiency of 28%. Another research team led by Kien Pham, et al. proposed a dual linearly polarized TA antenna [24]; the design is based on a bandpass filter using two rectangular patches separated by ground with cross slots. The UC phase response is controlled by varying the patch and the slot dimensions. Their project achieved horizontal and vertical polarised beams with an average of 20% for the 3-dB bandwidth and 24.9 dB gain.

The core issue of TA design is the design of a unit cell with the required transmission phase coefficient. Researchers developed some techniques to enforce radiated signals to be plane wave signals. For instance, one technique use variable length stubs that are connected to the same size patches [25, 26]. Another technique, variable size patches controls the phase shift [27]. Nevertheless, a 360° phase shift has not been achieved by these techniques. Accordingly, the quantization phase is limited. A TA antenna has been designed in [28], and the UC transmission matching bandwidth is less than 18%. The design in [29] achieved a full phase cycle. However, the total thickness is 11.22mm, and the transmission attenuation of the UC is less than 1.2 dB which has a negative impact on the TA gain. In [30], the TA antenna is designed with a 360° UC phase range is achieved. However, the aperture efficiency is 47%, bandwidth is 3.7%, cross-polarization -15 dB, and gain is 20.6 dBi. Another prototype of the TA antenna is shown in Figure 2.5(e). The design presented in [31] is based on two square stacked patches that operate as a receiver coupled through the slot to another stack patches as a transmitter. The design provides 38.7% aperture efficiency, 1.8% 2-dB gain bandwidth and 13.5% 3-dB gain bandwidth. They designed another TA surface consisting of five layers of Jerusalem cross-dipoles. This design is considered better than the first design because it provides measured results such as 34.64% aperture efficiency, SLL leas than -15dB, one and 2-dB gain bandwidths are 10.2% and 14.83%, respectively.

Table I illustrates the previous designs achievements in TA antenna gain, bandwidth, aperture efficiency, thickness, SLL, operating frequency, TA area, and cross-polarization. In this work, a modified version of the variable length strips technique is used to achieve a 360° phase shift and allow flexibility of phase quantization. Furthermore, old works suffer from moderate cross-polarization, so differential feeding is used as a technique for the first time. The aim here is to design a transmit-array antenna that operates at a millimetre wave region in which it can be used in many applications like imaging, beamforming, and 5G mobile applications.

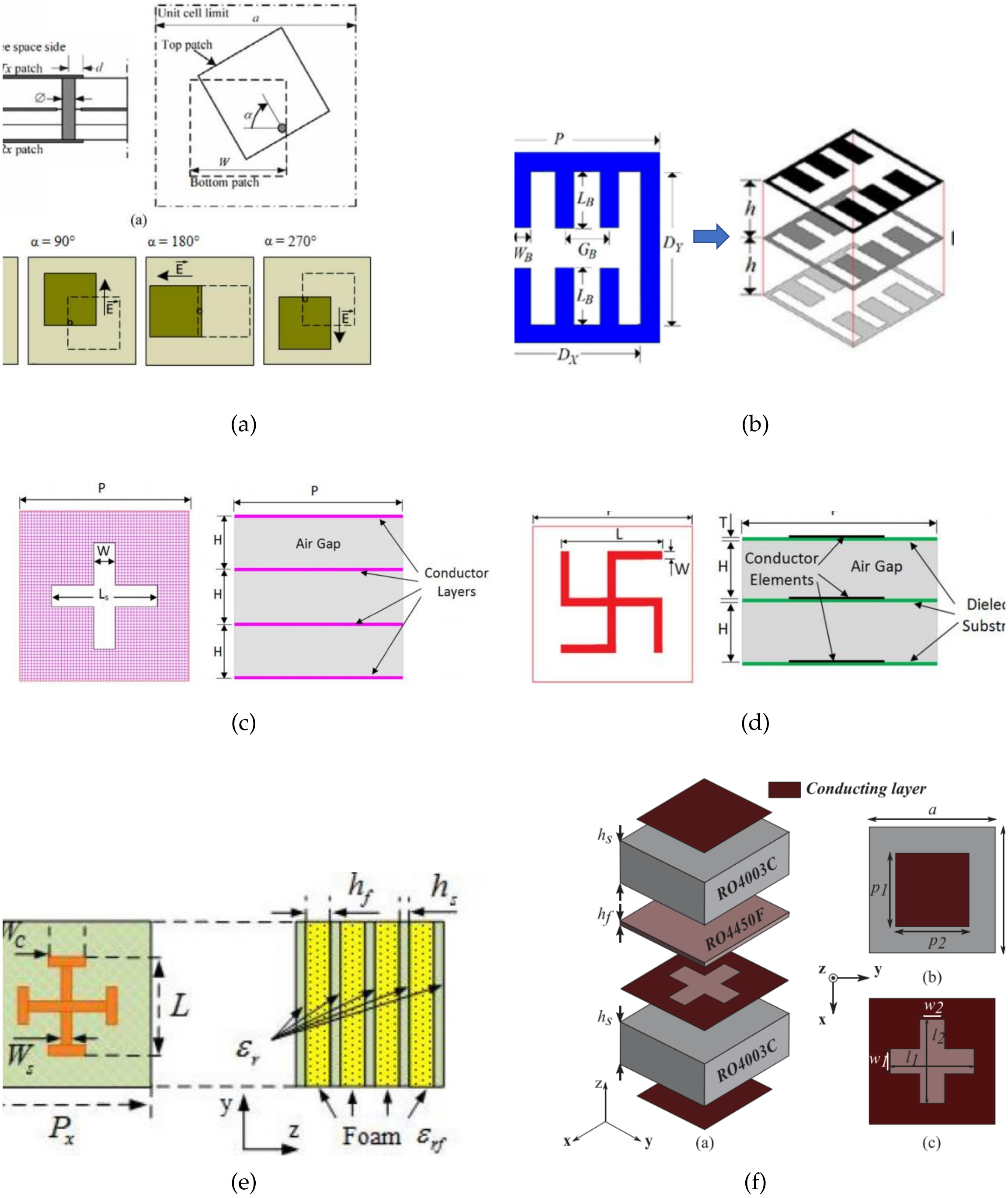

(a) (b)

(c) (d)

(e) (f)

Figure 2.5: Transmit-array antenna unit cells (a) [1], (b) [2], (c) [3].
, (d) [10], (e) [31]and (f) [24]

2.5 Transmit-array Antenna Consideration

The design procedure of a transmit-array antenna can be summarized in three steps; designing the phase-shift elements (UC), calculating the array configuration, and designing verification through full-wave simulation of the entire array. The TA system configuration consists of two factors, designing the feeding antenna and specifying the system requirements such as operating frequency, antenna gain and bandwidth. System gain and bandwidth are related directly to some factors: UC characteristics, feed antenna radiation pattern, and TA aperture efficiency. The TA antenna aperture is a 2D array of a tiny re-radiating element that controls the radiation pattern of all TA antennas as a system. The TA antenna designers should consider factors such as what will affect element characteristics and significantly impact the TA antenna gain and bandwidth. These factors are:

- Mutual coupling.
- Phase error on TA design.
- Quantization step and Phase range error.
- Incident angle approximation.
- Feed antenna characteristics and Coordinates.
- TA antenna shape.

All of the above-listed factors are discussed and concluded in this subsection.

2.5.1 Mutual Coupling

Transmit array is a 2D structure that contains several UCs arranged beside each other. Unit cell numbers depend on the size of the UC and the size aperture area dimensions. As known, computing the element's reflection coefficients is the main issue of TA antenna designers. Available simulation tools extract element amplitude and phase coefficients from an infinite periodic array, which assumes that the target element is surrounded by other identical elements [32]. This kind of calculation depends on Floquet boundary conditions, in which absorbing boundaries are considered on the UC's top, and bottom surfaces, and a normal incidence plane wave is used to illuminate the UC. Mutual coupling increases between adjacent unit cells as the substrate becomes thicker. The mutual coupling has a negative impact because it reduces the radiation pattern for the entire TA area. The Computer Simulation Technology (CST) considers mutual coupling when designers choose the periodic structure and Floquet port, but the computed coefficients are not accurate. According to the aperture phase distribution, each UC is surrounded by different UCs in size or phase, and the array is not infinite. Therefore, considering the TA aperture as a periodic structure leads to calculating refection coefficient error. H. M.-A. Milon; et al. [33] studied the mutual coupling effect for three excitation methods: the isolated approach, the infinite array approach, and the surrounded element approach. Their study shows that a UC's environment leads to varying element phase responses, and the surrounding experiment shows better agreement between the simulation and the measurement results, so it can be considered the accurate way to find the element phase characteristics.

2.5.2 Quantization Step and Phase Range Error

A feeding source illuminates a TA antenna's aperture. The incident waves are distributed over the surface at different arrival times because of path distance variation, so it has different phases. The dispersed phase is not continuous and uncontrolled. UCs with different phase delays are used to convert spherical waves to plane waves. According to Huygens, at the boundary, all of the incident rays at the boundry generate new radiator points, so it is essential to calculate the phase distribution to have the plane wave accurately.

Usually, the array phase distribution is created by generating a map between element coordinates and element transmission coefficients; this map is used to build the TA antenna [34]. Because of UC size and fabrication limitations, designers are forced to divide the antenna surface into a certain number of zones called quantization steps (k). Due to the quantization procedure, the experimental phase of an element on the antenna aperture may not be the computed phase [18,32]. According to the quantization theory, the difference between incident signal phase distribution and the quantization aperture phase distribution is called the quantization phase error. This error depends on the quantization step; increasing the number of quantization steps minimizes this error.

$$k = 2^N \tag{2.2}$$

Where: k Quantization steps, N Number of bits.

For example, two bits lead to; four quantization steps, four UCs with different phases, and the error is ±45°. Three-bit quantization steps lead to less error where the steps become closer and the phase distribution becomes wider, which means the maximum quantization error is ±22.5°. As we can see, the quantization error should be minimized as much as possible to enhance antenna directivity.
Since the maximum phase distribution over the TA aperture area is 360°, the UC should support the TA at least by 360° transmission phase to minimize aperture phase error. This phase error is connected directly to a UC of choice called a phase range. When element phase rage does not reach the required phase at aperture edges, designers are enforced to use the available UC with the closest phase. The substitute element reflects at least part of the incident power, and the reflected signal will inflict the incident signals and create some blockage. Also, this element becomes the source of destructive interference at the new wavefront and cause a gain reduction. A unit cell covering a 360° phase range is optimal for designing a TA antenna because it reduces the quantization phase error and enhances TA antenna gain.

2.5.3 Feeding Antenna Characteristics and Coordinates

Transmit array antenna is a surface re-radiates incident signals towards the desired direction. Knowledge of the feeding antenna location and radiation pattern are essential because they affect the TA antenna aperture efficiency [34]. The focal point location and the phase centre distance are essential because they are used to calculate the transmission coefficients and the effect of incident signal magnitude. Since the TA antenna aperture size is enormous compared with the feeding antenna, incident signals take different paths. At mm-wave, the wavelength is a fraction of a millimetre, so a small-displacement forward or backward of the feeder could vary the incident signal phase. For example, at 30 GHz 1.25mm is equal to 45° phase shift. In terms of phase centre errors, it can be corrected by repositioning the phase centre of the feeding antenna to the focal point. Different paths between different points affect the magnitude and the phase distribution over the aperture. Moreover, the TA antenna shape affects its efficiency because the feeding antenna radiation does not follow specific geometry. The Square and rectangular TA antenna aperture has a high sidelobe level and low efficiency compared to the circular one because of poor illumination at the edges. Frequently, feeding antenna position and radiation beamwidth controls TA antenna area and phase distribution over TA antenna aperture for optimal operation. In terms of feeding antenna coordinates, most of the available studies obtain a transmission phase coefficient according to the typical plane wave incident. Phase delay can vary from normal to oblique incidence. The feeding antenna radiation pattern is used to calculate the antenna aperture area. Typically, the -10dB beamwidth angle is used with respect to antenna location. Also, the characteristics of the feeding antenna radiation pattern affect both spillover and illumination efficiency.

According to [35] maximum value of illumination efficiency is about 80% if edge illumination is about -10 dB. The optimum aperture area is initial to enhance antenna efficiency because a small TA area causes spillover. Direct radiation that passes the edges of the TA area can create a sidelobe that exceeds the known sidelobe level, and it could affect re-radiated signals by causing a destructive area. On the other side, the big TA aperture area leads to weak edge surface illumination, which harms magnitude distribution over far edges of the aperture. Knowledge of the antenna radiation pattern model is the initial step to designing the TA antenna, balancing aperture efficiency and minimizing edge diffraction. The most common horn antenna radiation pattern model is $\cos^q \theta$ [36]. A feeder with a symmetric radiation pattern is preferable because an asymmetric field distribution negatively impacts the aperture efficiency, especially with a circular TA antenna aperture. Regular horn antenna can feed parabolic reflector because its curvature surface can compensate for path loss difference. Since the TA antenna has a flat surface, a special feeding antenna with high performance such as proper amplitude tapering, uniform aperture phase distribution, and the feeder should have a low side loop level. To deal with path loss differences, the optimum feeding antenna field should be distributed uniformly on the TA aperture. The author in [34] designed a horn antenna with a specific radiation pattern in which the radiation pattern model was chosen to be $\sec \theta$. The antenna is scaled up to be usable with the proposed TA antenna. The simulated and measured results are presented in chapter three. According to the author, the designed horn shows a more uniform field distribution on the aperture area than the conical horn. The designed horn even showed superior aperture efficiency. The conical horn with a cavity supports the design by 7% efficiency more than without a cavity, and both antennas have the same level of edge tapering. The designed conical horn increases aperture efficiency in spillover and taper efficiencies.

2.5.4 Aperture Efficiency

Usually, designers of TA antennas start by determining two factors: designing the UC and specifying the required TA antenna performance (system configuration) like the antenna directivity and the operating frequency [36]. Antenna gain is connected directly with the aperture efficiency because antenna directivity is proportional to the antenna area. This section discusses the aperture efficiency. By taking into account the loss, equation 2.3

comes in the form of gain, which indicates that the power profit is proportional to the effective antenna area [36].

$$D = \frac{4\pi A}{\lambda^2} \tag{2.3}$$

Where: D Antenna directivity, A Antenna aperture area, λ Signal wavelength

$$G = \frac{4\pi A_e}{\lambda^2} \tag{2.4}$$

$$A_e = \eta_a A \tag{2.5}$$

Where: G antenna gain, A_e antenna effective area, and η_a aperture efficiency

$$\eta_a = \eta_s \eta_i \eta_r \tag{2.6}$$

Where: η_i illumination efficiency, η_r radiation efficiency, and η_s spillover efficiency.

Effective area (A_a) depends on the aperture area and the aperture efficiency (η_a). Aperture efficiency is the multiplication of three factors which are spillover efficiency (η_s), illumination efficiency (η_i), and radiation efficiency (η_r) [37]. The first two factors are connected to the feeding antenna's radiation pattern, and the last factor related to the TA antenna's structure. Moreover, some factors are not considered connected to the UC, such as material loss, mismatching loss, polarization loss, and quantization phase loss. Maximizing both the spillover and the illumination efficiency values result in the overall aperture efficiency only being dependent on radiation efficiency. The spillover can be expressed as the ratio of total power radiated by the feeder over the entire spherical surface, and the incident power on the TA antenna aperture. Spillover efficiency can be increased by placing the antenna feeder at the optimal distance further away from the transmit array aperture. The spillover and illumination efficiency are expressed mathematically in [37]. The horn antenna radiation takes different paths to illuminate the TA antenna aperture, which affects the incident signal's amplitude. The relative difference in paths lost has a negative impact on the illumination efficiency (η_i).

2.6 Electromagnetic Wave Polarization

The electromagnetic wave comprises two orthogonal fields; an electric field and a magnetic field; those fields are orthogonal to the radiation direction. The tip shape and orientation of the electric field (E) is used to identify the polarization of the electromagnetic wave as the wave travels through that plane [38]. The most known forms of electromagnetic wave polarization are linear polarization (LP) and circular polarization (CP). The wave is defined as a linearly polarized electromagnetic wave in which the electric vector at a particular plane in space is pointed toward a fixed direction, although varying in magnitude. Generally, the linear polarization waves are either horizontal and vertical or parallel and perpendicular. The electric field of vertically polarized waves is perpendicular to the Earth's surface, and the waves are called horizontal polarization when the electric field is parallel to the Earth's surface. The polarization quality of the linear polarized antenna can be determined by considering the ratio of both co-polarized and cross-polarized responses. In general, the ratio indicates system power loss due to polarization mismatch.

Waves are called circularly polarized when the electric field vector component has a constant magnitude but its direction changes in a rotary manner on a plane perpendicular to the transmission direction as a function of time. The electric field vector represents a point on the circumference of the helix at any moment. The plane at that point can be considered a plane wave, which has a certain magnitude and direction of the electric field. The CP antennas specifications depend on their axial ratio (AR) over the frequency bandwidth. Equations (2.7), and (2.8) defined the axial ratio as the ratio of the orthogonal components (major axis to the minor axis) of the E-fields; this ratio represents the polarization quality for a circularly polarized antenna and the ideal CP antenna AR has 1 or

0dB. The circular polarization is divided into right-hand and left-hand circular polarization, and the hand rules are used to describe the sense of polarization. The right-hand circular polarization (RHCP), in which the electric field vector rotates on a right-hand sense and the thumb is pointed toward the direction of propagation, and left-hand circular polarization (LHCP), in which the vector rotates in a left-hand with respect to the direction of propagation. The CP wave becomes an LP wave when both RHCP and LHCP magnitude components are equal.

$$AR = \frac{majoraxis(E_{max})}{minoraxis(E_{min})} \tag{2.7}$$

$$AR(dB) = 20log\frac{majoraxis(E_{max})}{minoraxis(E_{min})} \tag{2.8}$$

Circular polarized antennas are preferred over linear polarization antennas because CP antennas are less sensitive to the antenna orientation. It is known that some wireless networks are designed to provide service to fixed and mobile subscribers, which leads to weakening the received power. The circular polarization links remove the need to align both transmit and receive antennas continuously. The Faraday rotation effect affects linear polarized waves at low frequency; as the electromagnetic waves pass through the atmosphere, the linear field vectors rotate due to interaction with the light field. The resulted wave causes misalignment problems between transmitting and receiving antennas that cause polarization mismatching error. Fortunately, circularly polarized antennas radiate energy in a circular shape in the horizontal and vertical planes; this feature allows for more flexible orientation of the transmitting and receiving antennas [39]. Moreover, the circular polarization waves with narrow beamwidth waves have less path loss than a linear signal. The multi-path interference suppression does not affect CP signals as much as liner polarized signals [40]. Waves at the receiving end are not only a direct line-of-sight radio wave but also via many different paths, and multi-path reception, such as reflected and scattered signals. These components of the wave interfere constructively or destructively. The multi-path waves reach the receiving antenna at a different time delay that causes channel degradation. The reflected linear polarized signal, which is not on the same planes, might lose signal strength, while circularly polarized signal energy is available on all planes. In LP signals, the reflected signal weakens the propagated signal, especially in the opposite phase. Out of-phase radio signals can result in dead spots, but the CP reflected signal has the opposite orientation. Moreover, CP signal energy is absorbed differently, so it is highly likely to be delivered. In [41], an explanation of the multi-path effects of circular and linear signals was included. The experiment clarified that the multi-path delay impact could be reduced to half by using the CP antennas instead of LP antennas.

2.7 Linearly Polarized Antenna Bandwidth Enhancement Review

The microstrip patch antenna is famous for its unique and attractive properties such as low profile, lightweight, ease of fictionalization, and ability to be integrated with other devices easily. Despite patch antenna advantages, it suffers from a narrow impedance bandwidth and a low gain. It also has disadvantages such as conductor losses and low radiation efficiency [42]. The patch antenna's gain is about 5 dBi for a single element and low loss antenna substrate. Size reduction, high-gain, and wide bandwidth antenna are required for many applications like mobile devices. Researchers have proposed many techniques to increase patch antenna impedance bandwidth to be usable for wideband antenna requirements.

Patch antennas loaded by U, E or C shape slots have a wide bandwidth. The established technique introduces other resonant frequencies that combine two resonances that cause a wide bandwidth. A symmetrical E-shaped patch antenna has been designed in [43], in which the centre wing resonates at a higher frequency, and the two side wings resonate at a lower frequency. The measured bandwidth is from 5.03 to 6.12 GHz for a reflection coefficient less than -10dB. However, the design suffers from air substrate and good mechanical stability. Another research articular has done by A.A. Kishk et al. designed a patch antenna that includes U and E slots. In [44], their designs are based on U-slot and E-slot patch antennas in which shorting pins and shorting walls are used. The half U-slot patch antenna with shorting pin design achieves a bandwidth of 20%, and the half E-shaped patch antenna achieves 25.2% bandwidth. Recently A. Kishk's group designed a new patch antenna with a narrow ground plane along the patch width direction compared with the conventional microstrip antenna. This technique provides the antenna with 15% impedance bandwidth [45].

A stacked configuration is a possible method to enhance the patch antenna's gain and bandwidth. Both apertures coupled and coaxial feeding techniques can be used to excite the lower patch antenna. The upper patch is excited due to the electromagnetic coupling. This combination could provide wider bandwidth when the lower patch substrate has a higher dielectric constant than the upper substrate. In [46], the designers use air as the second substrate layer and surround the design with a U-shape metal reflector to get good radiation and stable gain. An array of three elements provides stability gain of 12 dBi. Another design is based on four rectangular patch antennas placed on the top of the low dielectric substrate, which is etched on a rectangular patch. A bowtie slot excites the lower patch coupled to the upper patches. The antenna's measured realized gain and bandwidth are 11.2 dBi and 27%, respectively, at 10 GHz centre frequency [47].

A 2×2 array of a high dense dielectric patch using high permittivity fed by aperture coupled technique and covered by a perforated dielectric superstrate was designed or reported [48]. However, the antenna bandwidth was 15.35%, the gain 16 dBi, and the phase distribution along the superstrate is not uniform as we move away from the antenna centre to the edge.

The third approach to increase patch antenna bandwidth is the usage of low permittivity and tick substrate. The low permittivity material gives patch antennas charges the ability to generate more flux, while antennas with a high dielectric constant are a small area and narrow bandwidth. High permittivity material increases dielectric loss [49,50]. Thick substrate antennas with low dielectric boost the antennas' performance, such as antennas' bandwidth and radiation efficiency. However, this method increases both the material losses and the cross-polarization level [49]. The differential feeding technique is used to have a symmetric radiation pattern and decrease cross-polarization levels [51,52].

The differential feeding patch antenna is preferred in contrast to the single feeding antenna because the cross-polarization level of the differential feeding antenna is much weaker than the single feeding antenna's cross-polarisation. In contrast, the co-polarized radiation level is matched [53]. The following subsection illustrates some previous techniques used to feed patches differentially. The patch antenna can be fed using capacitive coupling to enhance antenna bandwidth. The Strip coupling technique is introduced to feed the patch antenna, in which the coaxial probe feeds the coupling strip. The probe introduces reactance impedance, and the gap between the patch and the strip introduces capacitance, both the capacitance and the reactance parts can produce extra resonance. As a result, the patch antenna and the coupling gap create dual resonance frequencies. Moreover, coupling techniques allow the patch to be excited only in a single-mode operation, in which the patch and the resonator are resonating, and suppressing other harmonics [54].

2.7.1 Differential Feeding Antenna Review

This subsection discusses the theory behind designing the patch antenna's wideband, broadside, and low cross-polarization. The differential feeding technique is used for cross-polarization discrimination purposes. The main focus of this work is to design a UC based on a differential feeding antenna technique. Examples of previous works are presented here.

In [55], Neng-Wu Liu, et al proposed a deferentially fed rectangular microstrip patch antenna where the operating bandwidth is enhanced using the TM_{10} and TM_{30} modes simultaneously. The TM_{10} mode is shifted up using four short pins, while the TM_{30} mode is shifted down using two long slots etched near this rectangular patch's edges that move close to the new TM_{10} mode. Since the shorting pins and probes feed introduce an inductance impedance, a short slot has been introduced in the middle to reduce this effect. However, this work provides only 13% impedance bandwidth and an average gain of 6.4 dBi. Furthermore, the antenna is air suspended, making it hard to be fabricated. Recently, Zubair, et al. [56], have used a TM_{30} rectangular patch antenna loaded by two slots to achieve a high-gain with a low sidelobe level. Since the feeding points are out of phase and located at the centre portion, which generates an out-of-phase surface current. The two etched slots are in an out-of-phase region to reduce the out-of-phase surface current while keeping the in-phase current. In addition, they added new radiation elements in-phase with the original antenna, enhancing antenna gain. The antenna achieves a gain of 12.8 dB with a side loop level of only -12.7 dB. Yet, the antenna has a narrow bandwidth of 21 MHz, around 3 GHz. In [57], two patch antenna arrays are designed and fed differentially to operate at 13 GHz centre frequency. The first array design depends on deploying the differential feeding to each array element. The second array design applies the differential scheme to the whole structure by feeding each pair of elements differentially (one feed for each element). The first array has an impendence bandwidth of 15.3% and a 10.41 dBi gain with -17.5 dB cross-polarization. The second array achieves a 12.32 dBi gain and a 12.8% impedance bandwidth with -17 dB cross-polarization. Its main idea is that the feeding pair of elements differentially reduces the feeding network losses and increases the gain with a negligible effect on the cross-polarization level. The main focus of this work is to design a UC with high performance. A feeding antenna and a UC based on capacitive and differential feeding techniques will be designed and presented in the upcoming chapters.

2.8 Circular Polarized Antenna Review

The simplest way to generate a circular polarization wave is by placing two half-wave dipoles orthogonal to each other. The dipole arms' lengths control the desired phase quadrature (90°), and the CP type can be achieved by the relative polarity of the wave components in dipole arms. As a result, the dipoles will generate circular polarization electromagnetic waves. Moreover, the circularly polarised antenna can be obtained by combining multi linear polarised elements, in which a sequential rotation feeding network is used to excite the linear elements [58]. The sequential rotation technique is used based on the distribution of the excitation power evenly using the progressive phase shift to excite linear polarized elements. The earlier method's axial ratio (AR) bandwidth depends on the sequential feeding network performances [40].

The New L-probe proximity-fed microstrip patch antenna uses the coplanar waveguide (CPW) line to feed the designed antenna. The new technique maintains a wide impedance bandwidth of over 35% and has a gain of around 7 dBi. For the high-gain purpose, a 4 × 4 linear polarized array was designed and fabricated; the designed array impedance bandwidth is 25.5% and has a gain of around 15.2 dBi. Then, the opposite corners of the rectangular radiating patch are truncated, so the patch can radiate CP. The 4 × 4 array elements are excited using eight pairs of differential output power dividers to increase the axial ratio bandwidth. The designed array exhibits a 3-dB axial ratio bandwidth of 15.6% and a gain of around 14.5 dBi [59].

Another way to generate a circular polarization wave is by exciting the CP elements with uniform distribution of equal phases [39]. The CP elements should be arranged in groups and excited using power dividers to broaden the axial ratio bandwidth, in which a strip or microstrip line is used for low profile purposes. In [60], the antenna geometry is a patch antenna with a U-slot patch slot. A stub supports the antenna at the patch corner to excite two orthogonal modes for the CP radiation. The designed antenna simulated $S_{11} \leq 10$ dB impedance bandwidth is 26.4%, but the AR bandwidth is 5.58%, and the gain is 5.7 dBi at the centre frequency. Then, to enhance AR bandwidth 4 × 4

U-slot patch antenna array with a stripline sequential rotation feeding scheme has been designed. The antenna measurement results are as follows; the maximum impedance bandwidth is 16.5%, the maximum AR bandwidth is 11.5%, and the maximum gain is 16 dBi. In [39], an antenna consists of a two-dimensional 8×8 antenna array. The array element is a pair of open rings. Each ring with feeding line is placed on the side of the substrate, and the other ring with feeding line is placed on the opposite sides of the antenna substrate. The antenna's measurements show $AR \leq 3dB$ is about 25%, and gain is near 20 dBi. Tingqiang Wu. et al. [61], designed a circularly polarized antenna consisting of two stacked patches fed by an $S-shaped$ network. Their CP design is based on truncating the two centre symmetric diagonal comers of the patches; they have four symmetric-L narrow slots. Additionally, the upper parasitic patch is rotated by 90° to support sequential rotation and enhance antenna impedance bandwidth. The designed antenna's results are an impedance bandwidth of larger than 15.1%, antenna $AR \leq 3dB$ is about 2.5%, and peak gain of 6.32 dBi. In [62], the authors introduced a circularly polarized antenna in which a circular patch with two peripheral cuts and four right-angle slits is embedded in the antenna. The peripheral cuts are used along the diameter 45° rotated around the centre to excite the CP orthogonal fields. The slits can extend the effective current lengths of the harmonic frequencies and shift the high-order harmonics to avoid interaction with the high-order modes that are generated from nonlinear components. The antenna results show a minimum axial ratio (AR) of a 3-dB AR bandwidth of 29 MHz.

Transmit-array circular polarized anteenas have been designed in [63].The designed UC contains patch antennas loaded by a U shape slot at the receiving side, while the re-transmitting side contains a truncated patch loaded by U slot. The designed CPTAA 3 dB measured gain bandwidth is larger than 4.6 GHz and AR bandwidth is 15.9% at 29 GHz and measured gain of 33.8 dBi. In [64] a design of CP UC based on two truncated corners patch antenna at the re-transmitting side whereas an LP rectangular patch is printed on the receiving layer. The receiving and the transmitting patches are connected using a metalized via hole. The designed CPTAA produces RHCP, measured gain of 22.8 dBi, 3-dB bandwidth of 20% and AR bandwidth of 24.4%. Another design UC configuration composed of the three-identical substrate layers separated by the air gap; each layer has a rectangle ring slot. The fabricated achieves 3-dB axial-ratio bandwidths of 16.7%, with a maximum gain of 20.1 dB [65]. A CPTAA design done by Yuan and others The circular polarization wave generation uses a pair of patches with U slot on receiving and transmitting layers connected by a via-hole. The CP wave is achieved by rotating the transmitting patch. The designed TAA achieved a maximum gain of 24.5 dBi and maximum fractional bandwidth of 7.5% [66]. The UC based on receiving and transmitting stacked patches connected by two microstrip delay lines; the design profile is 0.11 λ_o .The CPTAA measured peak gain is greater than 22 dBi, and bandwidth is wider than 12% [67].

2.9 Circular Polarizer

Mm-wave signals are sensitive to rain, atmospheric absorption, and interference. Circularly polarized waves could reduce rain echo and suppress interference [68], and CP waves overcome misalignment problems between transmitting and receiving antennas that cause polarization mismatching errors. Circularly polarized signals can be obtained by generating CP waves or picking out the CP components from LP waves using a circular polarization converter. Figure2.6 represents the CP converter configuration.

The circular polarizer is the surface used to convert linear polarized signals to circularly polarized ones. Either one layer or multiple layers polarizer produces CP wave, but the single-layer AR bandwidth is narrower than the multilayer. The required layer spacing of the multilayer polarizer is approximately 1/4 of the wavelength to realize the Fabry–Perot interferometer [69–71]. The polarizer could be built using a self-complementary composed of zigzag-shaped metal strips or meander lines printed on a dielectric substrate. The linear circular polarizer converter (LCPC) offers a low profile, a wide frequency band, and easy fabrication. The CP converters are helpful devices because they can be placed in front of any LP antenna to create CP waves with no negative impact on the designed antenna. The main drawback that limits the use of LCPC is the thickness of the structure compared to the wavelength. The LCPC has another limitation in that it operates at a narrow frequency band because it is frequency-dependent. In other words, the polarization purity depends on the 90° phase shift between the two orthogonal fields; this critical condition cannot be satisfied for a wide frequency range.

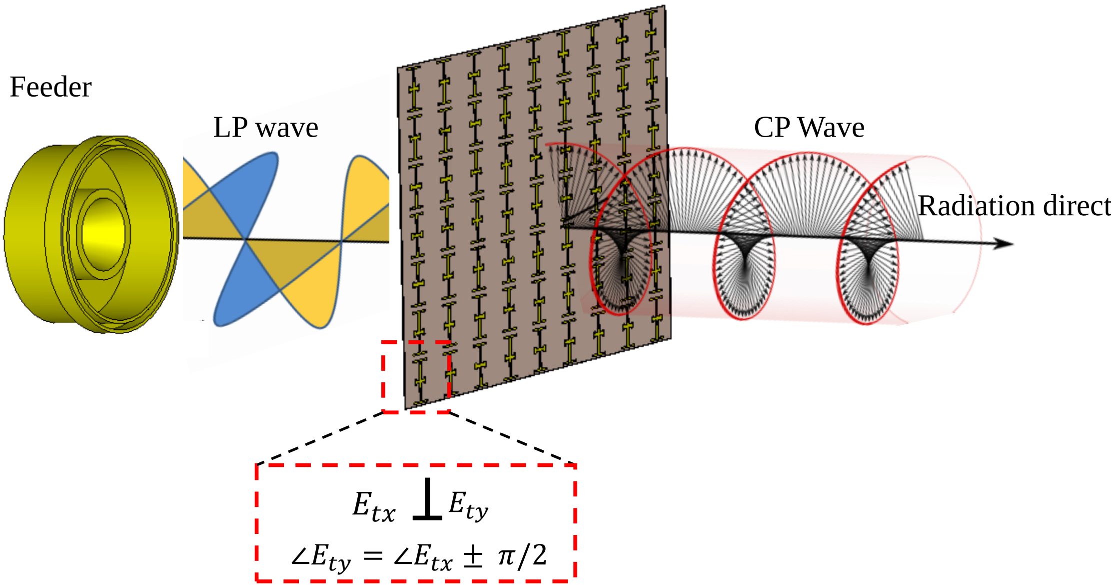

Figure 2.6: Linear to circular polarization converter.

2.9.1 Circular Polarizer Operating Mechanism

As we discussed in the literature review, a perfect CP wave can be generated by an antenna that simultaneously excites two orthogonal vectors of equal amplitude and in-phase quadrature. Figure2.6 describes the operating principle of the polarization converter. Generally, the horn antenna illuminates the 2D surface (CP converter) using LP waves; the CP converter transforms the LP waves into CP waves. The approach that considers an incident LP wave travels along the z-direction, with the electric field vector and the polarizer orientated at 45° relative to an incident signal. The converter acts on the incident LP wave to resolve the incidence signal components into two equal orthogonal components. The orthogonal E fields pass through the converter to introduce a relative phase shift of 90° between the two transmitted field components and a unitary module for the incident field. [72] clearfied the converter mathematics process, which expressed as follows:

$$|E_i|^2 = |E_{ix}|^2 + |E_{iy}|^2 \tag{2.9}$$

$$|E_{ix}| = |E_{iy}| \tag{2.10}$$

$$\overrightarrow{E} = \frac{1}{\sqrt{2}} |E_i| \, (\hat{a}_x + \hat{a}_y) e^{-jkz} \tag{2.11}$$

Where $(\hat{a}_x)$and $(\hat{a}_y)$ are the unit vectors in x- and y- directions respectively.

The mutual coupling between the electric field orthogonal components is neglected, so the transmission coefficient of the converter in x- and y- direction can be expressed as follows:

$$T_{xx} = |T_{xx}| \, e^{j\phi_{xx}} \tag{2.12}$$

$$T_{yy} = |T_{yy}| \, e^{j\phi_{yy}} \tag{2.13}$$

The magnitudes and phases of the transmission coefficients should satisfy the conditions as follows:

$$|T_{xx}| = |T_{yy}| \tag{2.14}$$

$$\phi_{yy} - \phi_{xx} = 90^\circ \tag{2.15}$$

In result, the orthogonal components are transmitted and form a CP polarization wave. The out-going E-fields at the output of the polarizer can be expressed as

$$\overrightarrow{E_o} = E_{ox}\hat{a}_x + E_{oy}\hat{a}_y \tag{2.16}$$

In result the orthogonal components are transmitted while they are within the operating bandwidth. The out-going E fields at the output of the polarizer can be expressed as follows:

$$E_{ox} = |E_{ix}|\,|T_{xx}|\,e^{j\phi_{xx}} \tag{2.17}$$

$$E_{oy} = |E_{iy}|\,|T_{yy}|\,e^{j\phi_{yy}} \tag{2.18}$$

The antenna axial ratio can be calculated as follows:

$$AR(dB) = 20log\frac{majoraxis(E_{max})}{minoraxis(E_{min})} \tag{2.19}$$

$$AR = \frac{|T_{xx}|^2 + |T_{yy}|^2 + \sqrt{a}}{|T_{xx}|^2 + |T_{yy}|^2 - \sqrt{a}} \tag{2.20}$$

$$a = |T_{xx}|^4 + |T_{yy}|^4 + 2|T_{xx}|^2|T_{yy}|^2\cos\left(2(\angle T_{xx} - \angle T_{yy})\right) \tag{2.21}$$

2.9.2 Circular Polarizer Review

Antenna designers and researchers aim to increase their knowledge about the desired topic by studying previous work, so this section aims to conclude some of the published work. In a published work in [73], a CP polarizer with a thickness of 0.18 times the wavelength was designed. The transmission coefficient phase, an equal magnitude between the two orthogonal components, was turned away from the required values; as a result, the bandwidth is just 40%.

In work done by [74], two FSS polarization converters have been designed based on single-layer two orthogonal cross slot and multilayer split slot ring geometry. The measured AR bandwidth of the cross slot is 17.3% and 3.38 dB insertion loss. The 3-dB AR bandwidth of the single-layer split slot ring is 20.4%, and 3.15 dB insertion loss. However, multilayer has decreased the insertion loss to 1.1 dB and negatively impacts AR bandwidth to be 12.2%. In another work by M. Euler, the transmission surface is used to retransmit the incident LP signal in the form of CP waves. The surface is one layer in which two concentric split ring slots are used to enforce the retransmitted horizontal and vertical components to be equal in magnitude and 90° phase difference. This structure achieves 11.75% measured 3-dB AR bandwidth with 3.38 dB insertion loss [75]. However, the designs [74,75] are metallized, making them hard to integrate with PCB applications.

In [76], a simple technique was proposed to design a multilayer circular polarizer based on a meander line. The two designed meander line spacing is $\lambda \setminus 4$ and $\lambda \setminus 8$ between layers.

In general, both designs' AR bandwidth is 35%. However, the designs are triple layers, and the total thickness exceeds $\lambda \setminus 4$ and to support the converter substrate, a foam layer has been added to increase the insertion losses. A single-layer LCPC is presented in [77]. It consists of two interlaced periodic meander lines connected at the centre to create a loop. The measured AR bandwidth and insertion losses are 46% and 3 dB, respectively. In [78], a self-complementary meta-surface polariser composed of zigzag-shaped metal strips is studied and fabricated. The meta-surface shows AR bandwidth of 53%. A flexible material LCP polarizer is proposed in [79]. A substrate of felt textile is used to design an LCP converter, in which a square-shaped loop UC is used to form the 2D array. The polarizer performance is 33.57% of 3-dB axial ratio bandwidth. The design of LPCP converter has been presented in [80]. The designed UC is a single-layer based on a circular diagonal split ring surrounded by a square ring. The meta-sheet works in transmission mode, and the AR bandwidth for each band is 21%. In [81] , LPCP TA antenna has been designed, in which the UC consists of three metallic layers. The upper and bottom layers are identical and composed of a patch and a split ring. A circular slot and rectangular patch has been designed as the middle layer. The designed polarizer achieves CP at two bands, where the AR bands are (19.7 – 20.2 and 29.5-30) GHz.

Chapter 3

Transmit-array Feeding Antennas

This chapter presents the design and preliminary results of two TA antenna feeders. The first design is a hybrid antenna, a patch antenna and a horn antenna combination. The performances of low profile broadside patch antenna are enhanced using capacitive coupling and differential feeding techniques. The second feeder antenna is a horn antenna with high radiation pattern characteristics, which improves TA antenna aperture efficiency.

3.1 Hybrid Antenna

The hybrid antenna configuration technique increases horn antenna bandwidth and gains simultaneously. Generally, a hybrid antenna consists of an active element, a parasitic element, and a metallic fence. In this technique, the active and parasitic elements have different resonance frequencies slightly apart, resulting in a broad bandwidth. While the metallic fence (horn antenna) is incorporated to increase the antenna gain [82–85]. This technique has the advantage of having a high gain with low profile antennas compared to conventional horn antennas. In [82], a hybrid dielectric resonator antenna is designed. A circular patch antenna is used to excite a ring dielectric resonator antenna, and a conical cavity is also incorporated to improve the antenna gain. However, the designed work achieved a gain of about 16.5 dBi with a -10 dB matching bandwidth in the frequency band from 57 to 64 GHz. Elboushi and Sebak [83] designed a hybrid antenna using a surface-mounted conical horn with a circular patch antenna to enhance the gain. They achieved a 12 dBi gain and 10% bandwidth around 31 GHz. However, similar to [82, 83], it has a narrow bandwidth of less than 12%. In [84], a Fabry–Perot resonance antenna with two layers of stacked superstrate is used to feed a conical horn antenna operating at a centre frequency of 12 GHz. The design achieved 19.1 dBi peak gain and 26% and 3-dB gain bandwidth. However, the antenna's aperture efficiency is 27%, which is considered low. Another hybrid configuration consists of a cross dielectric resonator antenna excited by a patch antenna and surrounded by a rectangular horn presented by Nasimuddin et al in [85]. However, the designer achieved a 21.3% impedance bandwidth and gained better than 9 dBi at a centre frequency of 6.8 GHz.

The proposed design combines a simple patch antenna and a rectangular horn antenna. A wideband capacitive differential fed patch antenna with high cross-polarization discrimination is designed at the mm-wave range. The capacitive coupling technique is used to increase antenna bandwidth. Also, differential feeding ensures broadside radiation and low cross-polarization. The differential feeding technique depends on equal power division and 180° phase difference. The feeding circuit includes a rat race, and probe stripline transitions are used. Then a gain enhancement has been achieved by adding a horn to the designed antenna with an efficient aperture efficiency.

3.1.1 Design Capacitive Feeding Patch Antenna

Several antenna design techniques have been adopted to serve the mm-wave technology. However, since achieving the goal of optimal antenna structures is still in its beginnings, the research stream opens the range for new and improved design ideas and concepts. This subsection presents the design of a wideband rectangle microstrip patch antenna fed by a capacitive coupling technique.

The single-layer patch antenna is known for its narrow bandwidth, so bandwidth incrimination brings a challenging task to the patch antenna design. Since the patch antenna is considered an *(RLC)* resonance circuit, introducing another resonance frequency enhances antenna bandwidth [54, 86]. Figure 3.1 shows the designed antenna, where the patch antenna can be fed using a gap coupling strip. The coupling strip technique is introduced to excite the patch antenna through the capacitive resonator, in which the coupling strip is connected to the coaxial probe. The probe presents reactance impedance, and the gap between the patch and the strip introduces capacitance; both the capacitance and the reactance parts can produce extra resonance. The coupling gap width is adjusted to make the two resonance frequencies close to each other to have a wide matching bandwidth. As a result, the patch and the coupling gap create dual resonance frequencies. Moreover, coupling techniques allow the patch to be excited only in a single-mode operation, in which both the patch and the resonator are resonating and suppressing other harmonics [54]. The equivalent circuit model of the designed antenna is shown in 3.2.

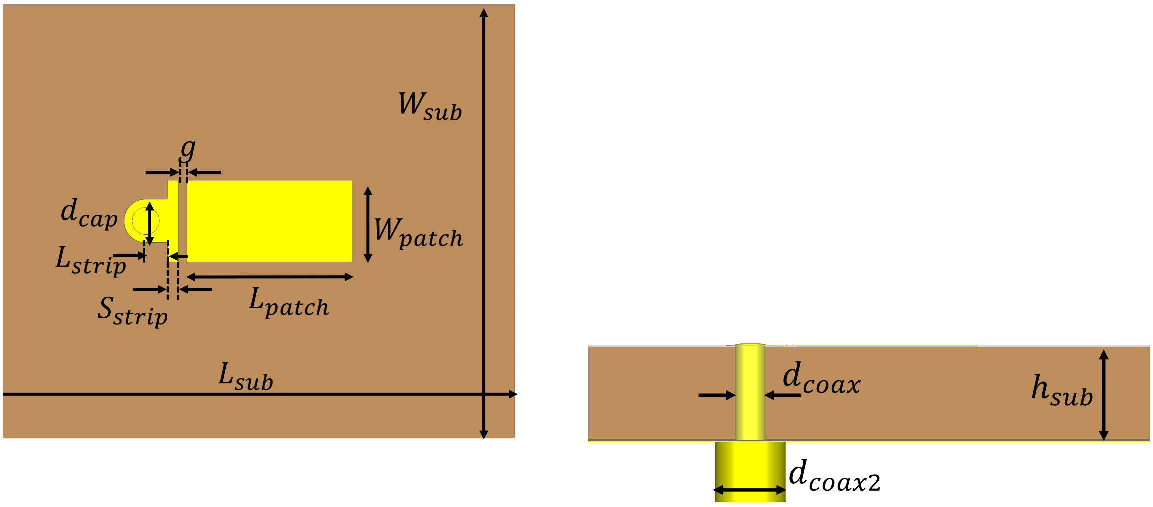

(a)

(b)

Figure 3.1: Configuration of capacitive feeding patch antenna. (a) Top view. (b) Side view

The resonator includes R_p L_p and C_p., representing the patch antenna. Also, C_f, R_f and L_f represent the feeding probe of the patch antenna. The π network C_{g1}, C_{g2} and C_{g3} represent the coupling gap. First, the feeding point, L_f represents the probe inductance, C_f represents the probe cap capacitance, and R_f represents the cap radiation loss. The capacitive coupling second, C_{g1} represents the edge capacitance between the patch and the rectangular strip ends, C_{g2} represents the strip edge capacitance, and C_{g3} represents the patch edge capacitance.

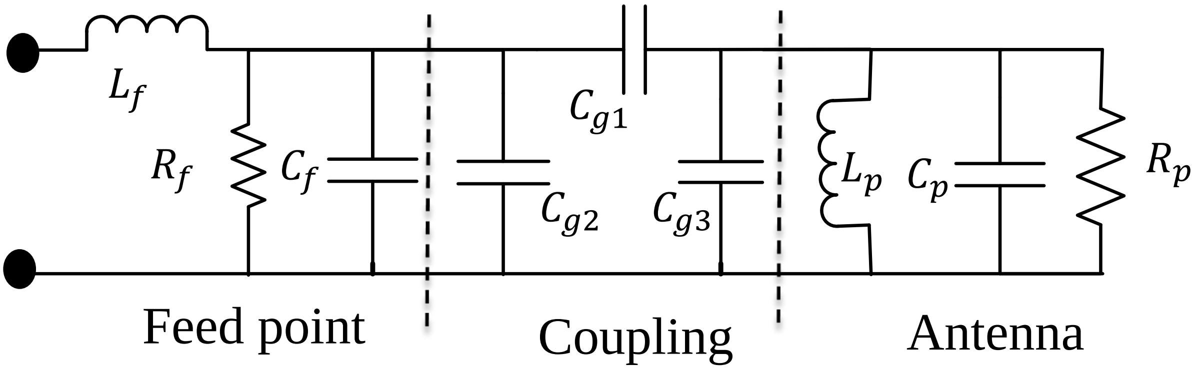

Figure 3.2: Capacitive feeding patch antenna equivalent circuit.

3.1.2 Single Capacitive Feeding Antenna Design

The antenna layout is illustrated in 3.1. The microstrip patch antenna is placed on a dielectric substrate (Rogers Ro 4350B, $\epsilon_r = 3.66$, $\tan\delta = 0.0037$, and thickness = 0.762 mm). Table 3.1 shows the antenna dimensions. A rectangular strip (resonators) is employed to generate another resonance frequency. Patch antenna can be fed using a gap coupling strip to enhance antenna bandwidth. In this technique, the coaxial probe feeds a short strip, which is used to excite the patch. The rectangular strip is placed at a coupling gap distance *(s)* from one patch's radiating edges and is connected directly to the probe.

The probe introduces an inductance, the gap between the patch and the strip introduces a capacitance, and the strip introduces radiation resistance. The three elements produce an extra new resonance circuit. The coupling gap is optimized to create another resonance frequency slightly close to the antenna resonance frequency. As a result, the patch and the coupling gap circuit create dual resonance frequencies. Moreover, coupling techniques allow the patch to be excited only in a single-mode operation, in which the patch and the resonator are resonating and suppressing other harmonics [87]. The computer simulation technology *(CST)* software package simulates the proposed antenna. It is first introduced to show the drawbacks of using a single feeding antenna. Figure 3.3 shows the designed antenna reflection coefficient and the gain. The simulated matched bandwidth is 56.8% at 30 GHz, wider than a regular patch antenna. In general low gain is

Table 3.1: Capacitive feeding patch antenna geometrical parameters

Parameter	W_{patch}	L_{patch}	W_{sub}	L_{sub}	S_{strip}
Value (mm)	1.5	6.1	10	8	0.15
Parameter	L_{strip}	g	h_{sub}	d_{coax}	d_{coax2}
Value (mm)	0.5	0.15	1.575	0.5	1.15

one of the patch antenna's drawbacks; the simulated realized gain is 6.5 dBi at the centre frequency. Figure 3.4 shows the antenna's *(3D)* radiation pattern at 28 GHz, clarifying the tiled beam.

The typical goal of a parametric study is to show the effect of specific parameters of the designed antenna on the gain and the impedance matching bandwidth ($S_{11} < 10$ dB). The selected parameters related to the capacitive feeding part are L_{strip}, S_{strip}, g, and L_{patch}. The L_{strip} effects are shown in figure 3.6, where the gain and the matching are improved at high frequencies as the value of L_{strip} decreases. Figure 3.5 shows the effect of S_{strip}, where there is a minimal effect on the antenna gain. However, the bandwidth is inverse proportion to the S_{strip} length. Figure 3.6 shows the effect of L_{strip}. The effect of S_{strip} and L_{strip} referring to when S_{strip} or L_{strip} increases so does the capacitance and hence shift in the resonance frequency of the feeding part toward the patch resonance which causes a decrease in the overall bandwidth. Figure 3.7 shows the effect of the coupling gap. The gap coupling does not affect the antenna gain in a low-frequency band. However, decreasing the gap space causes a slight shift in the resonance frequency of the patch toward the lower frequency band. The antenna gain and bandwidth increase when the gap coupling space decreases at high frequencies. Figure.3.8 shows the effect of changing the patch length (L_{patch}) where the gain increases at high frequencies by decreasing the patch length. Moreover, the first resonance in the reflection coefficient (near 22 GHz) shifts to higher frequencies as the patch length decreases.

Figure 3.9. shows the co-polar and the cross-polar radiation patterns at 45° for four different frequencies using Ludwig III definition. The 45° cuts have been chosen because it shows all the radiation patterns information and according to the Body of Revolution

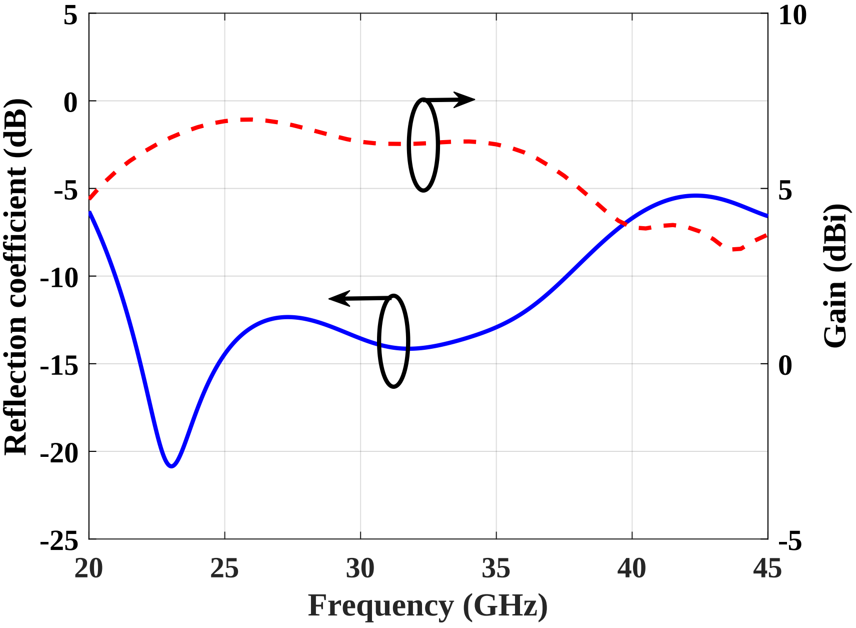

Figure 3.3: Patch antenna reflection coefficient and gain.

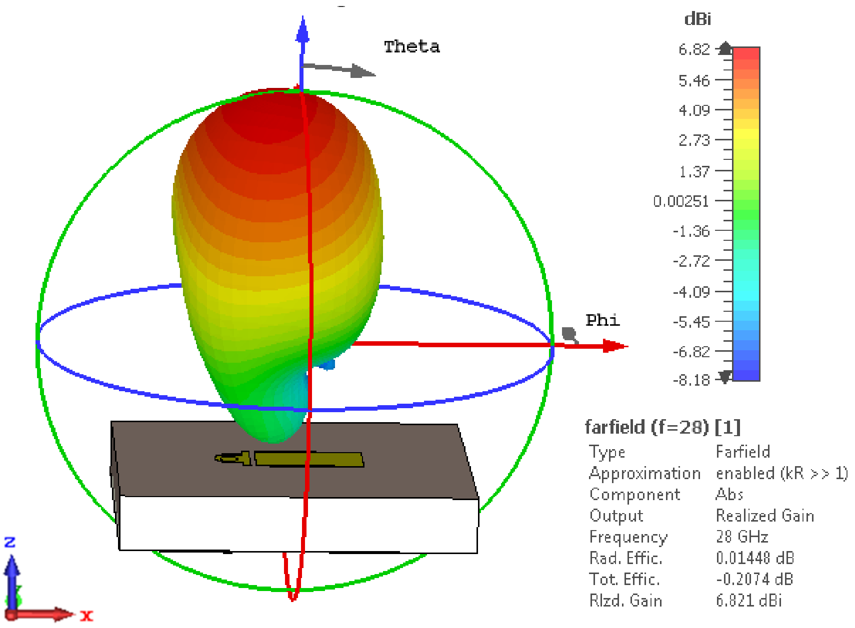

farfield (f=28) [1]
Type Farfield
Approximation enabled (kR >> 1)
Component Abs
Output Realized Gain
Frequency 28 GHz
Rad. Effic. 0.01448 dB
Tot. Effic. -0.2074 dB
Rlzd. Gain 6.821 dBi

Figure 3.4: Single feeding patch antenna radiation pattern.

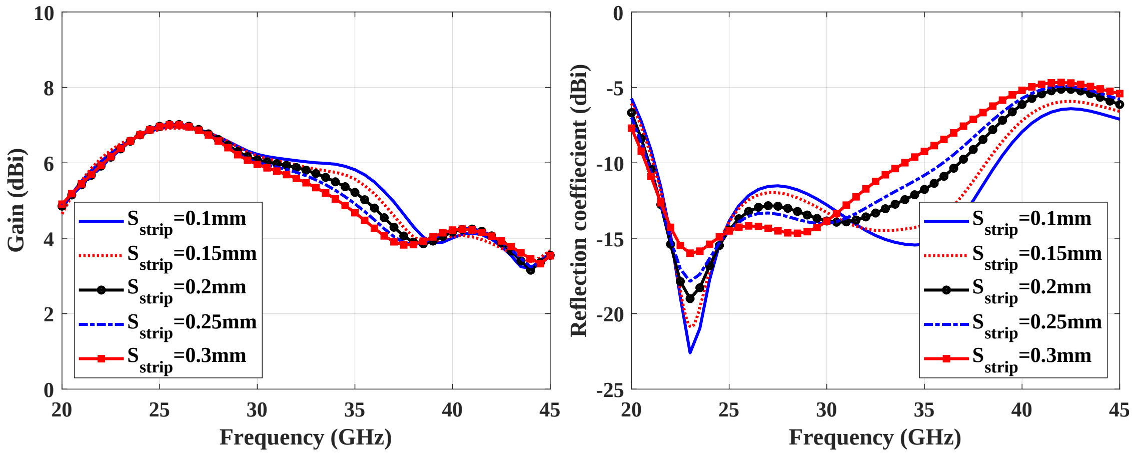

(a) (b)

Figure 3.5: Parameter study of the effect of S_{strip} on (a) antenna gain (b) antenna matching bandwidth.

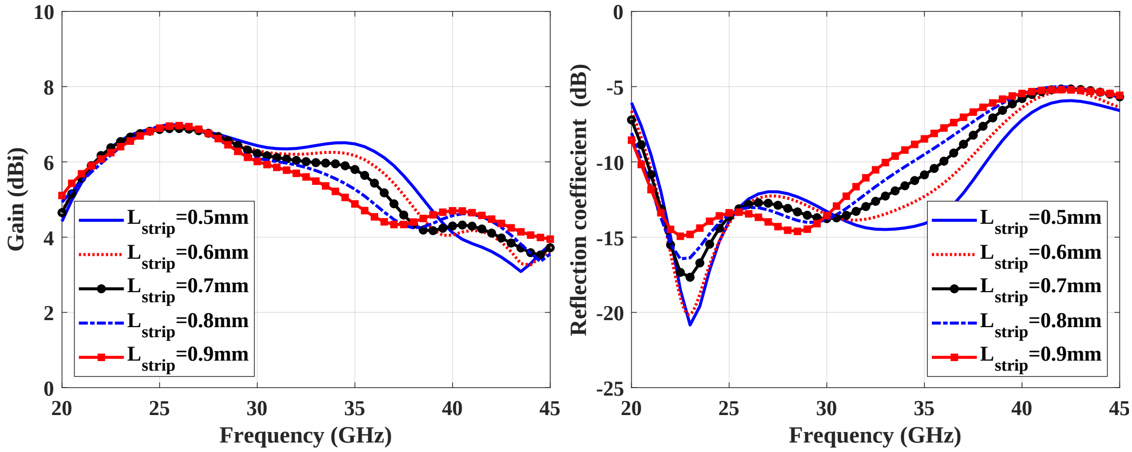

(a) (b)

Figure 3.6: Parameter study of the effect of L_{strip} on (a) antenna gain (b) antenna matching bandwidth.

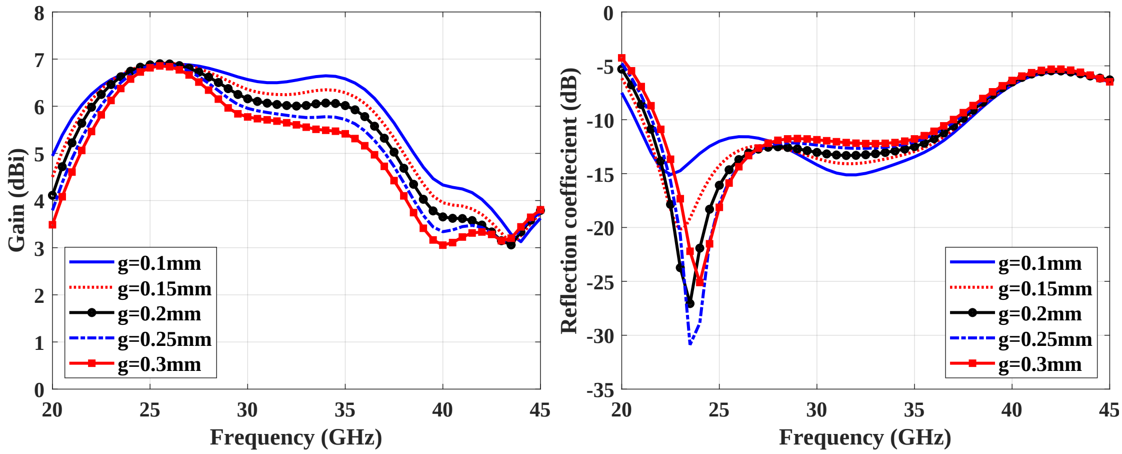

(a) (b)

Figure 3.7: Parameter study of the effect of g_{strip} on (a) antenna gain (b) antenna matching bandwidth.

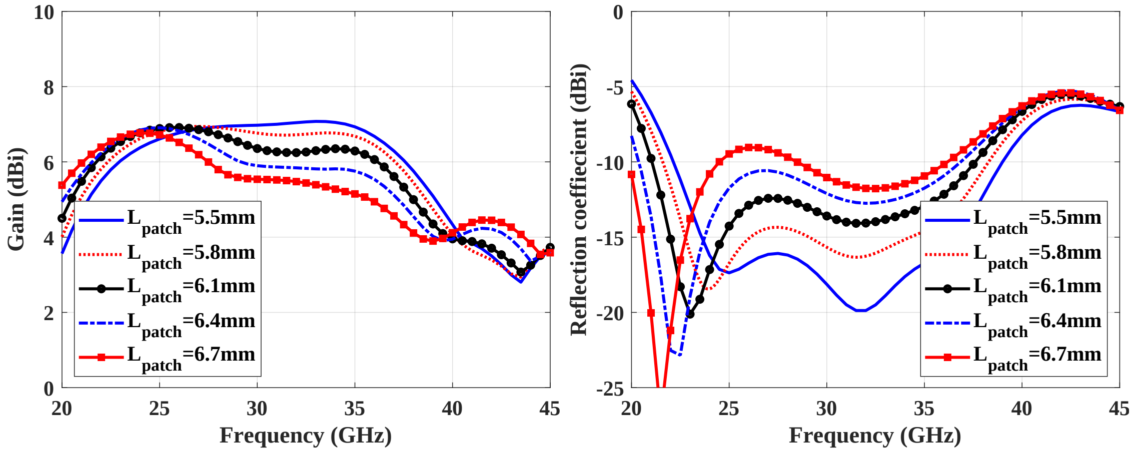

(a) (b)

Figure 3.8: Parameter study of the effect of L_{patch} on (a) antenna gain (b) antenna matching bandwidth.

(BOR) theory, the peak level of cross-polarization is at 45° [88]. Moreover, we can construct the radiation pattern of the desired antenna from 45° cuts in E and H planes. The figure shows that a minimum cross-polarization of about -8 dB is obtained. Moreover, the antenna's radiation pattern is asymmetrical in the E-plane due to the drawback of the single feeding. The antenna's main lobe is tilted with frequency ($-5°$ +7°); this tilt should be considered when designing an array antenna.

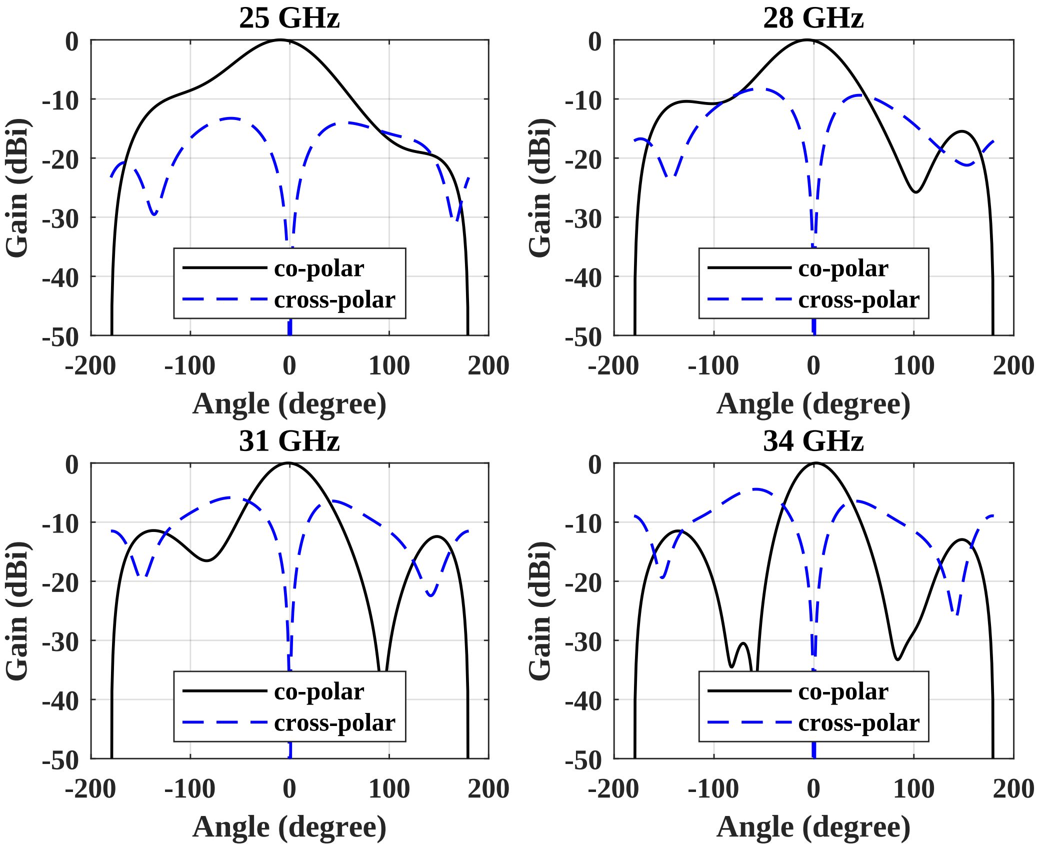

Figure 3.9: Single feeding patch antenna radiation pattern.

The antenna working principle can be explained by the electric field distribution shown in Figure 3.10. The solid arrows show that the synthetic electric vector on the coupling edge is along the x-direction and, hence, x-polarization is introduced. As a result, the capacitive feeding antenna electric field density is concentrated more at the feeding edge than at the far end, which causes beam tilting and high cross-polarization. Figure 3.4 and Figure 3.10 represent one-end patch antenna disadvantages such as radiation pattern tilting and asymmetry electric field density distribution. To overcome these drawbacks understanding the antenna field distribution are essential. The patch antenna's E-field lines distribution can be expressed using the cavity model (TM_{100} mode) with a perfect magnetic conductor (PMC) walls surrounding the antenna, while the fringing fields' effect is excluded [35]. The antenna radiation pattern can be expressed by two radiating slots separated by a distance equal to patch length *(L)*. Each slot radiates a field like a magnetic dipole [51]. Accordingly, the patch field distribution has a cosine shape and uniform shape along the antenna length and width, respectively, as shown in Figure 3.11.

The desired field vector component is a co-polarized field, and the field vector perpendicular to it is a cross-polarized field. The cross-polarization is associated with the fields on the non-radiating edges of the patch. Figure 3.11 shows that the E-field amplitude is not symmetric along the antenna length, and hence the cross-polarization field's intensity becomes weak when it moves away from the feeding point, resulting in the non-zero cross-polarization field in the broadside direction. Accordingly, the cancellation of this asymmetry is the crucial factor for cross-polarization suppression. One known way to cancel this difference is to feed the antenna at the two ends with the same signal with a 180° phase shift. Due to the equalization of vector field intensity at both ends of the patch antenna, a symmetric radiation pattern is generated, and the cross-polarization level is suppressed.

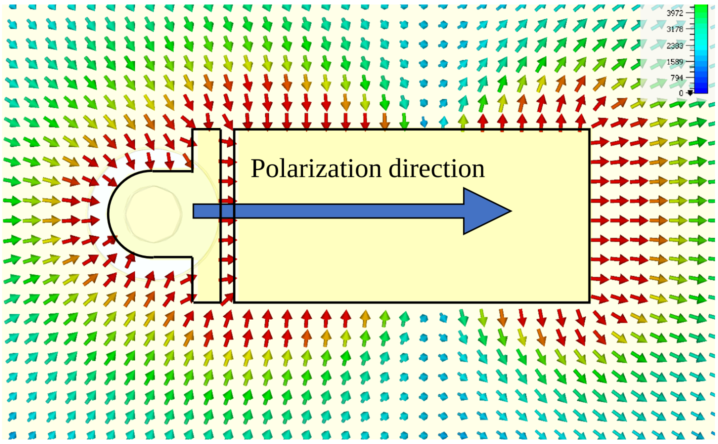

Figure 3.10: Electric field distribution of single feed patch antenna.

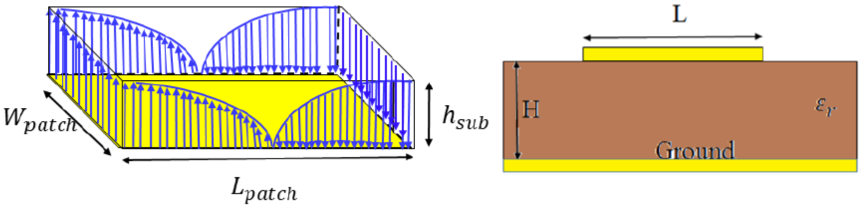

Figure 3.11: Patch antenna cavity model E-field distribution.

3.1.3 Differential Feeding Antenna Design

The patch antenna is excited deferentially at both radiating ends in this section. This technique, presented in the previous section, can overcome the tilting in the radiation pattern and the high cross-polarization level. Although the differential feeding is achieved by adding another capacitive feeding strip at the other end of the patch antenna, the physical symmetry of the feeding points' location should be seriously considered. The antenna is designed with the same substrate, Figure 3.12 shows the antenna layout, and its dimensions are presented in Table 3.2. Figure 3.13 shows the antenna simulated reflection coefficient and gain, achieving a wide bandwidth (more than 55% at 30 GHz). Moreover, the antenna gain is increased to 8 dBi instead of 6.5 dBi for the single feeding antenna. The antenna's radiation pattern becomes symmetrical and extreme broadside direction, as shown in Figure 3.14.

The antenna E-field distribution is presented in Figure 3.15. The solid arrows show

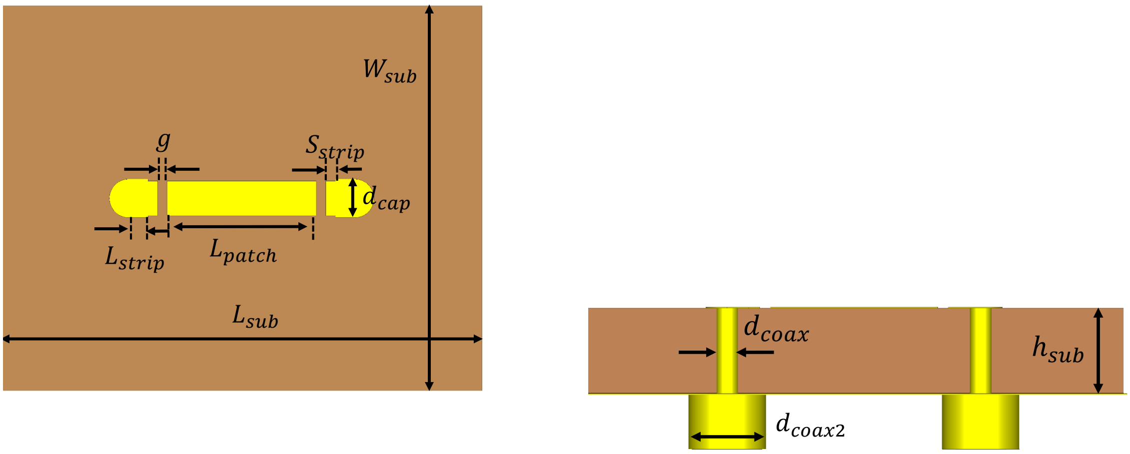

(a) (b)

Figure 3.12: Differential feeding antenna. (a) Top view (b) Side view.

Table 3.2: Optimized geometrical parameters for the differential feeding patch antenna

Parameter	W_{patch}	L_{patch}	W_{sub}	L_{sub}	S_{strip}
Value (mm)	0.72	3.1	10	8	0.2
Parameter	L_{strip}	g	h_{sub}	d_{coax}	d_{coax2}
Value (mm)	0.2	0.2	1.575	0.4	0.4

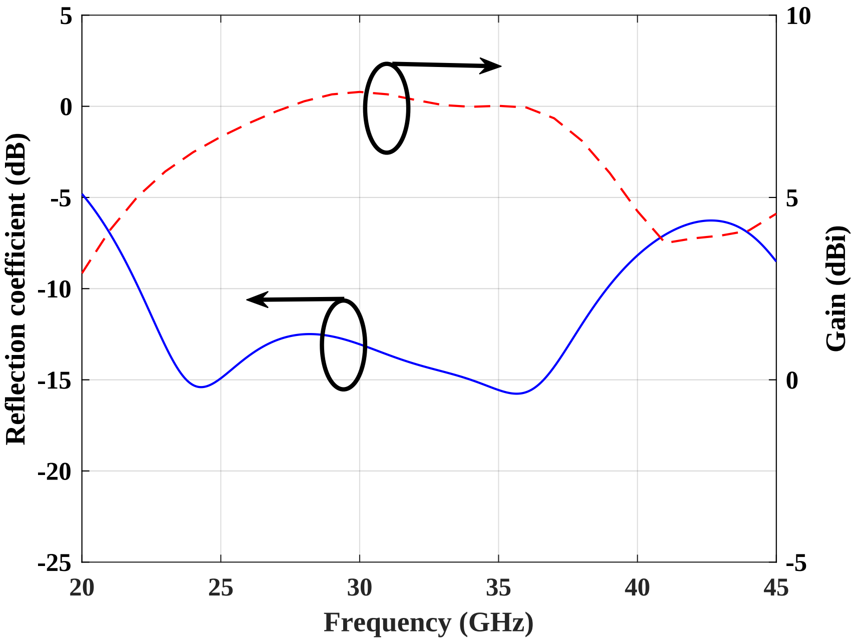

Figure 3.13: Capacitive differential feeding patch antenna reflection coefficient and gain.

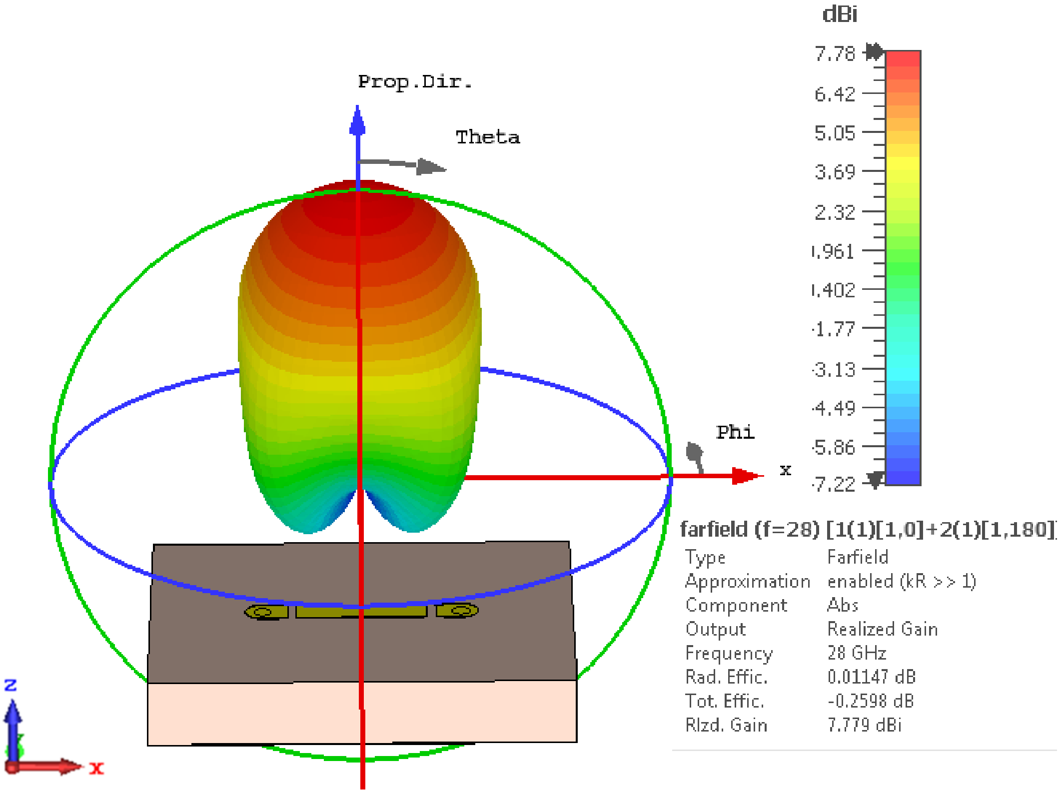

farfield (f=28) [1(1)[1,0]+2(1)[1,180]
Type Farfield
Approximation enabled (kR >> 1)
Component Abs
Output Realized Gain
Frequency 28 GHz
Rad. Effic. 0.01147 dB
Tot. Effic. -0.2598 dB
Rlzd. Gain 7.779 dBi

Figure 3.14: Differential feeding patch antenna radiation pattern.

that the synthetic electric field vector on the coupling edges is along the x-direction, and co-polarization is introduced. The electric field's distribution density is equal in value and symmetrical with respect to the xz- and yz-planes. The excitation through both ends of the patch antenna deferentially generates two different voltage pols *(+v and –v)*.

The pols at the coupling gaps generate symmetrical E-fields in the same direction; moreover the E-field's distribution along the x-axis is uniform. The E-field's orthogonal to the YZ-plane constructs the co-polar radiation pattern, whereas the fields orthogonal to XZ-plane produces the cross-polar radiation pattern. The cross-polar E-fields are opposite each other in direction, so the resulting cross-polar in the far-field region is zero along YZ-plane. Figure 3.16 shows Ludwig III co and cross-polar radiation patterns of the differential feeding antenna at four different frequencies, covering the whole operating band. The differential feeding technique positively impacts the radiation pattern compared to the single-feeding antenna. The figure indicates a high level of symmetrical radiation pattern and a lower cross-polarization level. Moreover, the radiation pattern is broadsided with no tilting angle; for reference, the single-feeding antenna radiation pattern has about 14° tiltings. As a result, the differential feeding antennas have a bit higher gain.

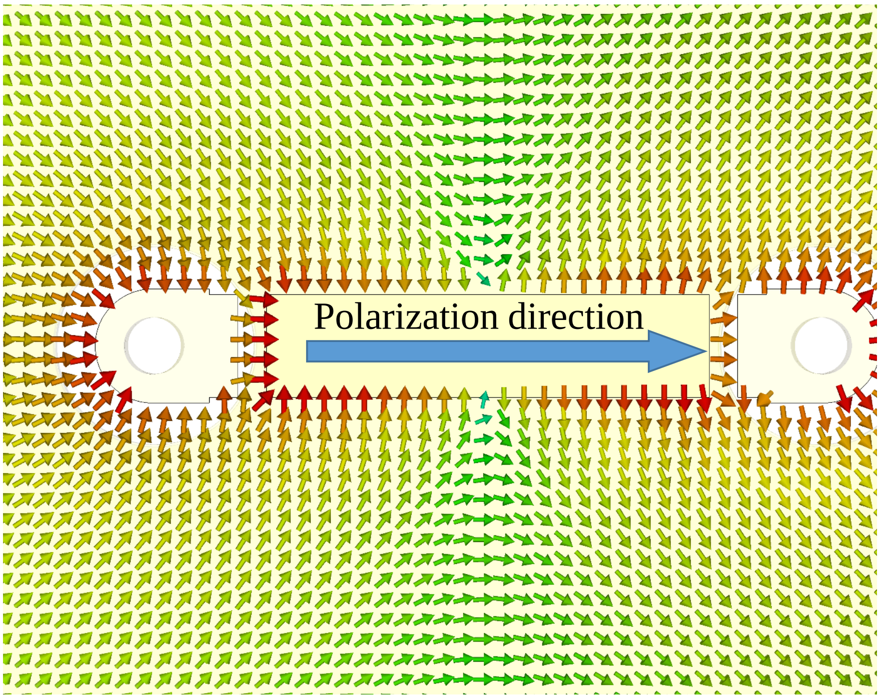

Figure 3.15: Electric field distribution of differential feeding antenna.

3.1.4 Differential Feeding Circuit Design

The feeding circuit is implemented by employing a strip rat-race coupler, which is used to feed two probes (+v and-v) by equal amplitude and out-of-phase signals. The transition from the stripline to the antenna probe and the stripline rat-race coupler are designed as shown in Figure 3.16. This feeding circuit is considered the candidate choice because it is easily fabricated, has no radiation loss, and is inexpensive compared with the conventional waveguide. The transition circuit is shielded using vias around the probe and the stripline to prevent leakage. The shielding technique is designed based on two factors, d_{via} and the distance between the two adjacent vias s_{via}, similar to the substrate integrated waveguide technique [89, 90]. The rat-race coupler's isolated port is usually terminated with a matched load.

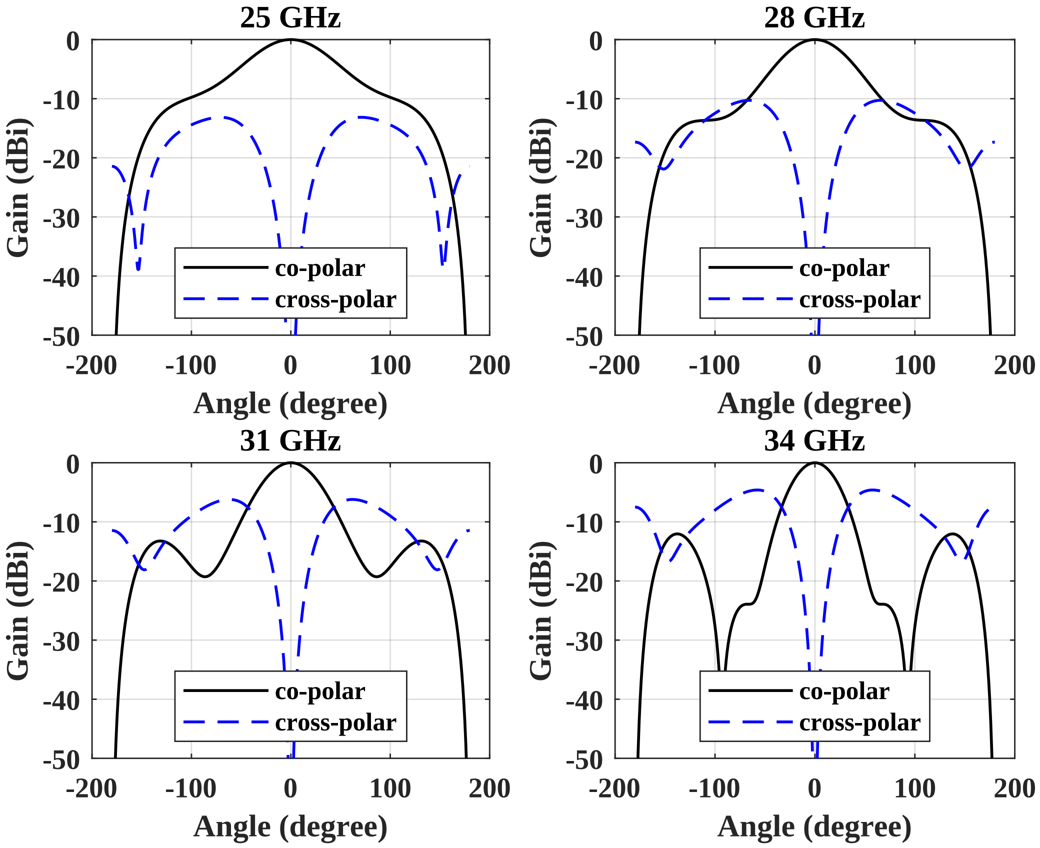

Figure 3.16: Ludwig III Co and cross polar radiation pattern of differential feeding antenna ($\phi = 45°$).

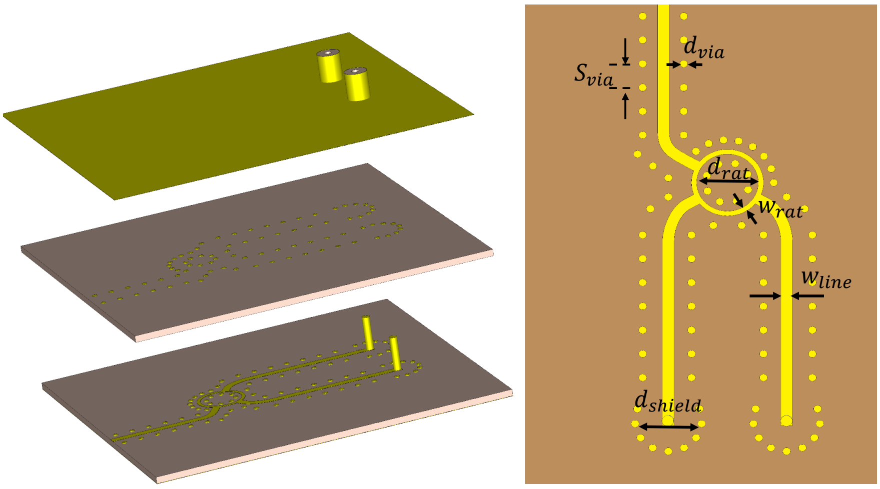

Figure 3.17: Rate race and transition line configuration.

Table 3.3: Optimized geometrical parameters for the rat race and the transition component

Parameter	d_{via}	S_{via}	d_{shield}	d_{rat}	w_{rat}	w_{line}
Value (mm)	0.15	0.3	1.4	2.4	0.2	0.45

$$d_{via} \leq \frac{\lambda_g}{5} \tag{3.1}$$

$$s_{via} \leq 2d_{via} \tag{3.2}$$

The matched load is a 50Ω lumped element that is not easy to fabricate in the mm-wave band. However, the designed coupler's isolation level is better than 15 dB; hence, this port is removed without affecting the rat race behaviour. As a result, the rat race coupler has almost equal power division in the required bandwidth. Dimensions of the rat race and the transition part are presented in Table 3.3. The simulated reflection coefficient amplitude and phase of the feeding circuit, including the rat race and the transition, are shown in Figure 3.18. The figures indicate that $S_{11} \leq -15$ dB for the whole operating band of the antenna and equal power division with 180° phase difference.

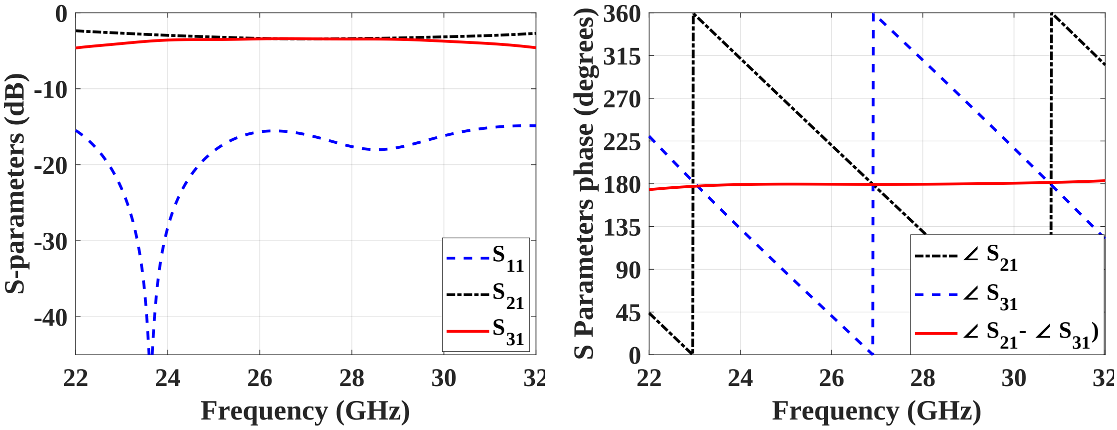

(a)

(b)

Figure 3.18: Rat race and transition circuit (a) S-parameters (b) Phase response.

3.1.5 Hybrid Antenna Design

The proposed wideband patch antenna can be used to achieve a high data rate at the mm-wave band. However, a high gain antenna is also required due to mm-wave characteristics. Antenna gain is by employing a horn antenna on top of the designed patch antenna. The proposed horn antenna is designed based on the equations in [35], where the phase error coefficients: t, and s values are chosen as 0.375 and 0.25, respectively, for the optimum horn design. The following equations show that the t and s are a function of the antenna geometric parameters L_{ap}, w_{ap}, R_1, and R_2.

$$t = \frac{L_{ap}^2}{8\lambda_0 R_1} \qquad s = \frac{w_{ap}^2}{8\lambda_0 R_2} \tag{3.3}$$

where L_{ap} and w_{ap} are the dimensions of the horn antenna aperture and R_1 and R_2 are the dimensions from the horn aperture to the phase center in the E and H-planes. The following equation determines the antenna gain.

$$G = \eta_a \frac{4\pi}{\lambda_0^2} L_{ap} w_{ap} \tag{3.4}$$

Table 3.4: Horn antenna parameters

Parameter	L_{ap}	w_{ap}	h_{horn}	w_{base}	l_{base}
Value (mm) Ant. 1	23.95	23.95	11.37	8	11.3
Value (mm) Ant. 2	23.95	23.95	12	10	7.9

where the aperture efficiency η_a is taken as 51 %. Finally we get the following design equation for and optimum horn antenna.

$$\frac{3}{2}\left(\frac{G\lambda_0^2}{4\pi\eta_a}\right)^2 - \frac{3G\lambda_0^2}{8\pi\eta_a}Ab = L_{ap}^4 - w_{base}w_{ap}^3 \tag{3.5}$$

The horn design parameters are first calculated based on having a gain of 15 dBi at the centre frequency, and the value of the inner feeding aperture is 8 × 8 mm^2 (the patch antenna size). Since the inner feeding aperture controls the designed horn antenna, the antenna parameters have been optimized for good impedance matching and high gain. The resulted hybrid antenna configuration can be seen in Figure 3.19, and it is associated dimensions listed in Table 3.4.

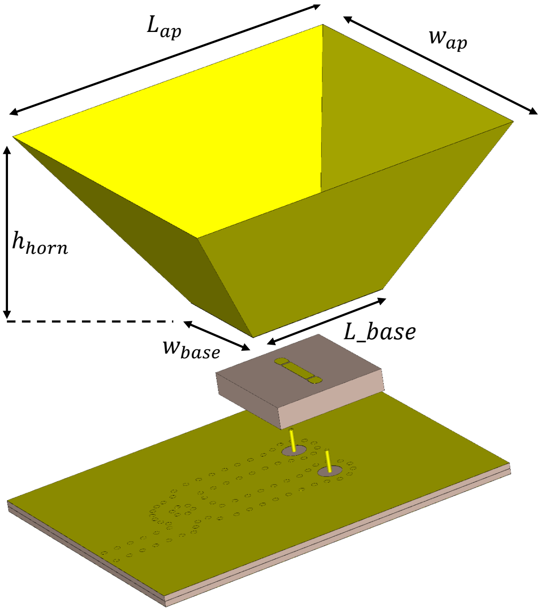

Figure 3.19: Hybrid antenna configuration.

3.1.6 Result and Discussion

Prototypes of the proposed antennas are fabricated using PCB multi-layer technology, while the horn part has been made using four pieces of coppers and assembled by conducting tape, then soldered together. The prototype antenna is shown in Figure 3.20. The programmer network analyzer (PNA N52271A) is used to measure the reflection coefficients, and the Anechoic chamber is used to measure antenna's radiation pattern and gain. Figure 3.21.shows the radiation pattern measurements set up in the chamber. The measured and simulated S_{11} and gain are shown in Figure 3.22. The maximum realized gain of the designed antenna is 14.5 dBi at 30 GHz , and the ($S_{11} \leq -10$ dB) is 34.48%.

The maximum realized gain of the designed antenna is 14.5 dBi at 30 GHz , and the

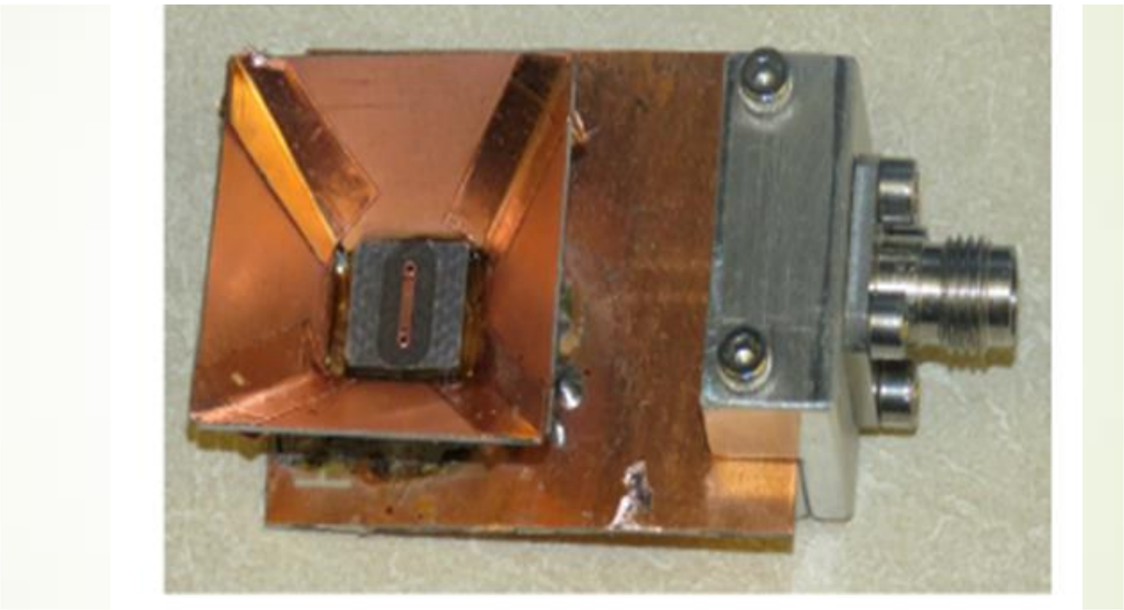

Figure 3.20: Hybrid antenna prototype.

Figure 3.22 shows the horn antenna simulated and measured gain and reflection coefficient results; it provides 14.2 dB gain at 29 GHz and fractional impedance bandwidth of 34.4%. Figures 3.23, and 3.24 show the simulated and the measured E and H-plane patterns of the hybrid antenna at four different frequencies. The E and H-planes are almost identical over the operating frequency range, with a gain of around 14 dB at 26 GHz. Figure 3.25 shows the far-field phase error distribution of the hybrid antenna radiation pattern at 28 GHz. The phase is calculated based on the phase difference between the

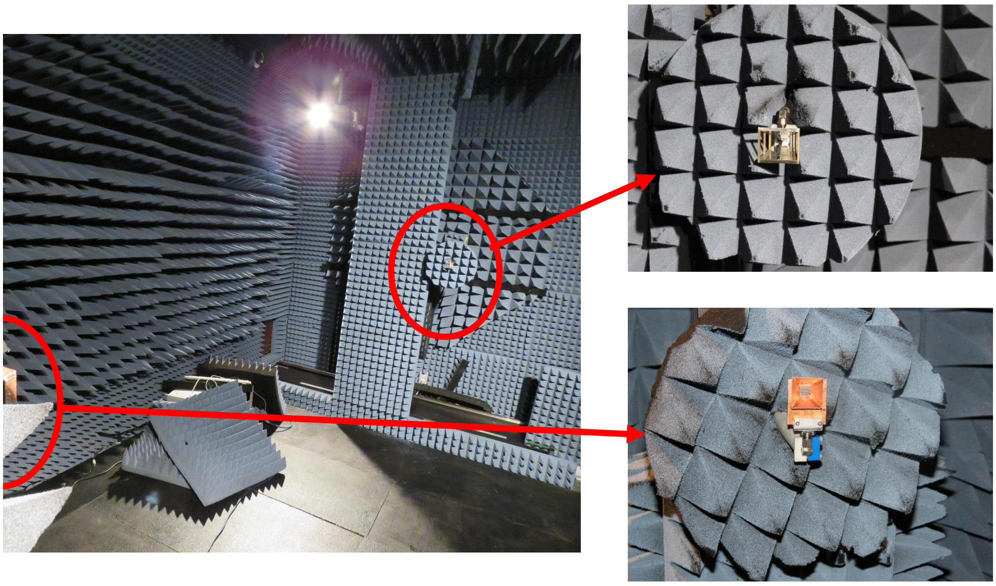

Figure 3.21: Antenna radiation pattren measurements setup.

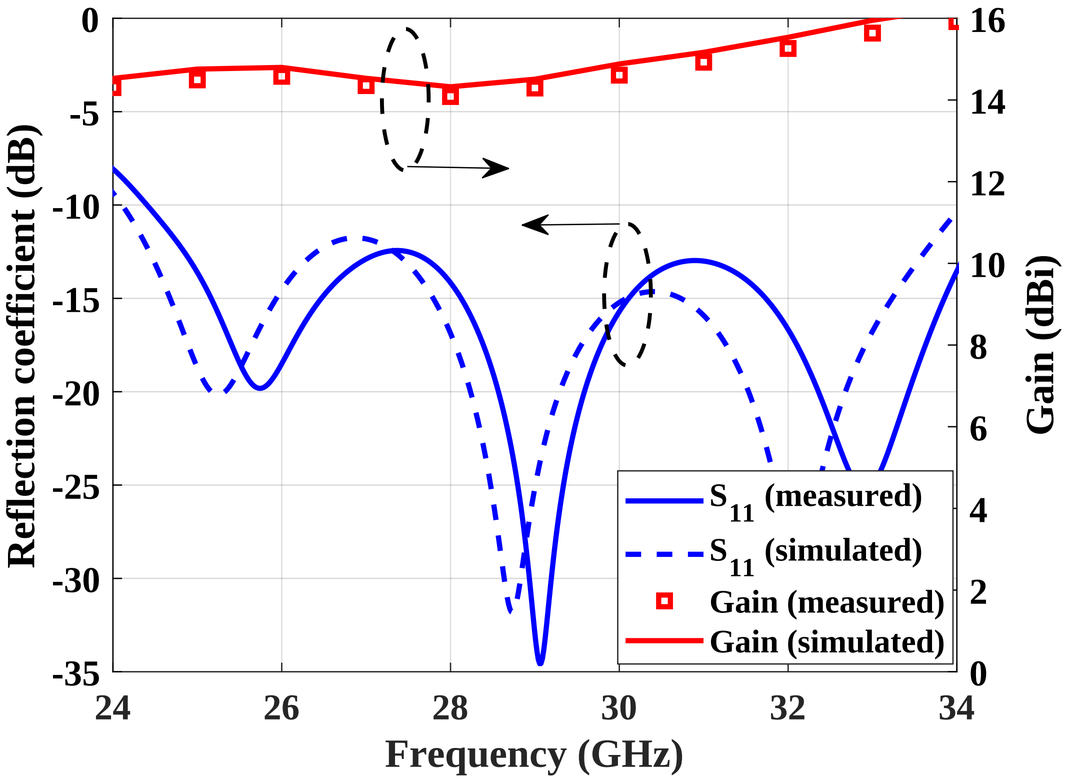

Figure 3.22: Hybrid antenna simulation and measurements reflection coefficient and gain.

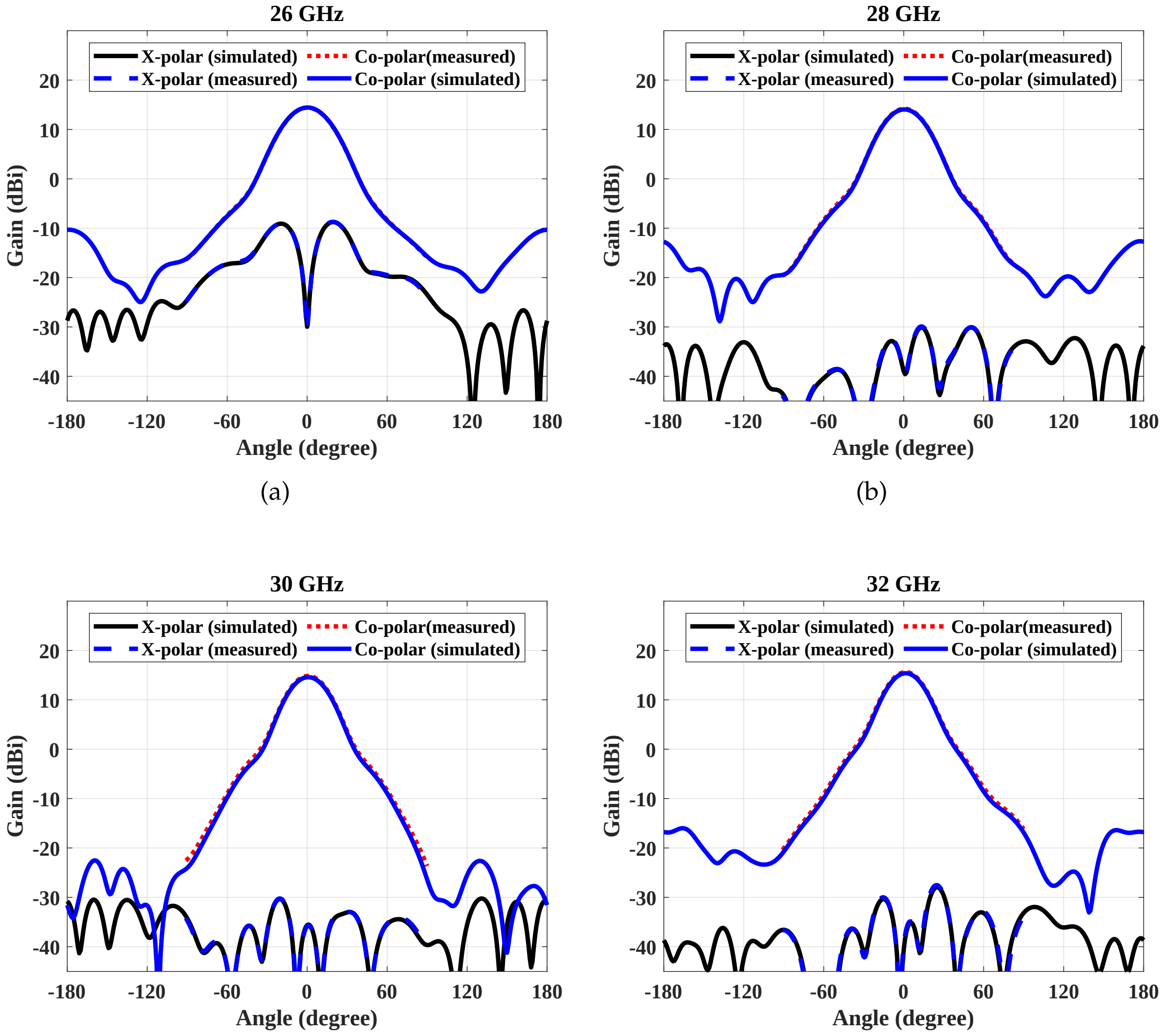

(a)

(b)

(c)

(d)

Figure 3.23: E-plane simulated and measured radiation pattern of the hybrid antenna at different frequencies. (a) 26 GHz (b) 28 Ghz, (c) 30 GHz, (d) 32 GHz

centre and surrounding points. The radiation pattern phase error range is 40°, and the phase error could affect the TA antenna gain.

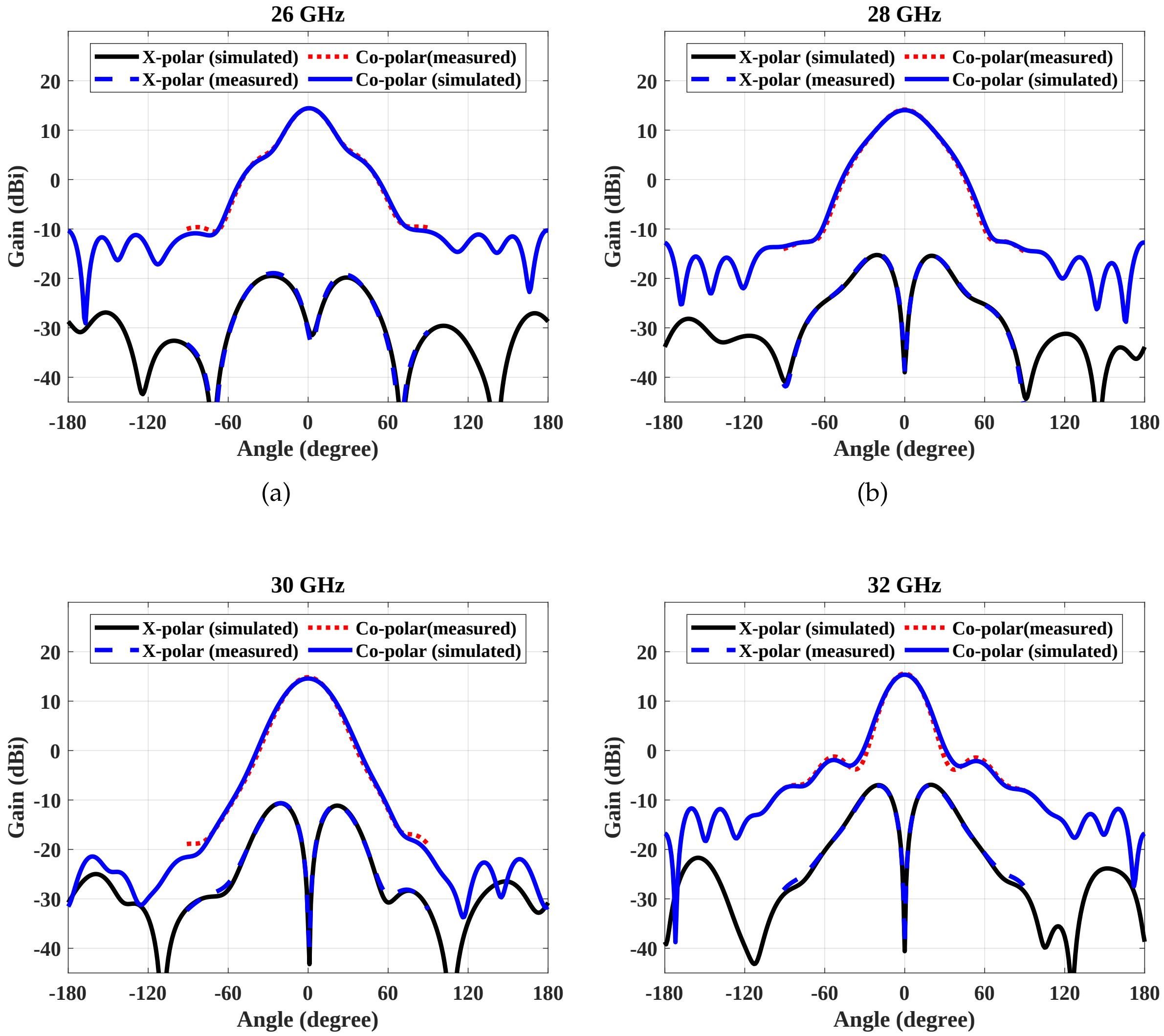

(a) (b) (c) (d)

Figure 3.24: H-plane simulated and measured radiation pattern of the feeder hybrid antenna at different frequencies. (a) 26 GHz (b) 28 Ghz, (c) 30 GHz, (d) 32 GHzr

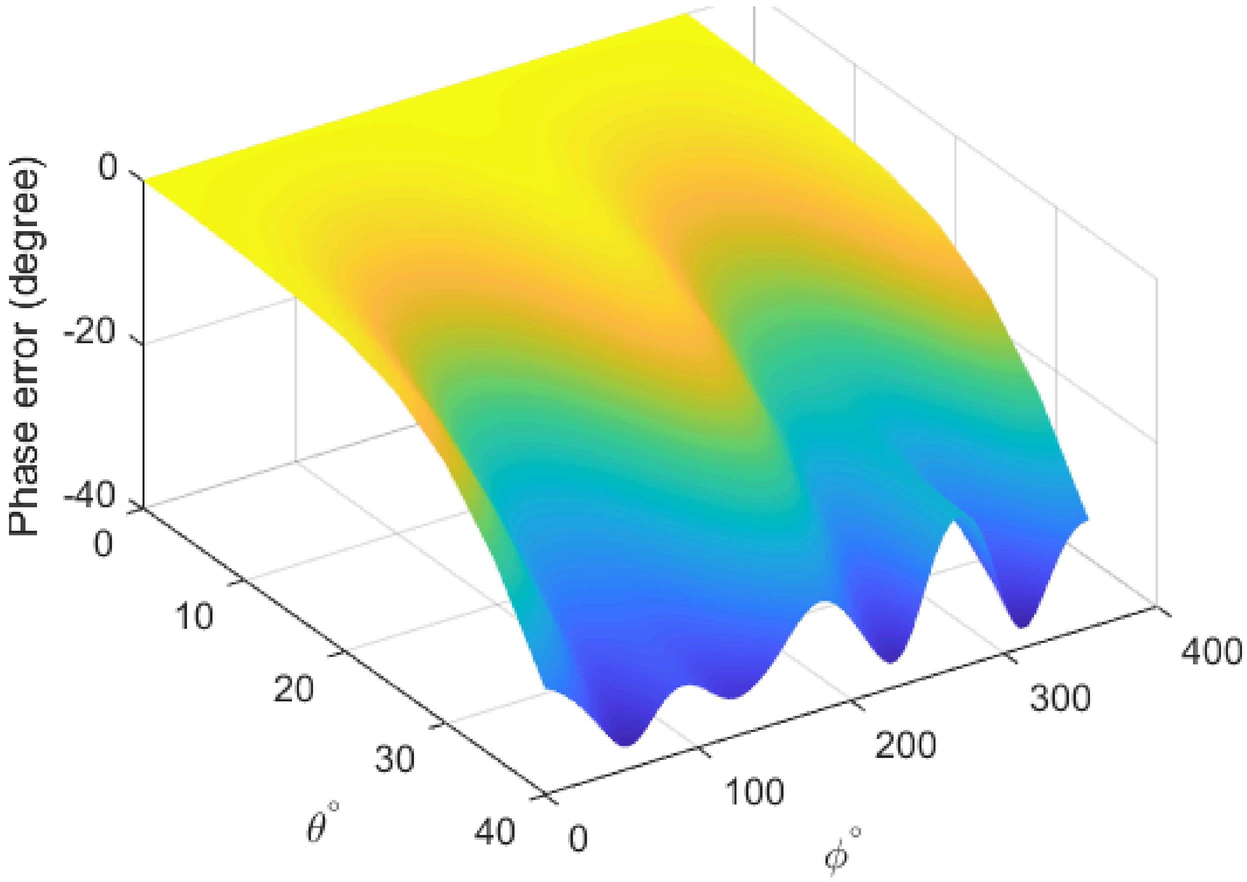

Figure 3.25: Hybrid antenna radiation pattern phase error

3.2 Conical Horn Antenna Design

The illumination of the TA surface depends on an external source. Hence, a wideband horn antenna is required to excite the TA antenna aperture area. Regular horn antennas have reduced the TA aperture efficiency because they can not overcome path loss difference over TA surface. The optimum feeding field amplitude distribution should enhance aperture efficiency. A horn antenna designed in [34] is scaled, fabricated and used as a feeder. The radiation pattern model of the horn antenna was chosen to be $(\sec\theta)$. This source provides radiation patterns with specific characteristics that improve the spillover and tapering efficiencies. The designed horn is better than the conventional conical horn and increases the aperture efficiency by 7% [34]. Figure 3.26 shows the horn antenna geometry.

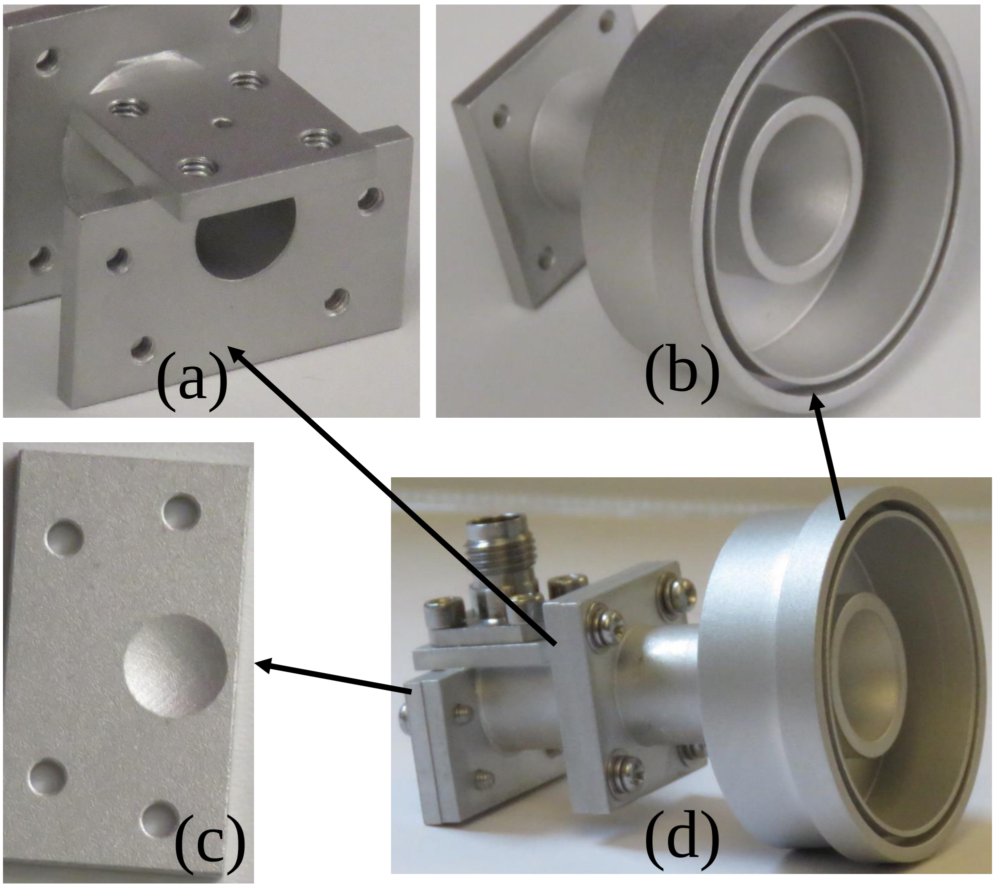

Figure 3.26: Horn antenna structure

Figure 3.27 shows the horn antenna simulated and measured gain and reflection coefficient results, and it provides 10.4 dB gain at 28 GHz and a wideband impedance matching over the frequency range from 25 to 34 GHz. Figure 3.29 shows horn antenna's simulated and the measured E and H-plane patterns at four different frequencies. The E and H-planes are almost identical over the operating frequency range, with a gain of 10 dB at the centre frequency. Figure 3.30 shows the far-field phase distribution of the horn antenna radiation pattern at the centre frequency. The phase error is within the acceptable range in which the maximum value is 12° and less than the quantization step error.

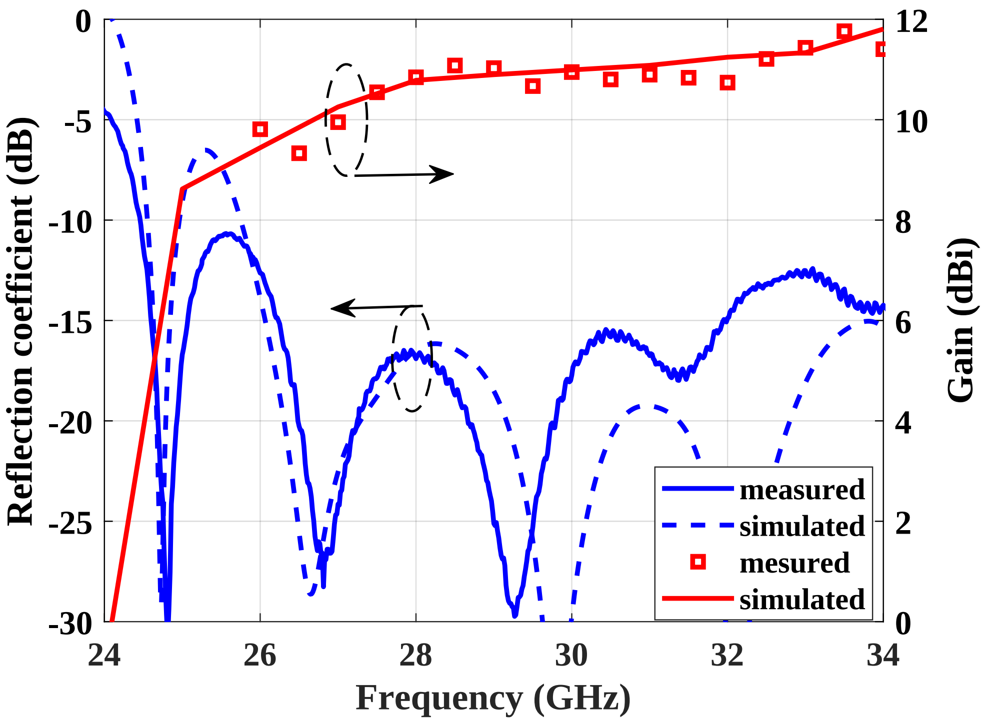

Figure 3.27: Horn antenna simulated and measured gain and return loss

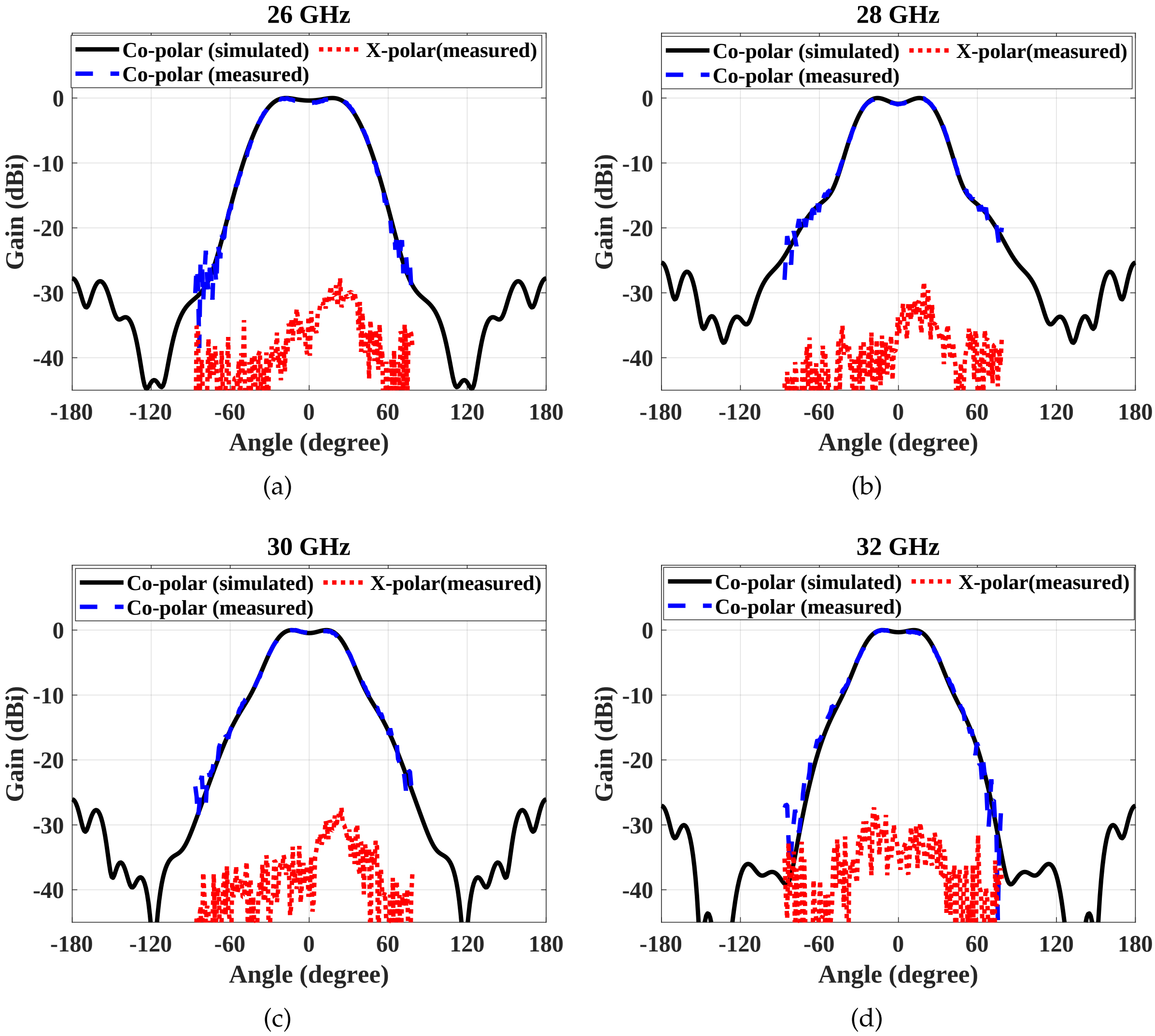

(a) (b) (c) (d)

Figure 3.28: E-plane simulated and measured radiation pattern of the feeder horn antenna at different frequencies. (a) 26 GHz (b) 28 Ghz, (c) 30 GHz, (d) 32 GHz

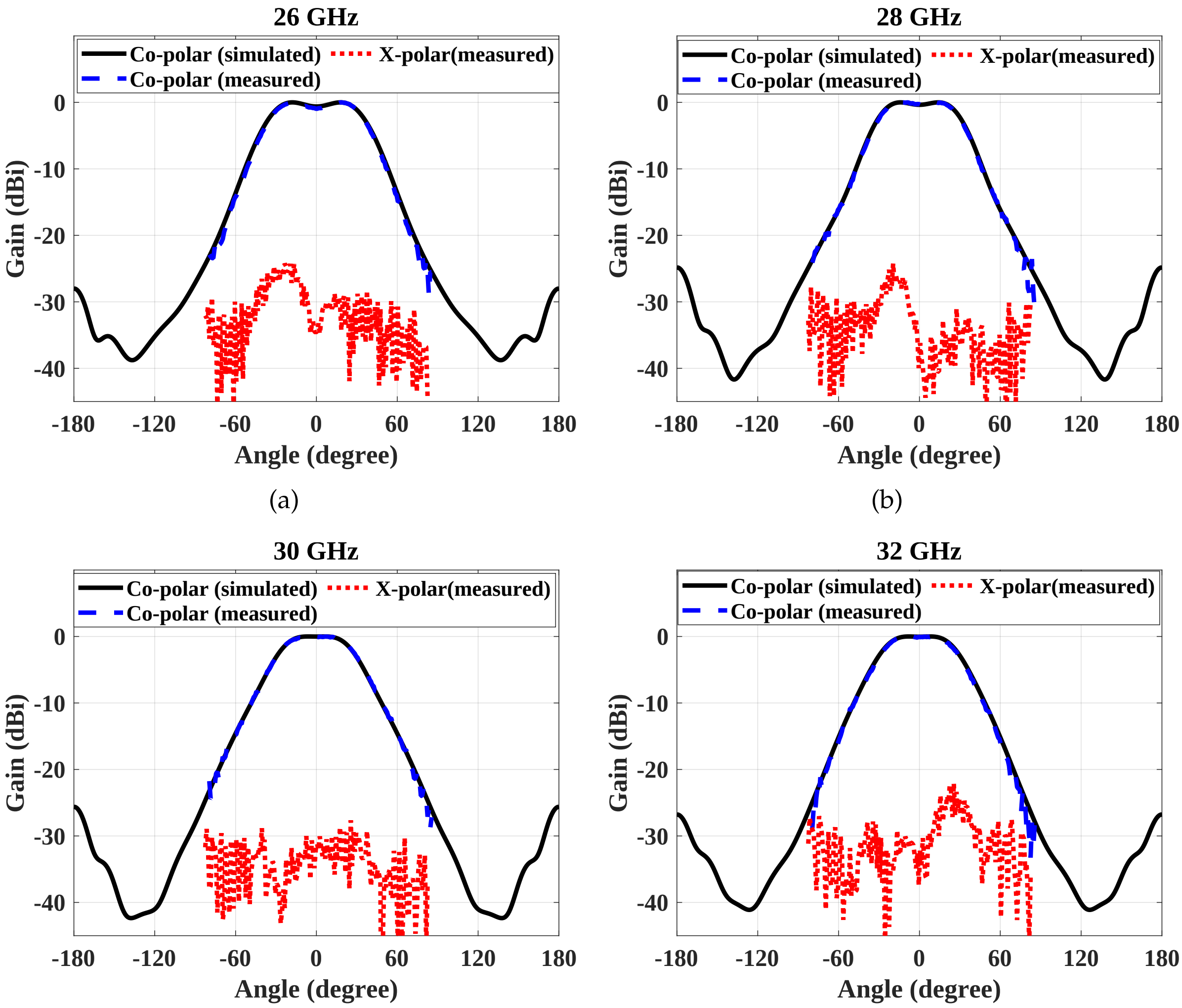

(a)

(b)

(c)

(d)

Figure 3.29: H-plane simulated and measured radiation pattern of the feeder horn antenna at different frequencies. (a) 26GHz (b) 28Ghz, (c) 30 GHz, (d) 30GHzr

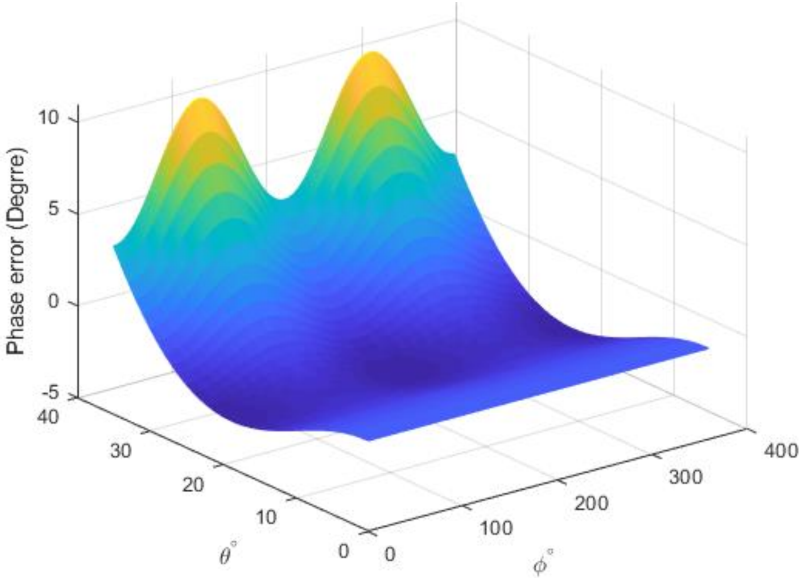

Figure 3.30: Horn antenna radiation pattern phase error

3.3 Summary

The differential feeding antenna would be the base of the proposed UC, because of it's features such as wide bandwidth, low crosspolarization, and broadside directional beam. Moreover, the capacitive differential feeding patch antenna could be used as a feeder in two cases. First, the patch antenna could be used to illuminate the TA aperture area. Also the patch can be used to design folded TA antenna to reduce the focal point distance. which the TA aperture and the feeder become a combination of one low-profile surface. The second application of the differential feeding patch is designing a hybrid feeding antenna that will also be used to feed the TA antenna. Also, the conical horn antenn, which has some features will be examind on the TA antenna surface. The next chapter presents the design and the preliminary results of both the UC and the TA antenna.

Chapter 4

Linear Polarized Transmit-array Antenna Design and Results

This chapter presents the design and preliminary results of the UC and the TA antenna. The linear polarized UC was designed based on receive/ transmit (R/T) technique. The unit cell was designed using capacitive coupling and differential feeding techniques for a linear polarised TA antenna.

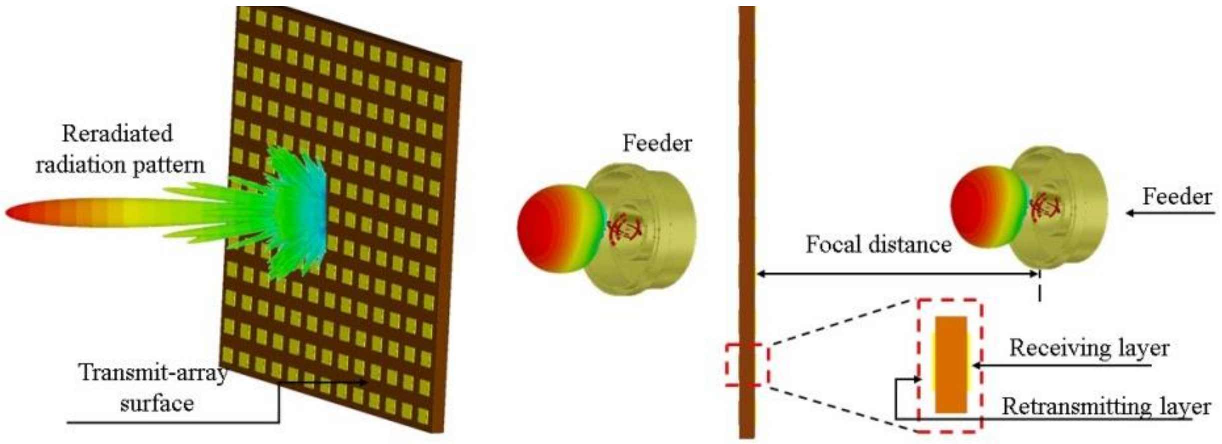

Figure 4.1: Transmit array antenna configuration.

4.1 Linear Polarized Unit Cell Design

Henceforth, the main focus of this proposed work is to design UC with high performances such as wideband and low loss. Exploiting the differential feeding and the capacitive features have been discussed in [91], in which wideband and low cross-polarization antenna has been obtained. The designed UC receives/transmits true-time delay; this design is based on a capacitive differential feeding patch antenna. The UC structure contains a dual capacitive coupling differential feeding patch antenna which layout is illustrated in Figure. 4.2. The microstrip patch antenna is placed on a dielectric substrate (Rogers Ro 4350B, $\epsilon_r = 3.66$, $\tan\delta = 0.0037$, and thickness = 0.762 mm). Two back to-back identical patch antennas have been utilized for receiving and re-transmitting purposes. The re-transmitting patch antenna is rotated by 90° and has an opposite view. Since the UC has to correct the incident signal phase to become a plane wavefront [37], a transition layer (phase delay layer) is placed in between. The phase delay layer contains two strip lines that are built-in dielectric layer RO3006 (ϵ_r=6.15, $\tan\delta = 0.002$, thickness= 0.13 mm). Typically the strip lines connect the receiving patch to the re-transmitting patch. Different unit cells have different strip line lengths to compensate for the phase difference, forcing the front of the re-transmitted signals to be a plane wave. The delay lines are designed alone carefully. The vias shield the transition lines for two reasons: isolate the incoming signals and reduce strip line loss. The shielding technique is designed based on the radius d_{via} and the distance between the two adjacent vias s_{via} [32, 91]. Rotating the phase delay layer by 90° allows UC to produce 180° phase shifts in addition to the original UC phase.

$$d_{via} \leq \frac{\lambda_g}{5} \tag{4.1}$$

$$s_{via} \leq 2d_{via} \tag{4.2}$$

Finally, five dipoles are printed on Rogers RT5880 ($\epsilon_r = 2.2$, $\tan\delta = 0.0009$, and thickness = 0.127 mm) and placed on the top of the patch antenna layer on both sides

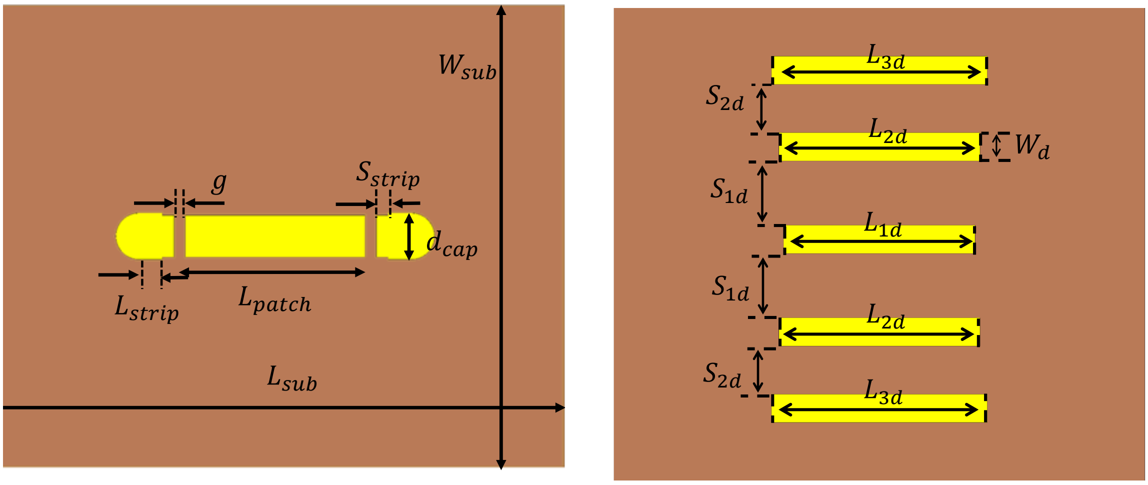

(a) (b)

Figure 4.2: UC structure (a) Differential feeding patch layer. (b) Dipoles layer

Table 4.1: Optimized geometrical parameters for the differential feeding patch antenna

Parameter	W_{patch}	L_{patch}	W_{sub}	L_{sub}	S_{strip}
Value (mm)	0.72	3.1	10	8	0.2
Parameter	L_{strip}	g	h_{sub}	d_{coax}	d_{coax2}
Value (mm)	0.2	0.2	1.575	0.4	0.4

of the UC. Because printed patch antenna suffers from limited bandwidth, these dipoles have different resonant frequencies besides the patch resonant frequency; this technique makes the total bandwidth wider and enhances antenna gain by increasing the radiating area. Figure 4.2 shows the five dipoles layer and its dimensions are $L_{1d} = 0.6$ mm, $L_{2d} = 0.6$ mm, $L_{3d} = 0.6$ mm, $w_d = 0.6$ mm, $S_{1d} = 0.6$, and $S_{2d} = 0.6$ mm. The 3D UC structure is shown in Figure 4.3. The UC dimensions are tuned to obtain a wide bandwidth, a good transmission magnitude, and the required transmission phase. The final UC dimensions are summarized in Table 4.1, the UC size is fixed at $6.6 \times 6.6\,\text{mm}^2$ and the thickness is less than a quarter wave length of the free space at the centre frequency. Moreover the designed UC has small dimensions that minimize quantization phase error.

In terms of the operating mechanism, the receiver layer is illuminated using a feeder source. The incident signals are transferred through the dipoles to the patch antenna, which transfers the energy through the strip lines to feed the re-transmitting layer. The re-transmitting patch excites the dipoles that generate the new in-phase wavefront.

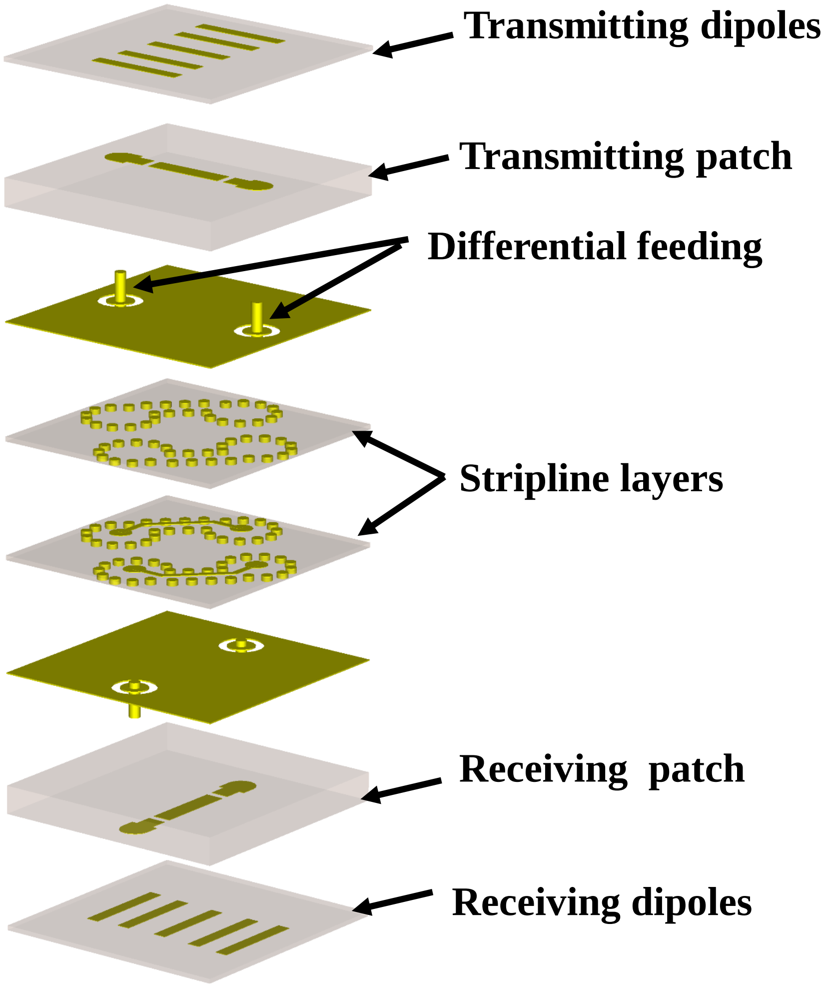

(a)

Figure 4.3: 3D structure of the designed unit cell

4.1.1 Unit Cell Frequency Response

The computer simulation technology microwave studio (CSTMWS) software package is used to simulate the proposed UC to obtain the UC frequency response. Each UC operates as a radiating element, and its transmission behaviour is the function of the frequency; the transmission phase depends on its stripline length. The UC is simulated by defining two Floquet ports, one above the UC and the other below it, each port has two orthogonal TEM modes. The boundary conditions are periodic to present an infinite array of UCs. Figure 4.4 shows the excitation structure of the UC. The E_{in-x} mode from port 1 is reflected and is not considered in the following discussion, as it is orthogonal to the upper dipoles. On the other hand, the E_{in-y} mode from port 1 is the desired incident mode that excited the UC. The E_{tr-x} is the port 2 desired output mode, which is rotated by E_{tr-x} relative to the incident polarization due to the structure of the re-transmitting part of the UC. The principle operation of the UC is explained by the electric field distribution shown in Figure 4.5.

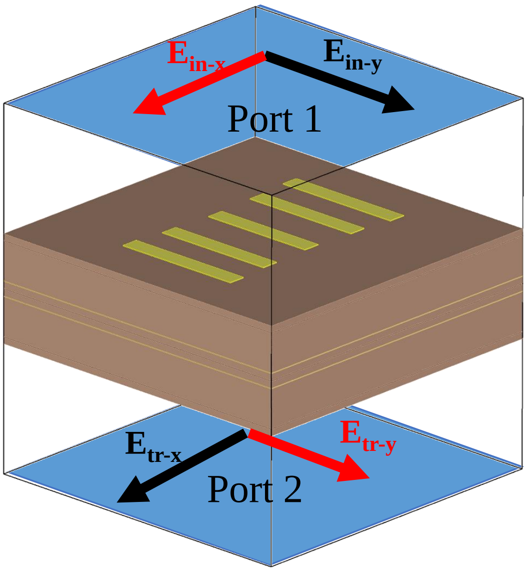

Figure 4.4: UC under Floquet ports excitation.

The TA antenna is designed based on the 3-bit quantization phase. Therefore the required phases of the UCs are 0°, 45°, 90°, 135° 180°, 225°, 270°, Figure. 4.6 shows the simulated reflection and transmission coefficients of four UCs (0°, 45°, 90°, and 135°), while the other four UCs have the same amplitudes with a 180° additional phases for the transmission coefficient. The UCs reflection coefficient is better than -10 dB. Moreover, the designed UCs provide a wide transmission bandwidth of 24%, around 28 GHz, with insertion loss better than 0.5 dB. Figure 4.7 shows the undesired reflection and transmission coefficients. They are less than -30 dB for all the UCs in the range of 26 to 31.5 GHz.

The transmission coefficients' phase is presented in Figure.4.8. The phase-frequency response covers a 360° phase range. The 3-bit quantization phase is achieved; therefore, a 45° phase shift is arranged between two adjusted phase steps. Figure 4.19 shows the calculated phase, the quantized phase distribution, and the phase error for the 27 × 27

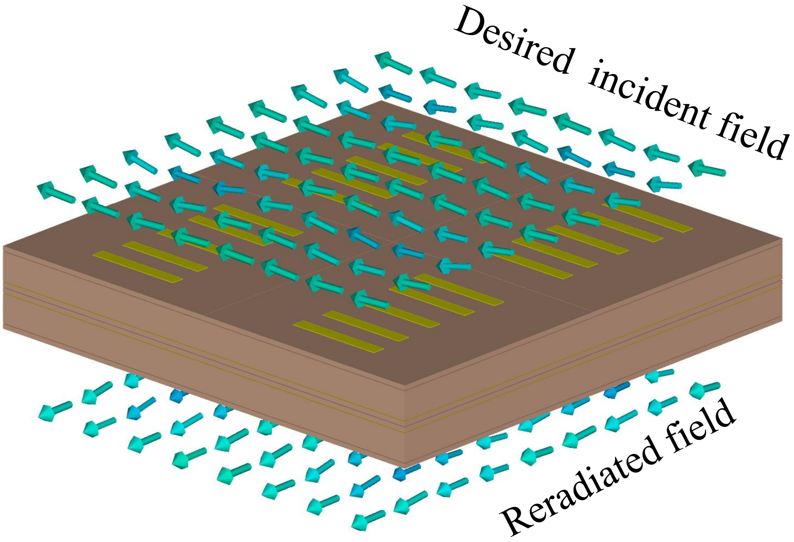

Figure 4.5: Incident and re-transmitted electric fields.

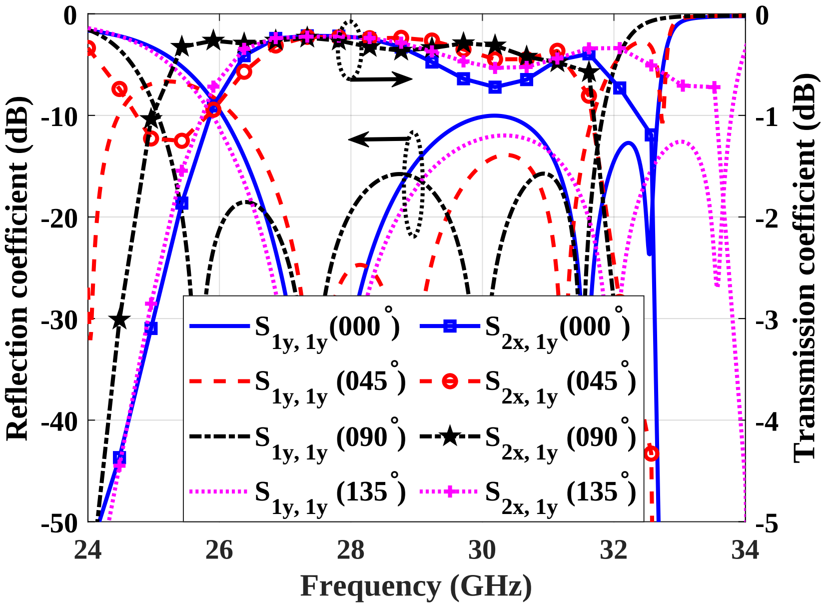

Figure 4.6: Reflection and transmission coefficients for four UCs (0°, 45°, 90°, and 135°.

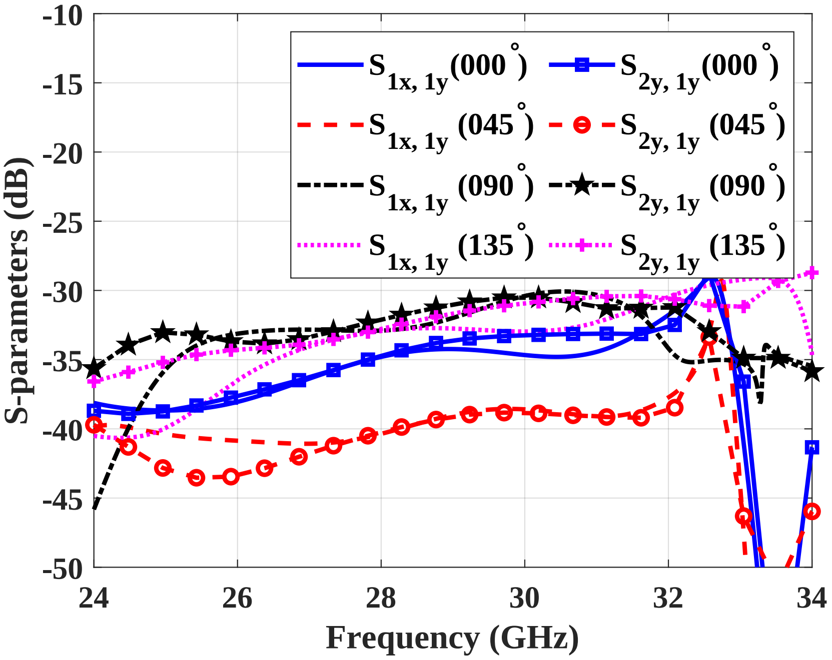

Figure 4.7: Undesired reflection and transmission coefficients

TA antenna. The figure indicates that the maximum phase error is equal to ± 22°. Thus wideband and high gain transmit-array antenna is expected. Thus wideband and high gain transmit-array antenna is expected.

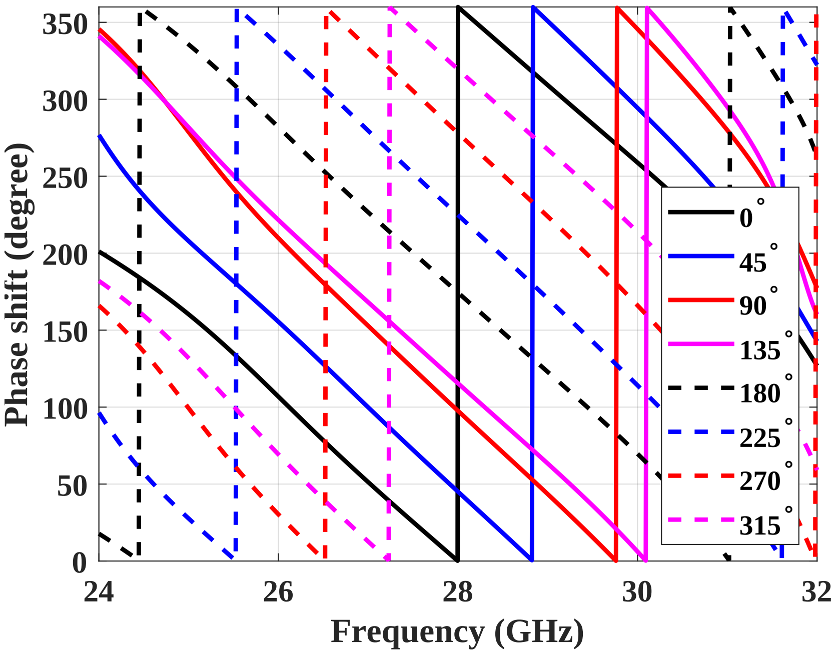

Figure 4.8: Simulated transmission coefficients phase

4.2 Linear Transmit-array Antenna Results and Discussion

This section includes the stimulated and the measured results of TA antenna surface under illumination of both hybrid and conical horn antennas. Moreover, a patch antenna has been used to illuminate the TAA, but the results are not included in this section. Arrays of two patch antennas are used because one element radiation pattern beamwidth is very wide, which requires a big TAA surface, which requires high computation performances and processing time. This experiment proves that the designed TA elements are able to re-transmit the incident signals toward the desired direction and encourage us to reduce the patch antenna beamwidth using a hybrid antenna technique to be useable as a TAA feeder. The TAA with the patch as a feeder radiation pattern results will be concluded in a comparison table with the hybrid and the conical feeders.

4.2.1 Conical Feeding Antenna

The horn antenna is placed at the focal point of the TA aperture for illumination purposes. The array size and the focal point position are the main factors that affect the TA performance. The focal source radiation pattern model is considered ($(\sec\theta)$) with 10 dB gain and 35° half-power beamwidth at the centre frequency. Assuming the TA required gain is 30 dBi, and the aperture efficiency is about 50%. According to parabolic theory, the theoretical values of the aperture area and the focal length are calculated. In order to verify the UC concepts in which it acts as a phase compensation and a polarization rotation, the TA antenna surface has been examined. Figure 4.9 shows the horn incident fields extracted just above the TA surface. The phase distribution is uniform, and as moving far from the centre of the TA surface, the phase varies. Also, the electric field amplitude decays as moving toward the aperture edges, which harms the tapering efficiency. Figure 4.10 shows the electric field distribution of the re-transmitted signal, in which the electric fields are in phases. The TA unit cells convert the accepted field polarization to the normal direction. Also, that ensures the TA aperture gives maximum efficiency. A parametric study of F/D effect on antenna gain has been carried out to find the optimum value of the F/D. The TA antenna size is kept fixed,18 × 18, while the value of F/D is changed from 0.3 to 1 by 0.1 step. Based on Figure 4.11, which shows the realized gain for different values of F/D, the best value for F/D is between 0.7 and 0.8; therefore, a more fine parametric study has been carried out for values of F/D between 0.7 and 0.8 as shown in Figure. 4.12. The optimum value of F/D is 0.76 as it gives the highest gain at the centre frequency and the widest 2-dB gain bandwidth, among other values of F/D. Therefore, F/D=0.76 is used to design other TA antennas, with 24 × 24 unit cells and 27 × 27 unit cells.

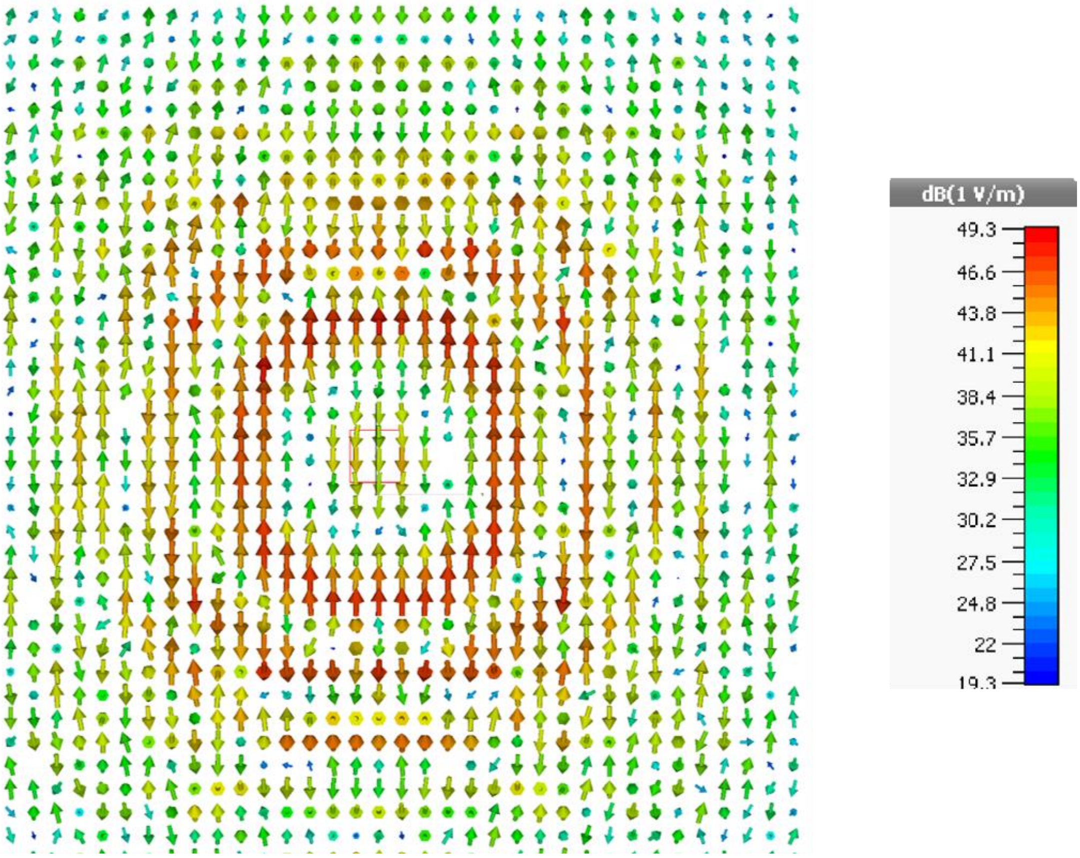

Figure 4.9: The incident electric filed distribution

Figure. 4.13 and Figure. 4.14 shows the simulation realized gain and aperture efficiency for the 18 × 18, 24 × 24 and 27 × 27 TAs. The 24 × 24 has a gain improvement of 2.68 dBi over the 18 × 18 TA, while the 27 × 27 has an improved gain of 3.7 dBi. The maximum aperture efficiency is above 54% for all the designs.

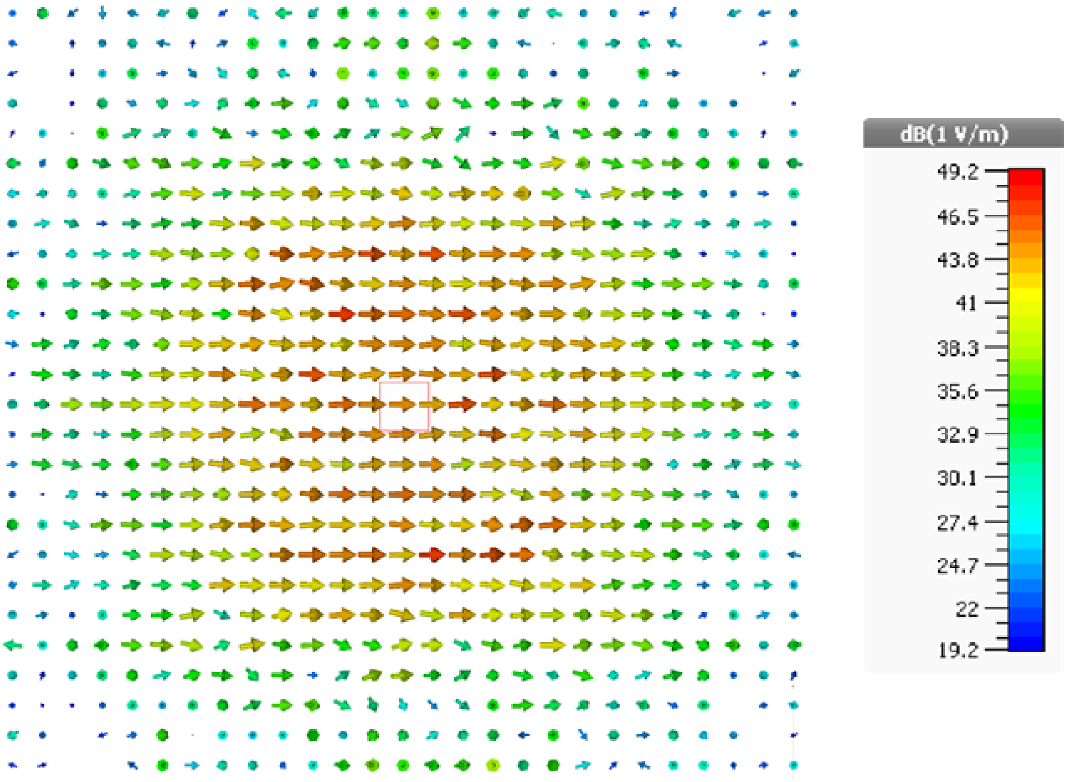

Figure 4.10: The re-radiated electric filed distribution

The 27 × 27 unit cell TA antenna is fabricated and measured as shown in Figure. 4.15 to validate the proposed work. The measurement has been carried out using a near-field scan system (NSI 5913), the PNA network analyzer, WR42, and WR28 waveguide probes. The probes are used to receive the re-radiated fields after the TA surface; then the far field directivity is calculated using NSI2000 software. A comparison between the simulated and measured directivities is presented in Figure. 4.16. The discrepancy between the simulated and measured results may come from the fact that material loss and material variation in thickness. Also, Rogers's material dielectric constant is given at 10 GHz, but our design centre frequency is 28 GHz. Fabrication tolerance could have a significant impact on a design at high frequency. Figure. 4.17 presents the antenna's measured and simulated E-plane radiation patterns at different frequencies. The maximum gain is 31.14 dBi, and the sidelobe and the cross-polarization levels are less than -28 dB and -27 dB,

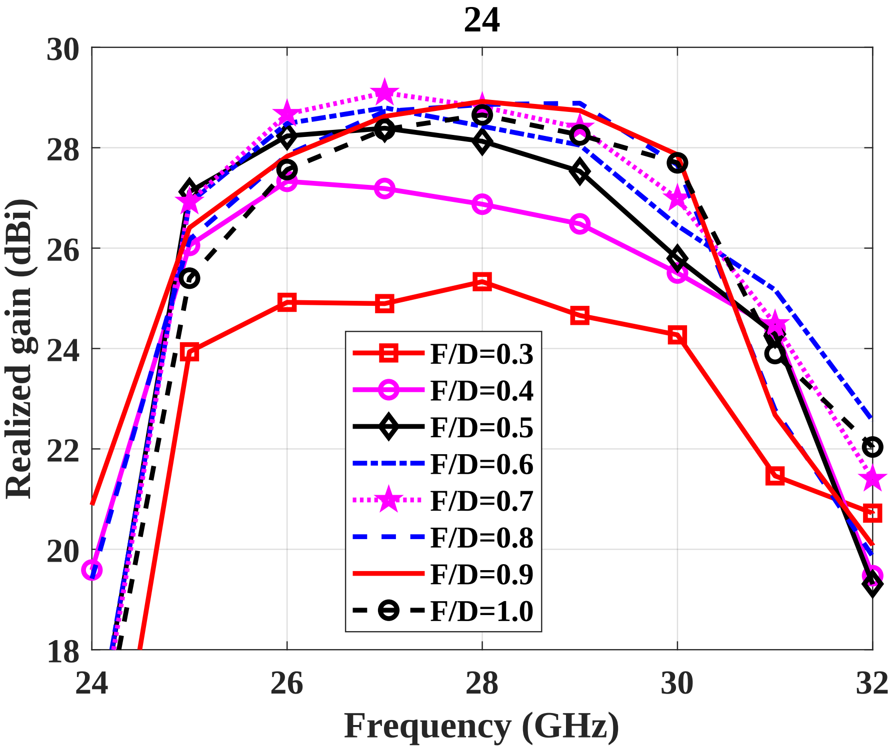

Figure 4.11: 18 × 18 Transmit-array antenna gain for different values of F/D

respectively, over the operating bandwidth. On the other hand, Figure. 4.18 shows the H-plane radiation patterns where the sidelobe and the cross-polarization levels are less than -28 dB and -27 dB, respectively. A study of the hybrid horn antenna on the TA antenna will take place in the next section.

A study of the hybrid horn antenna on the TA antenna will take a place in the next section.

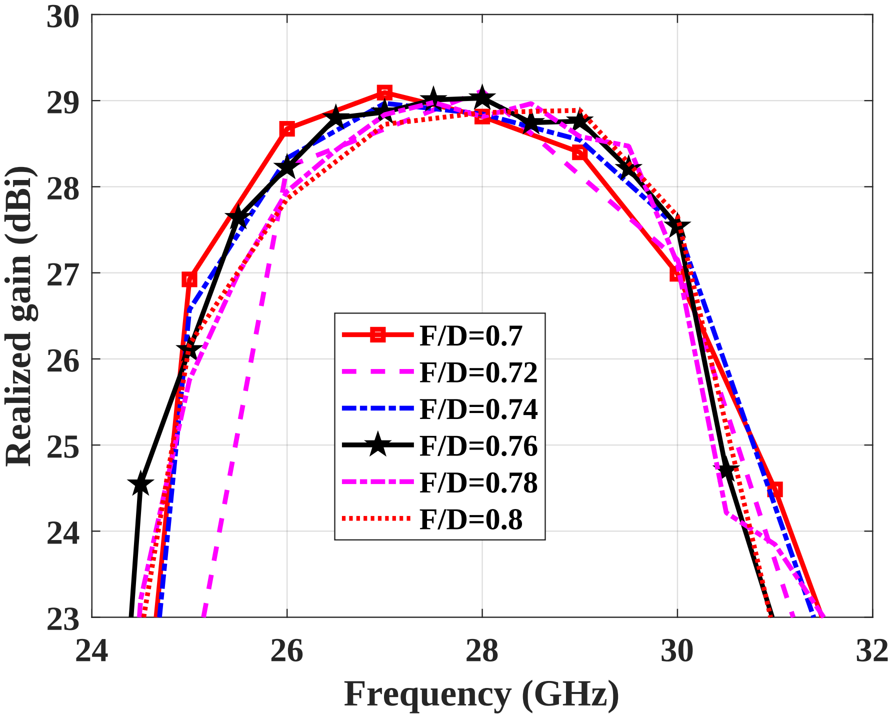

Figure 4.12: 18 × 18 Transmit-array antenna gain for different values of F/D between 0.7 and 0.8.

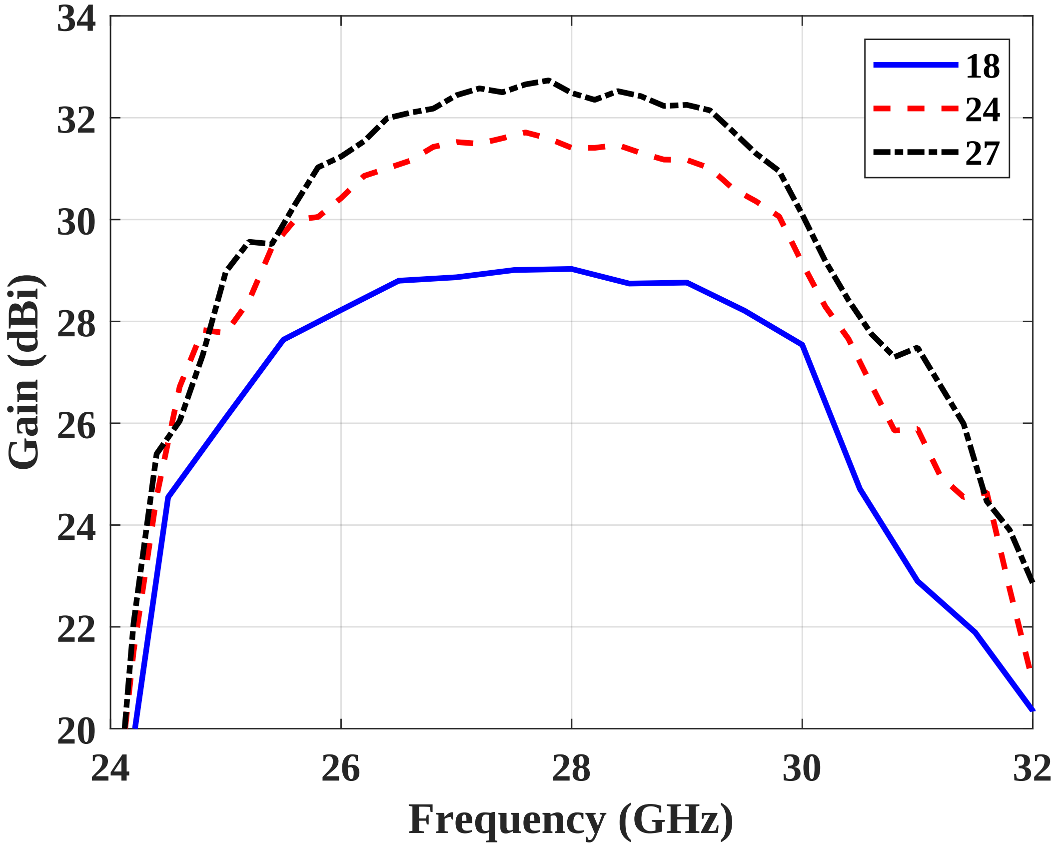

Figure 4.13: Transmit-array antenna gain for different aperture areas (18 × 18, 24 × 24, and 27 × 27), and F/D=0.76

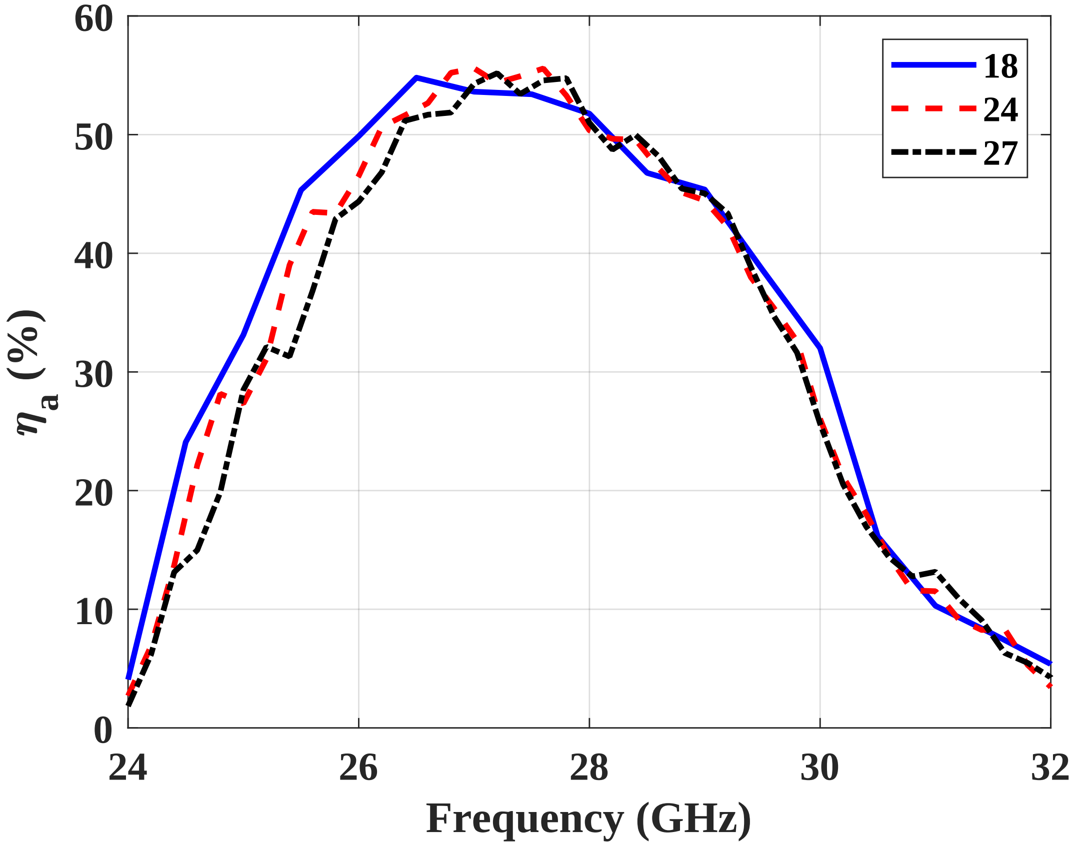

Figure 4.14: Transmit-array antenna efficiency for different aperture areas (18 × 18, 24 × 24, 27 × 27), and F/D=0.76

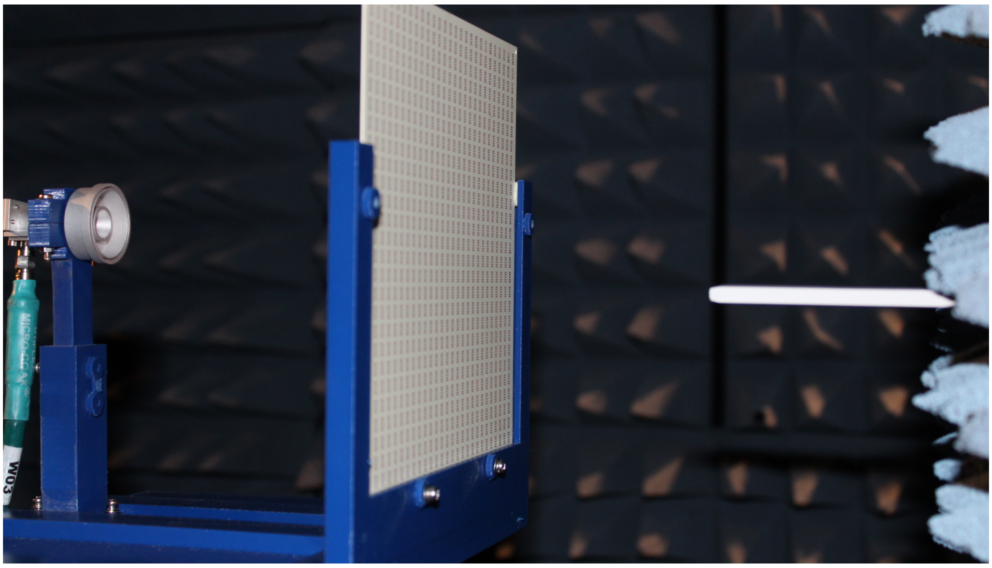

Figure 4.15: Transmit-array antenna measurement setup

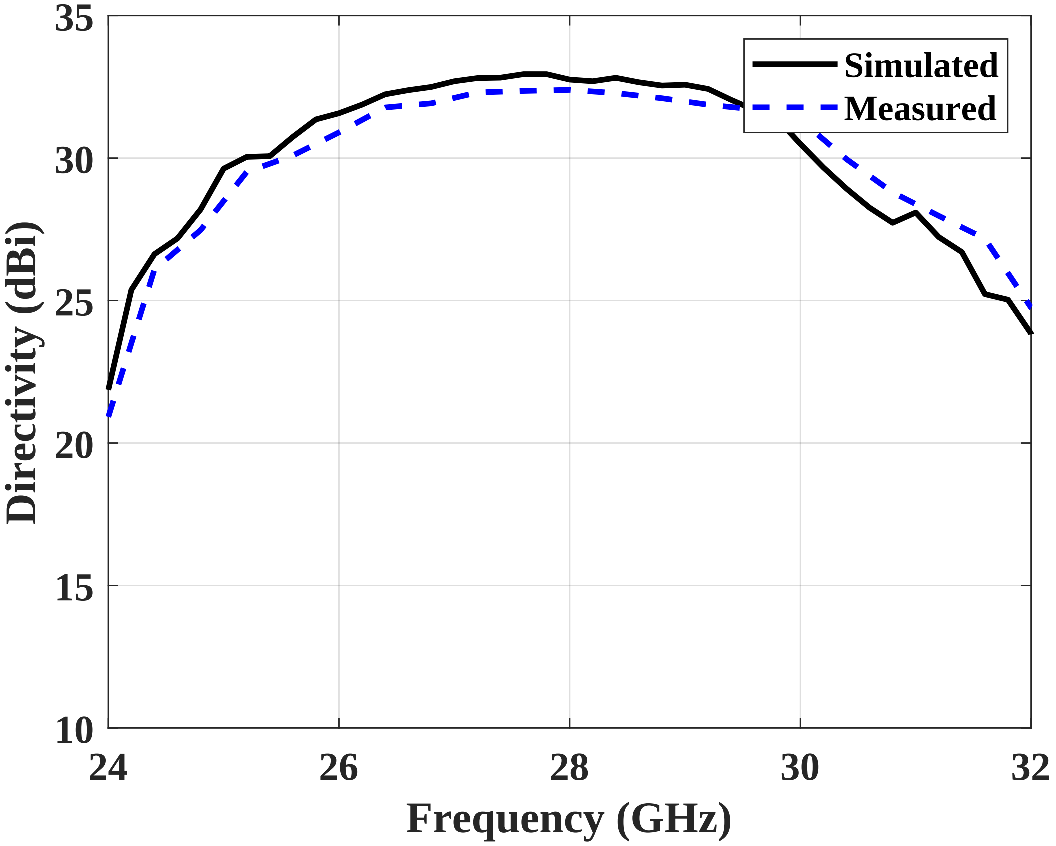

Figure 4.16: Simulated and measured directivities of the 27 × 27 TA

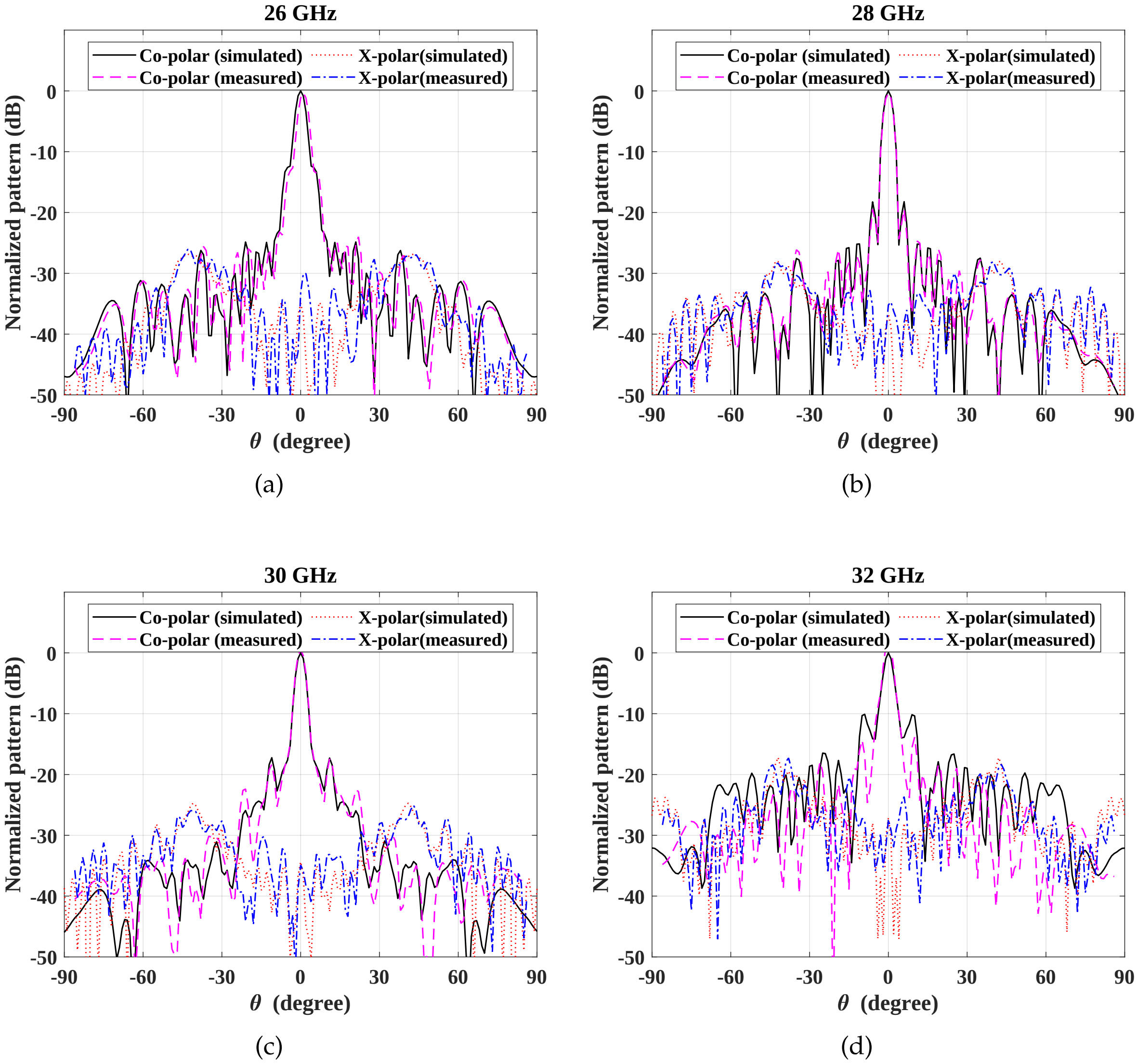

(a) (b) (c) (d)

Figure 4.17: E-plane radiation patterns of the TA antenna at four different frequencies.

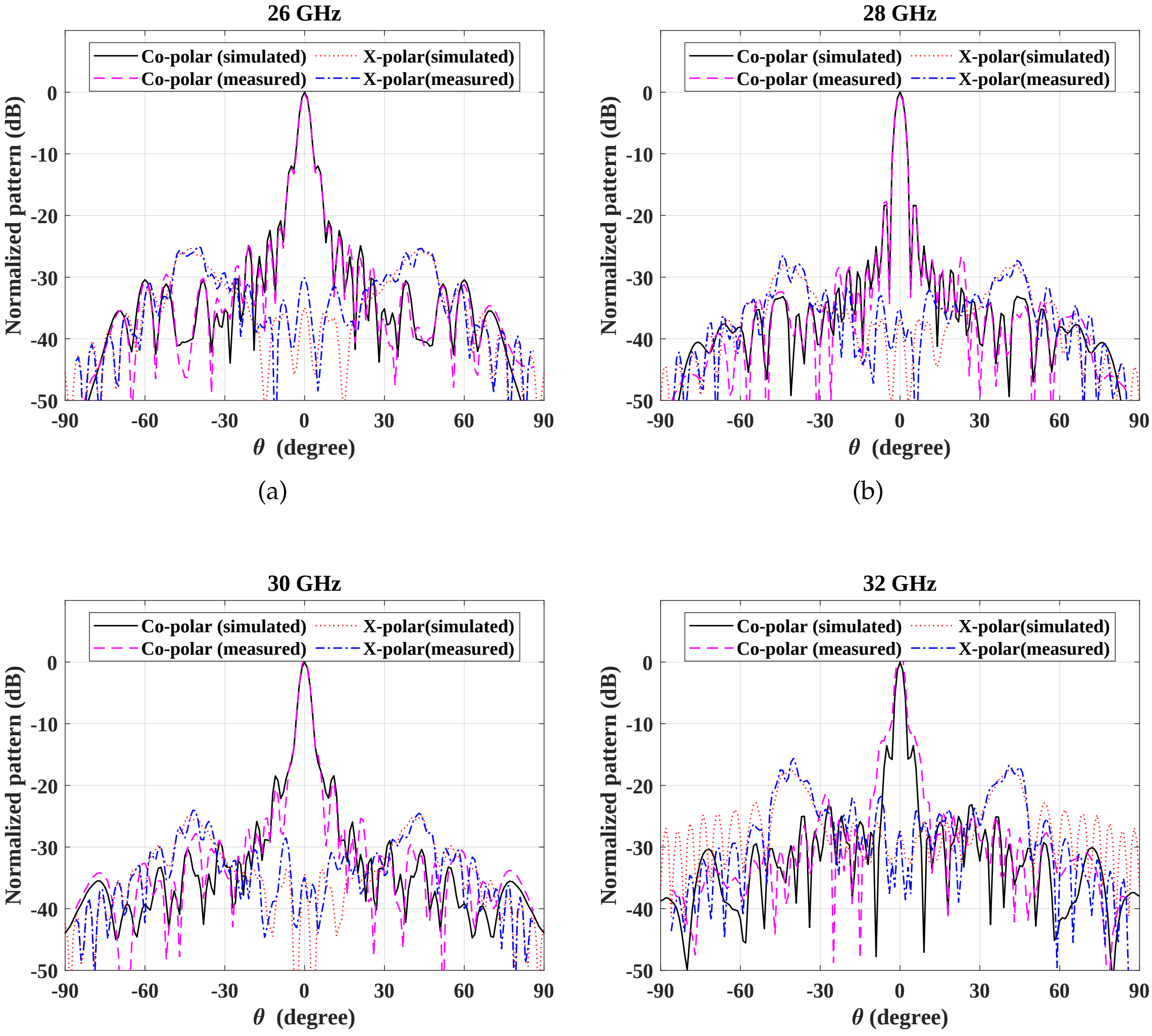

(a) (b) (c) (d)

Figure 4.18: H-plane radiation patterns of the TA antenna at four different frequencies.

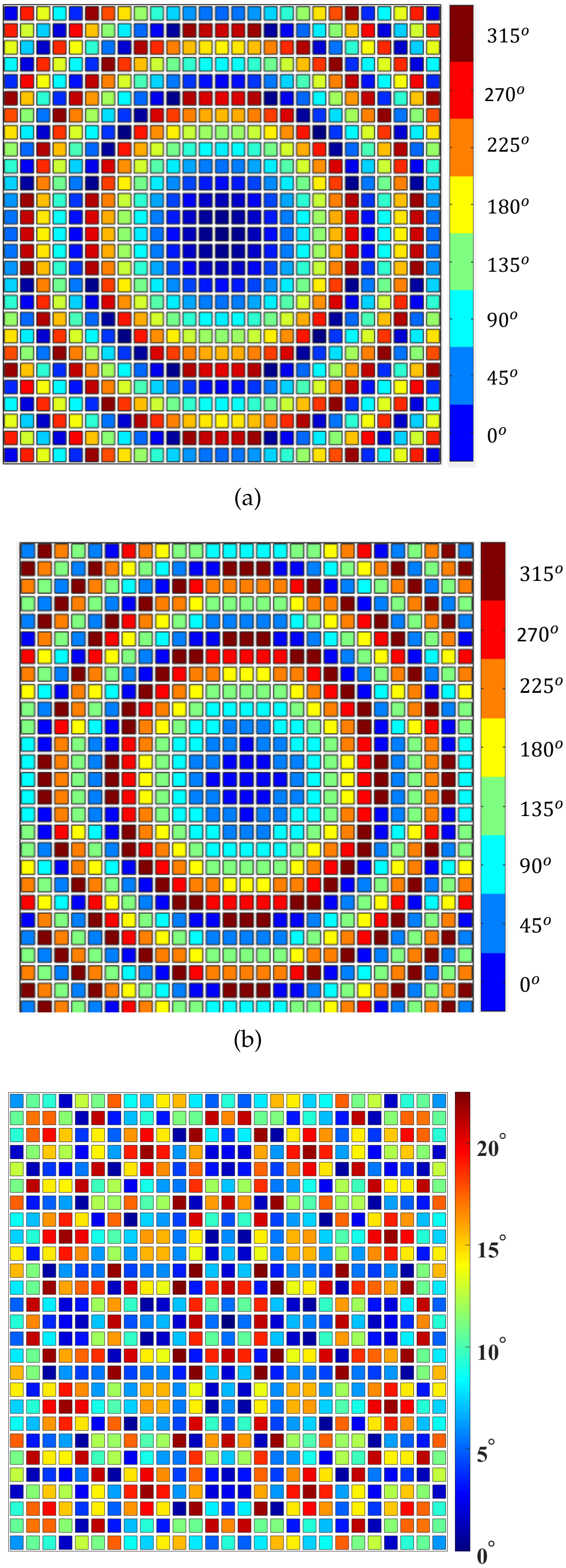

(a)

(b)

(c)

Figure 4.19: The phase distribution of 27 × 27 TA antenna. (a) The calculated phase. (b) The quantize phase. (c) The phase error

Table 4.2: Table of comparison

Reference	Gain (dBi)	1-dB BW (%)	3-dB BW (%)	A_e (%)	Area (λ_0^2)	x-pol (dB)	SLL (dB)	Thickness (λ_o)	Frequency (GHz)
[14]	28.9	9	19.4	30	206.1	-21	-14	0.5	11.3
[13]	23.7	4.2	9.4	13.8	133.14	-30	-13	0.75	11.3
[11]	24.8	15.5	—	55	40.9	-29	-24	0.433	10
[12]	22.8	12.1	—	28	100	—	—	0.096	60
[3]	24.8	—	5.4	24.6	100	-28	-15	0.105	60
[29]	24.8	—	—	31.3	38.45	-20	-20	1.87	28
[30]	20.6	3.7	—	47	72.4	-15	—	1.9	9.5
[13]	24.45	10.2	14.83	34.64	201.06	—	-15	0.58	12
This work	31.15	11.5	21	50	218.5	-37	-28	0.198	28

4.2.2 Hybrid Feeding Antenna

A hybrid horn antenna is used to illuminate the TA surface. The hybrid antenna gain is 14.2 dBi, and the 3 dB radiation beamwidth is 31.3° at 28 GHz. Then the TA antenna aperture area is determined to be 18 × 18 UCs for computing limitation. The effect of the focal point distance over the TA aperture area is studied, the antenna area is kept equal to 18 × 18 while the value of F/D is changed from 0.4 to 1 by 0.1. Based on figure 4.20, which shows the realized gain for different values of F/D, the best value is F/D = 0.9 and the realized gain is 28.5 dBi. This study gives us a sense of the feeding antenna radiation pattern beamwidth and gain effect over the TA antenna gain. The Figure shows gain enhancement as much as F/D increases; however, the TA antenna gain drops at F/D= 1. The value F/D=0.9 is the optimum value, and the increment of TA area leads to a decrease in the aperture efficiency. The TA aperture is calculated according to the required gain, which is mainly equal to 27 × 27, and the F/D is kept equal to 0.76.

Figure 4.21 represents the simulated and measured directivities. The discrepancy between the simulated and measured results could be related to focal point measurements and TA antenna tolerance. Figure. 4.22 represents the measured and simulated E-plane radiation patterns of the antenna at different frequencies over the operating bandwidth. On the other hand, Figure. 4.23 shows the H-plane radiation patterns.

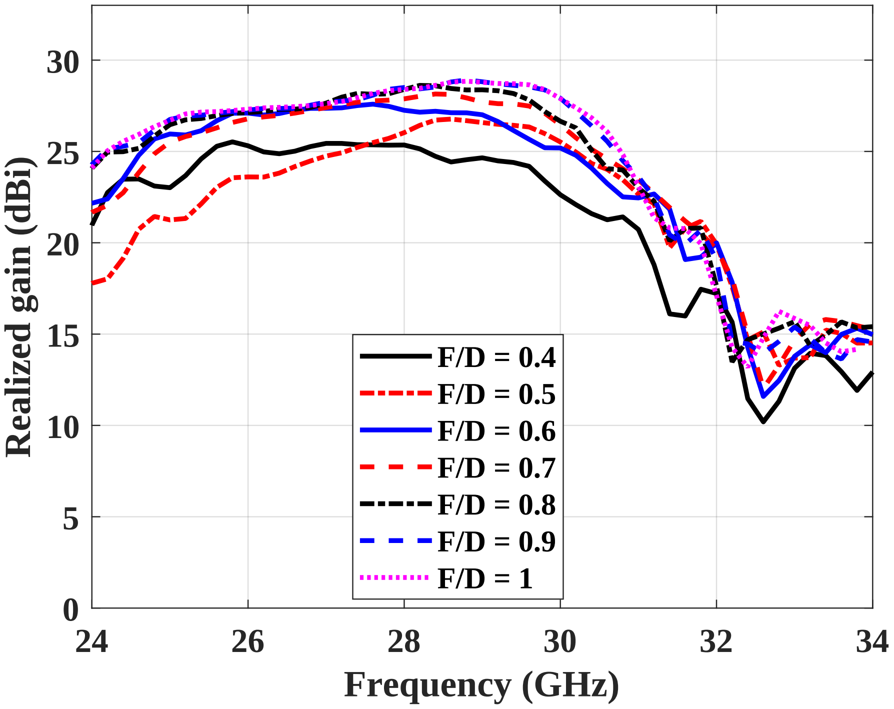

Figure 4.20: 18 × 18 Transmit-array antenna gain for different values of F/D between 0.4 and 1.

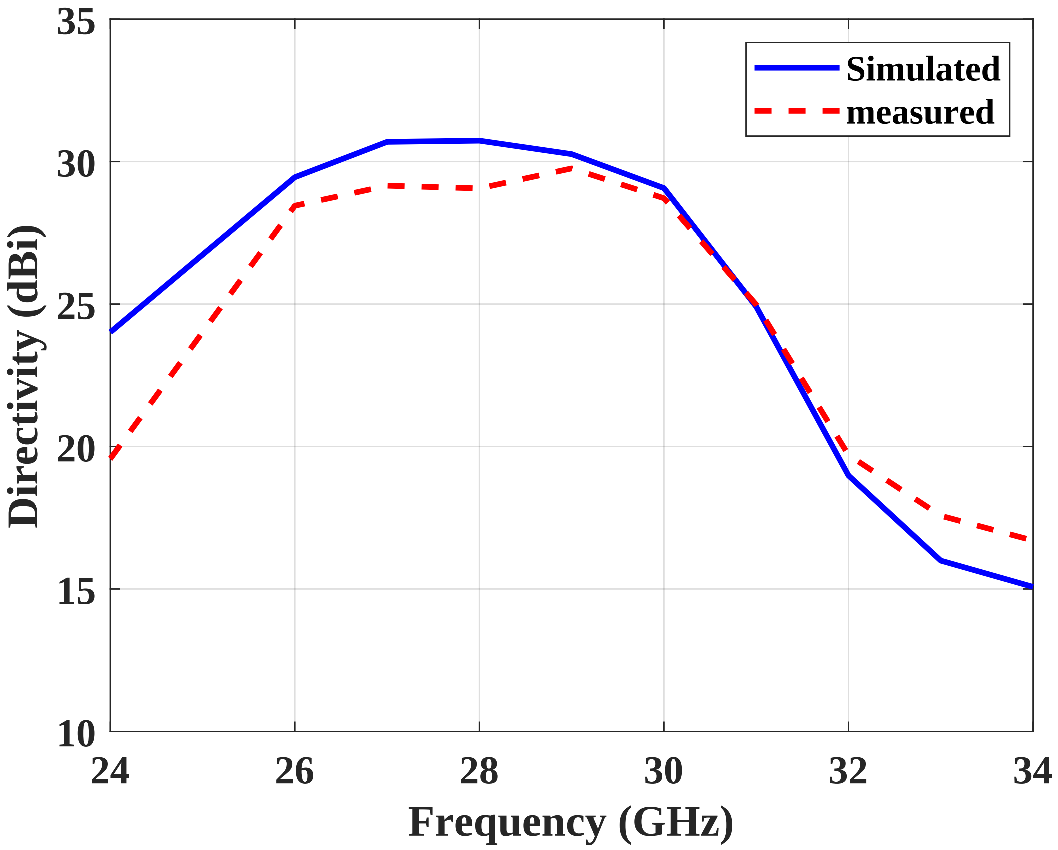

Figure 4.21: Simulated and measured directivities of the 27 × 27 TA antenna

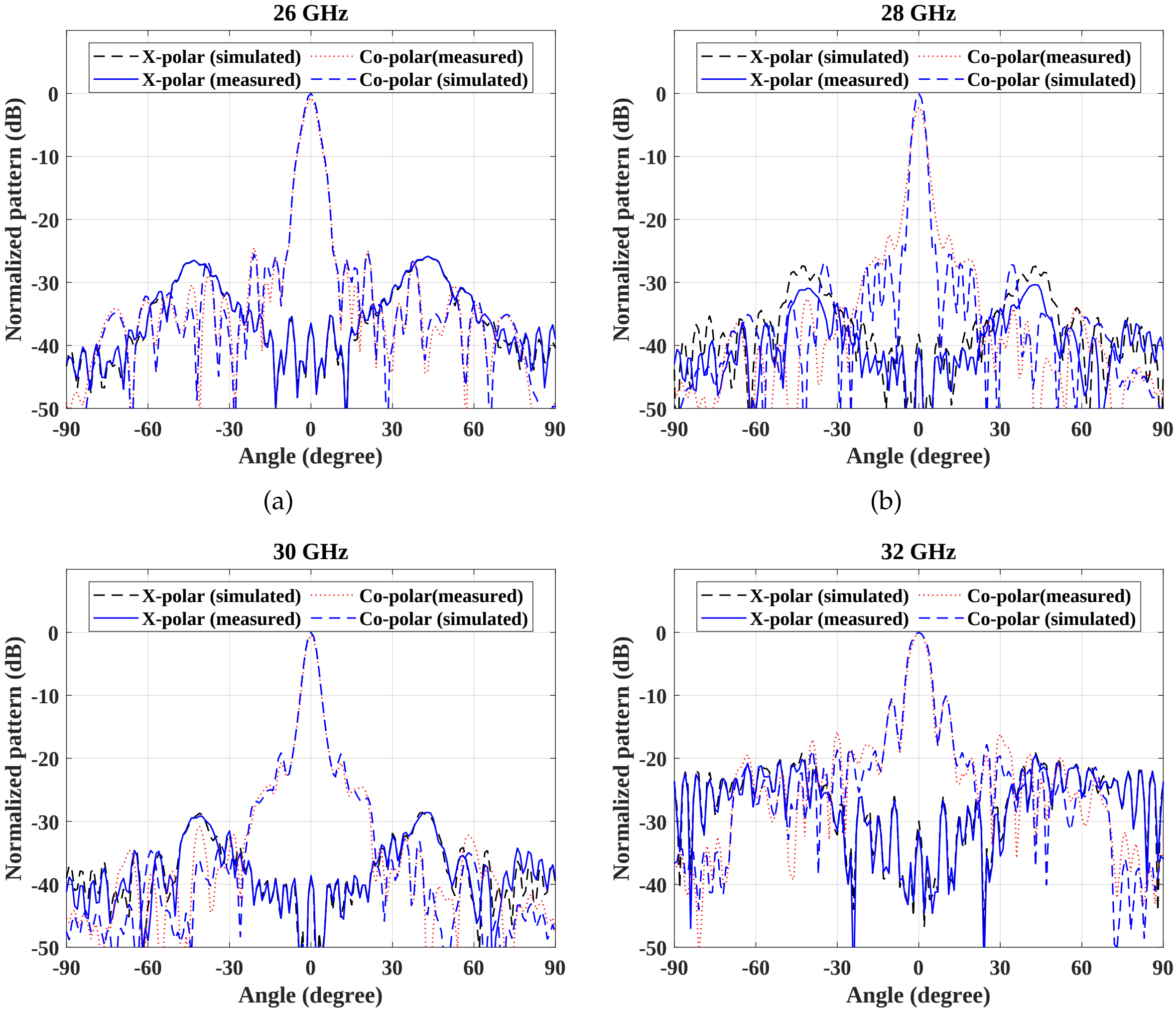

(a) (b) (c) (d)

Figure 4.22: E-plane radiation patterns of the TA antenna at four different frequencies.

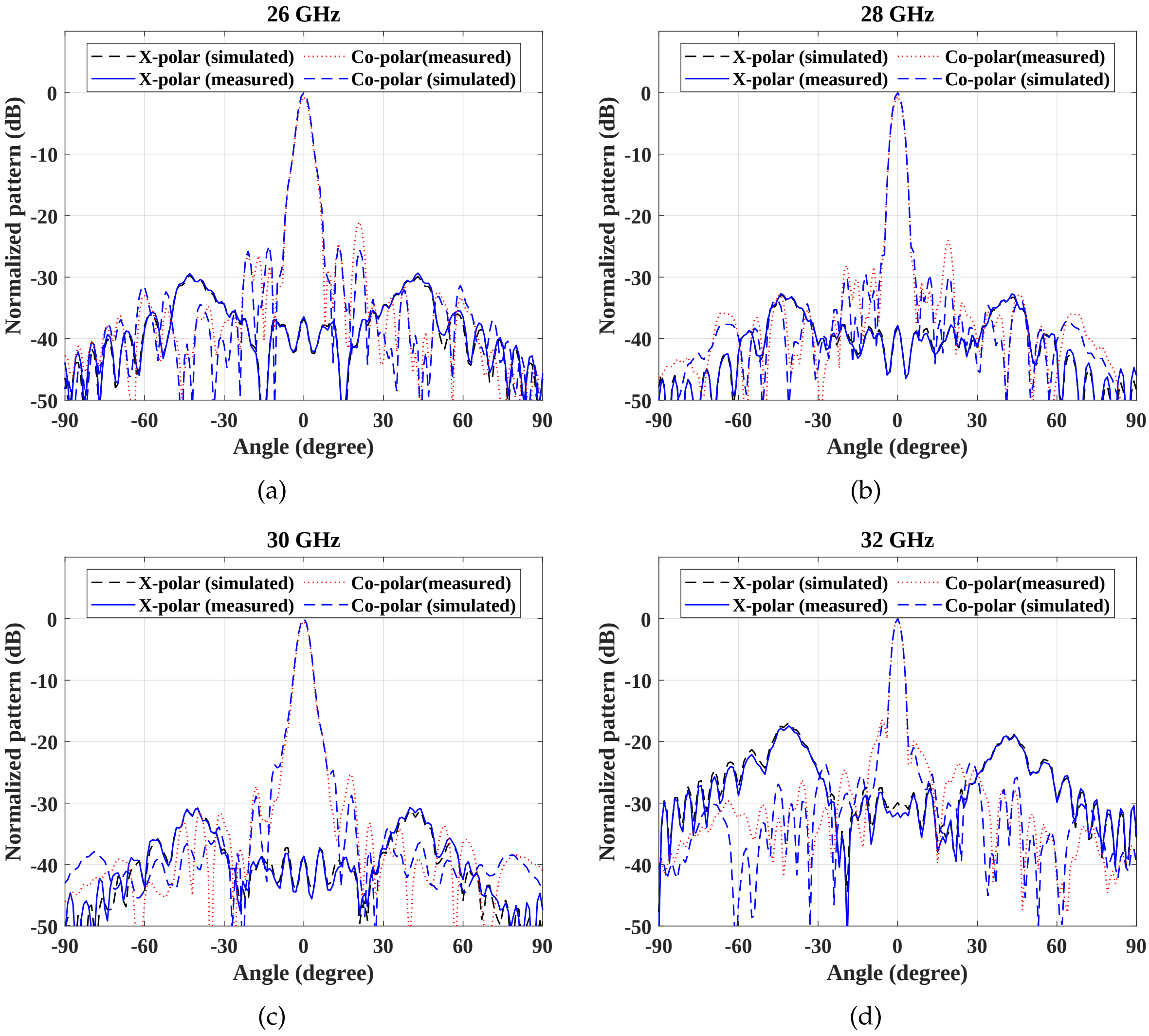

(a) (b)

(c) (d)

Figure 4.23: H-plane radiation patterns of the TA antenna at four different frequencies.

4.3 Feeding Antennas Radiation Effect on Transmit-array Antenna

The feeding antenna is the source to illuminate the TA antenna surface; therefore, the incident signal amplitude and phase have a massive impact on the TA antenna efficiency. The TAA efficiency is calculated based on equation 4.4. Figure 4.24 shows the efficiency of TA antennas, in which 51% and 47.85% aperture efficiency using conical and hybrid antennas.

$$G = \frac{4\pi A_e}{\lambda^2} \tag{4.3}$$

Where: G Antenna gain, A_e Antenna effective area, λ Signal wavelength

$$A_e = \eta_a A \tag{4.4}$$

Where: A Antenna aperture area, and η_a aperture efficiency

Since the incident signal varies in amplitude and phase according to the incident coordinates, the feeding antenna radiation pattern affects the TAA efficiency. The parabolic reflectors interact with the incident signal radiation because of its curvature surface regardless of the feeding antenna's pattern. The TAA is a flat surface, so the illumination signal affects the TAA efficiency, as stated in equation 4.5.

$$\eta_a = \eta_s \eta_i \eta_r \tag{4.5}$$

Where: η_i illumination efficiency, η_r radiation efficiency, and η_s spillover efficiency.

Knowledge of the feeding antenna radiation pattern as a function of the broadside spherical coordinates θ and ϕ is required [34]. The conventional rectangular horn antenna beamwidth in E-plane is unequal to that in H-plane [92].

Figure 4.25. illustrates the simulated radiation patterns of the designed hybrid horn antenna at the centre frequency where (ϕ=0°), and (ϕ=90°). The radiation pattern is symmetric at about ± 18°, then the beamwidth in E-plane is much broader than in H-plane. However, the radiation pattern of the conical horn antenna at (ϕ=0°), and (ϕ=90°) is shown in Figure 4.26. Both E-plane and H-plane are symmetric to a certain degree, which is ± 30°, and then the beamwidth in H-plane is a little wider than that in E-plane. A feeder with a symmetric radiation pattern is preferable because asymmetric field distribution harms the aperture efficiency. In terms of amplitude tapering efficiency, a parabolic reflector shape is used to compensate for path loss difference, but the TA antenna has a flat surface; therefore feeder with acceptable amplitude tapering is required. In addition, the hybrid antenna radiation pattern has a narrow beam that harms TA antenna amplitude tapering efficiency. However, the radiation pattern distribution of the designed conical horn antenna is different. The conical horn antenna concentrates at ± 18°, while at ϕ=0° is leas by 0.4 dB, compensating for incident signal path loss difference and enhancing tapering efficiency.

As known UCs are created and distributed to compensate for the path phase difference of the incident signals, while the feeding antenna radiation has uniform phase distribution. The TA aperture phase distribution is calculated based on the distance between the focal point and the coordinates of the points on the surface. In contrast, the incident signal phase is not considered. As a result, there is a phase error, which impact can be minimized by using a feeding antenna with uniform phase distribution.From Figure 3.30 and Figure 3.25 we can clarify that the phase of the feeding antenna radiation pattern impacts the TA antenna efficiency.

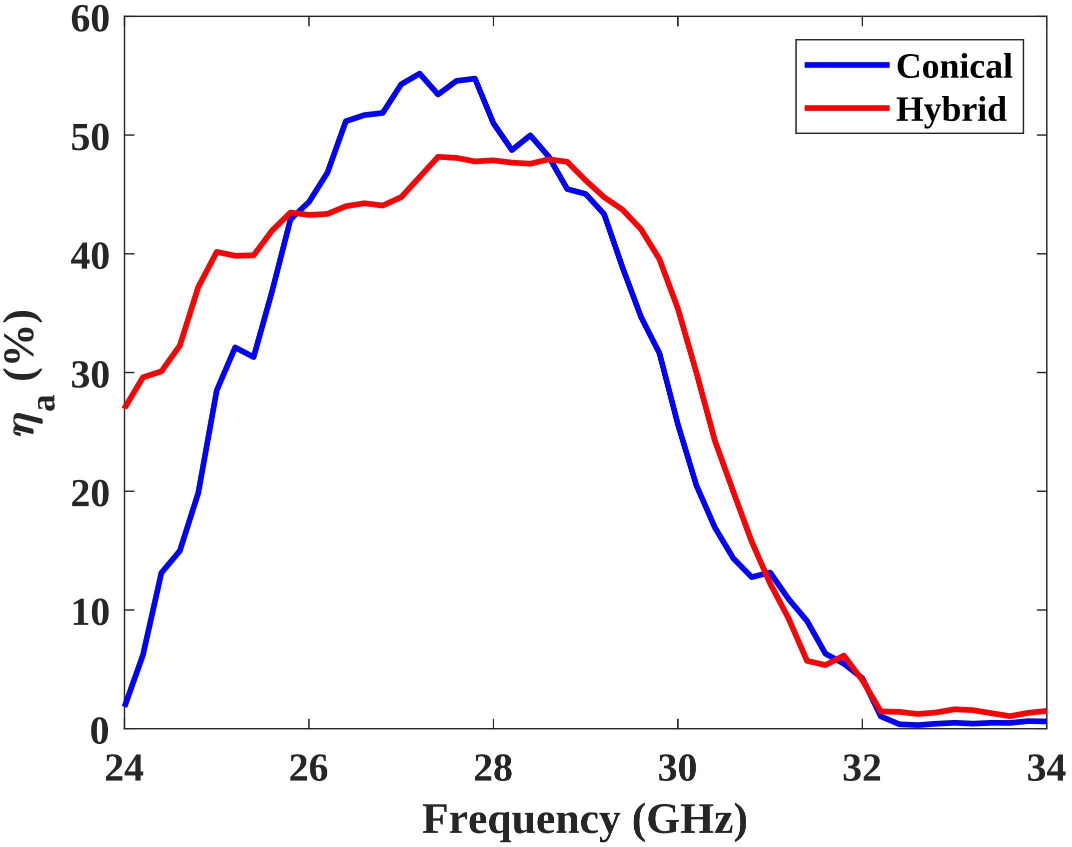

Figure 4.24: Efficiency of TA antenna using conical and hybrid antennas

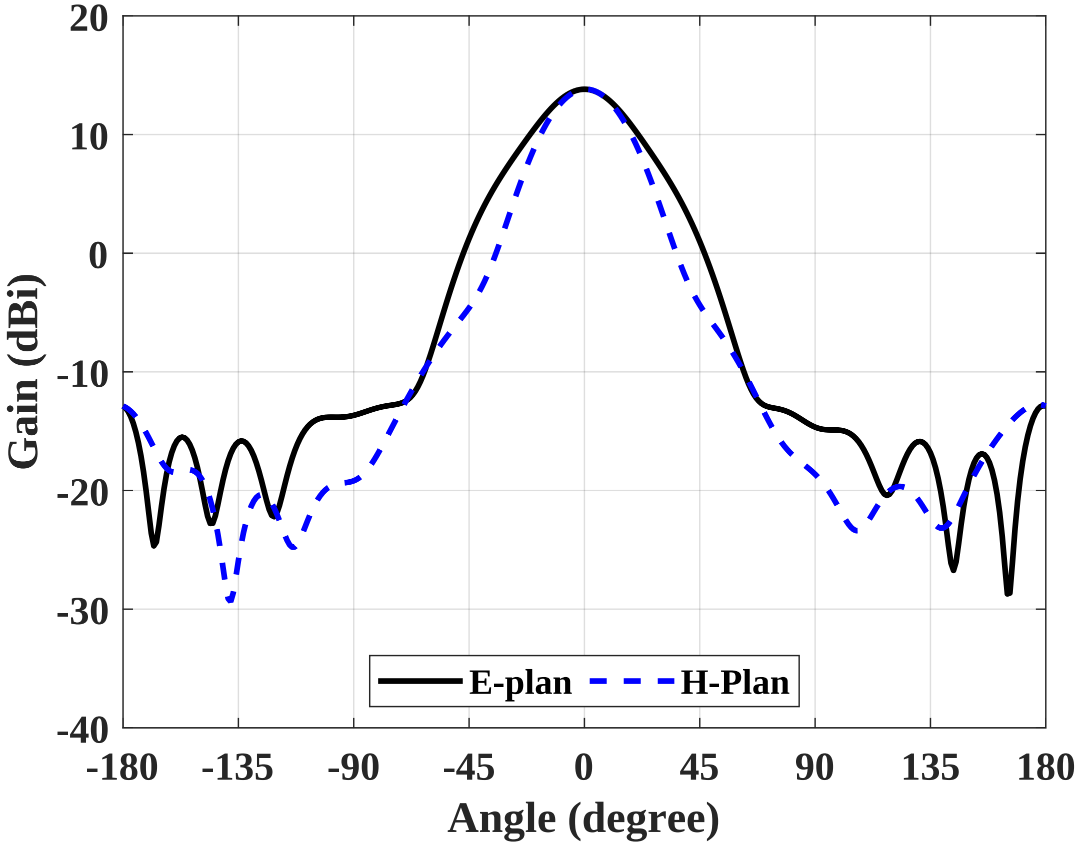

Figure 4.25: Simulated E-plane and H-plane radiation pattern of the hybrid antenna at 28 GHz

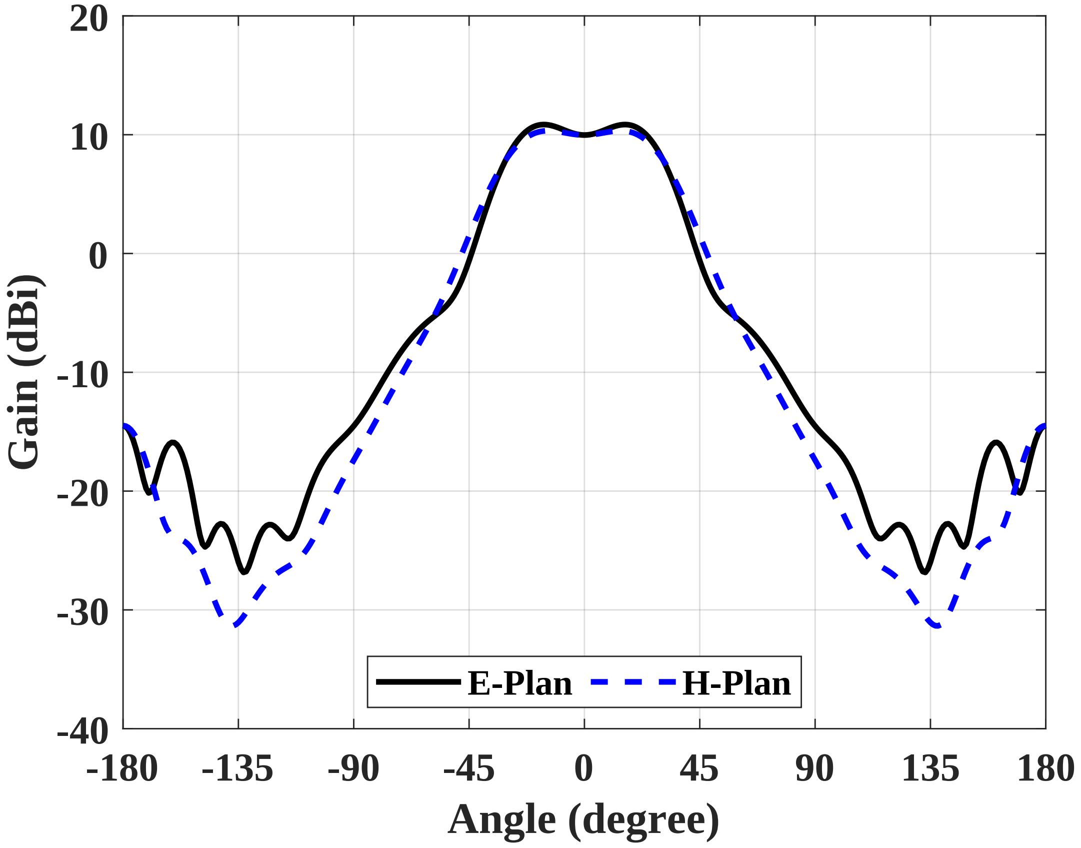

Figure 4.26: Simulated E-plane and H-plane radiation pattern of the conical horn antenna at 28 GHz

Chapter 5

Circular Polarized Transmit-array Antenna Design and Results

Linear polarized transmit-array antenna design and results have been discussed in the previous chapter, in which ultra-wideband and high gain are achieved. Since antennas with high gain, wideband, and circularly polarized are in high demand, this chapter concludes with the design and the results of the circular polarized UC and the CPTA antenna. The circularly polarised wave is obtained based on extracting the CP components from the LP wave, in which the UC transmission coefficients satisfy the CP wave requirements. Then an array of the UCs is assembled with the LPTA antenna to form the final CPTA antenna.

5.1 Circular Polarizer Unit Cell Design

The main aim of this section is to apply a high-performance Jerusalem cross (JC) to create a CP signal. The design of the LPCP converter has been presented in [72]; the designed UC is a single layer based on the JC unitcell. Since the TA antenna with circularly polarized waves is in high demand, the JC has been extended to mm-wave and serves as a CP unit cell. The UC provides two orthogonal electric fields equal in magnitude and 90° phase-shifted combined with wideband and low loss. The UC polarizer is designed in Jerusalem cross (JC) form and the 3D UC structure is shown in Figure 5.1. The designed polarizer UC consists of two layers of metal and two layers of dielectric substrates

Table 5.1: Optimized geometrical parameters for the CP unit cell

Parameter	W_{x1}	w_{x2}	W_{x3}	w_{x4}	h_{sub}
Value (mm)	1.74	0.36	2.5	0.413	0.168
Parameter	w_{y1}	w_{y2}	w_{y3}	w_{y4}	h_{space}
Value (mm)	5.3	0.255	2.5	0.413	2.36

spaced by 2 mm. The Jerusalem cross (JC) is printed on the top layer of the dielectric substrate RO4350B (ϵ_r=3.66, $\tan\delta = 0.00037$, thickness= 0.168 mm). In order to enhance the capacitance values, the JC ends are loaded, and the layers of the Jerusalem cross (JC) are identical for re-transmitting CP wave purposes. The top metal layout is illustrated in Figure 5.1. The UC dimensions are tuned to obtain a wide AR bandwidth, in which the re-transmitted fields are orthogonal, equal and 90° phase-shifted. The final parameters of the designed LCP polarizer are summarized in Table 5.1; the UC size is similar to TA antenna UC dimensions. Moreover, the UC thickness, including the space between layers, is less than half the wavelength of the free space at the centre frequency.

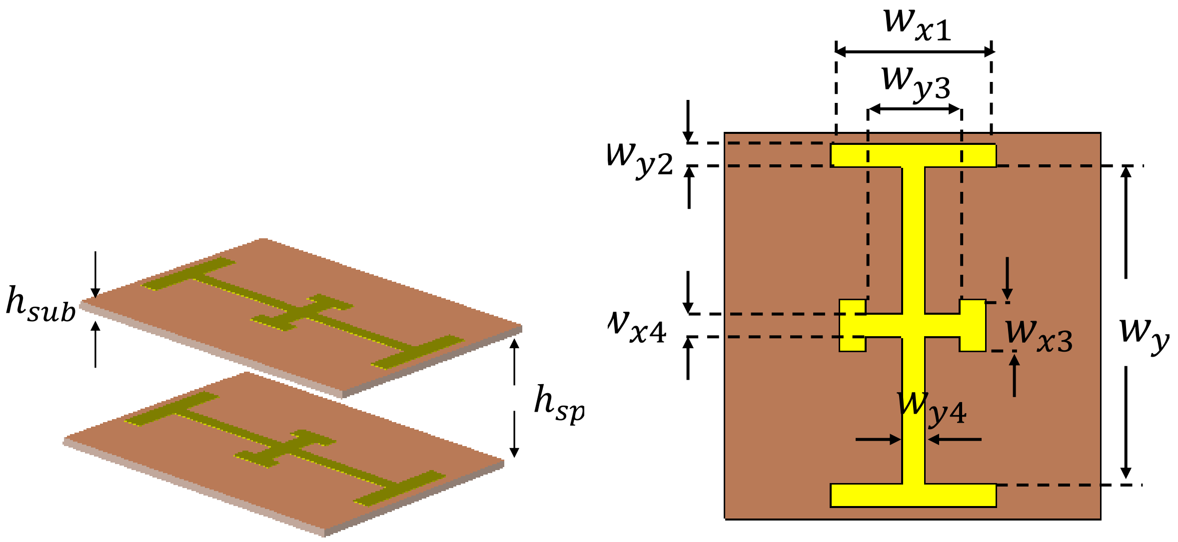

(a) (b)

Figure 5.1: CP polarizer UC structure (a) 2 D UC structure. (b) Top layer

5.1.1 Unit Cell Frequency Response

The computer simulation technology microwave studio (CSTMWS) software package simulates the proposed UC. Figure 4.4 shows the excitation structure of the UC, the excitation modes, and the boundary conditions arranged. Each JC-UC operates as a polarization converter element, and the transmission coefficients' magnitude and phase are represented in figure 5.2. and Figure. 5.3, respectively. From Figure 5.2, we can observe that the transmission coefficients are variable in the frequency domain. There are two outgoing signals at the x and y polarizations. Both the x-polarized and y-polarized signals are re-transmitted in equal amplitude in terms of the transmission magnitude. However, there is an intersection at 28 GHz. This result indicates the JC-UC $|T_{xx}| = |T_{yy}|$, in which one of the CP requirements exists. The insertion losses of the transmitted signals are less than 0.5 dB. Besides that, Figure 5.3 presents the phase of the x- and y-polarized signals transmission coefficient. The black line presents the phase difference fulfilled by the CP condition over the required band. The tolerance range is within ± 10°; that range is acceptable for a wideband CP antenna [79]. The UC axial ratio is presented in Figure 5.4 where the 3-dB bandwidth is from 21.34 GHz to 33.58 GHz. As aresult, the UC is promising for designing a wideband CPTA.

5.2 Circular Polarized Transmit-array Results and Discussion

This section investigates and concludes the characteristic of the designed CPTA antenna. As we concluded in the previous chapter, the optimum size of the TA surface is $178.2 \times 178.2\ mm^2$, and the focal distance is 119.2 mm. Also, the CP polarizer size is 178.2 × 178.2 mm2, and is placed at 2mm apart from the TA surface. The CST software package computes the CPTA behaviour, such as AR bandwidth and radiation pattern. The initial concept of the CP UC is to convert the LP incident signal to become CP re-transmitted signals and achieve the required AR bandwidth. The CP characteristic of the proposed

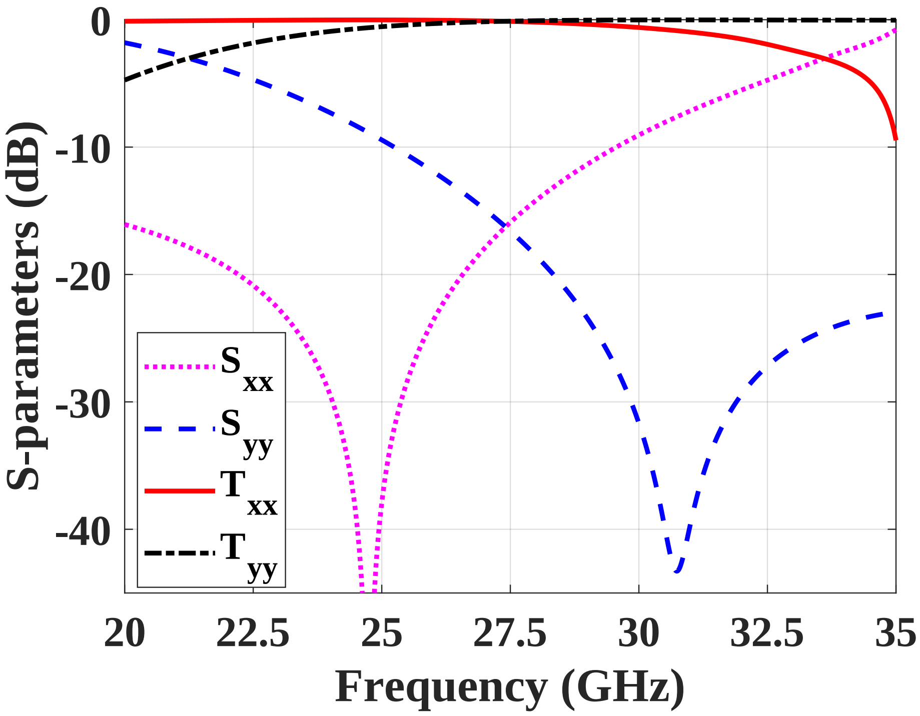

Figure 5.2: Simulated transmission magnitude of the circular polarized UC .

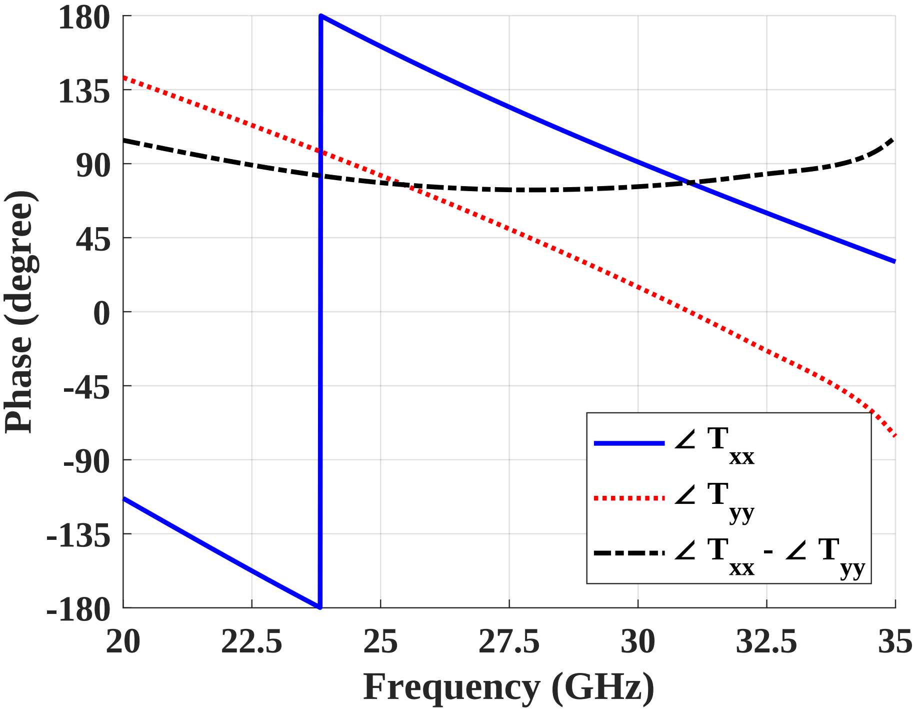

Figure 5.3: Simulated transmission phase of the circular polarized UC.

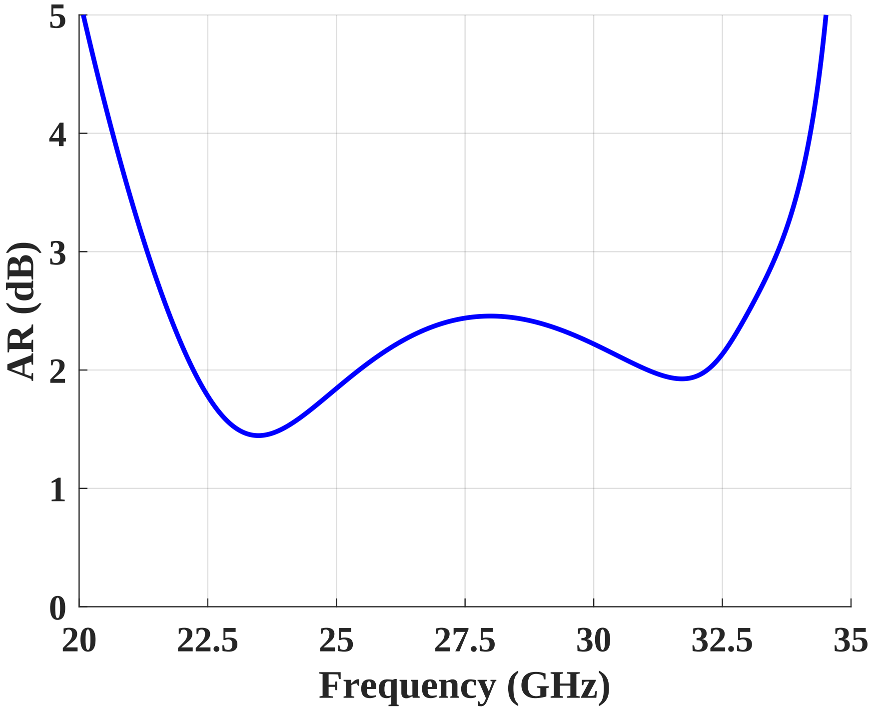

Figure 5.4: Simulated AR of the circular polarized UC.

antenna can be examined using the simulation tool (CSTMWS). Because of computing limitations, the designed UC is arranged in an array of 3 × 3 UCs and excited using a LP patch antenna to figure out the electric field distribution, as shown in Figure 5.5. Figure. 5.6 and Figure. 5.7 shows the extracted electric field distribution above the radiation surface at different frequencies, 25 and 28.5 GHz.

The electric field distribution of different phases (0°, 90°, 180° and 270°) is a function of the frequencies. The figure shows that the electric field amplitude is constant while the direction rotates around the axis at different phases. The produced electric field at the mentioned frequencies is rotating anti-clockwise, which indicates that the designed LCPC produces a RHCP over the designed frequency range. An array of the JC-UC has been assembled.

The CP characteristic of the proposed TA with the LCPC such as AR bandwidth and radiation pattern is examined using the simulation tool (CSTMWS). After that, an array of UC was assembled and fabricated in order to be combined with the TAA.

Figure. 5.8 shows the circular polarization TA antenna measurements setup. The TA antenna surface is placed in front of the feeding source, which is placed at the focal point. The CP converter is placed at the radiation side of the TA antenna to convert the output LP signals into CP signals. The near field scan system (NSI 5913), the PNA network analyzer, WR42, and WR28 waveguide probes are used for antenna measurements. First, the probes are used to receive the re-radiated fields after the TA surface, and then the far-field directivity is calculated using NSI2000 software. The gain and the AR bandwidth of the proposed antenna are shown in Figure. 5.9, in which the maximum realized gain is 30.6 dBi, and 23% AR bandwidth. Figure. 5.10, and Figure. 5.11 represent the radiation characteristic at both (ϕ=0°), and (ϕ=90°) planes of the CPTA antenna at different frequencies. The proposed CPTA antenna at the centre frequency achieves a side lobe level of less than -20 dB, and a RHCP to LHCP ratio of around 20 dB as well.

Table 5.2 shows a comparison between the proposed work and other listed works. The proposed antenna has a high gain compared to [66, 67, 68 and 69]. Also, it has a wide AR bandwidth compared to [65, 67, 68, and 69]. Moreover, its aperture efficiency is higher than those in [67, 68, and 69].

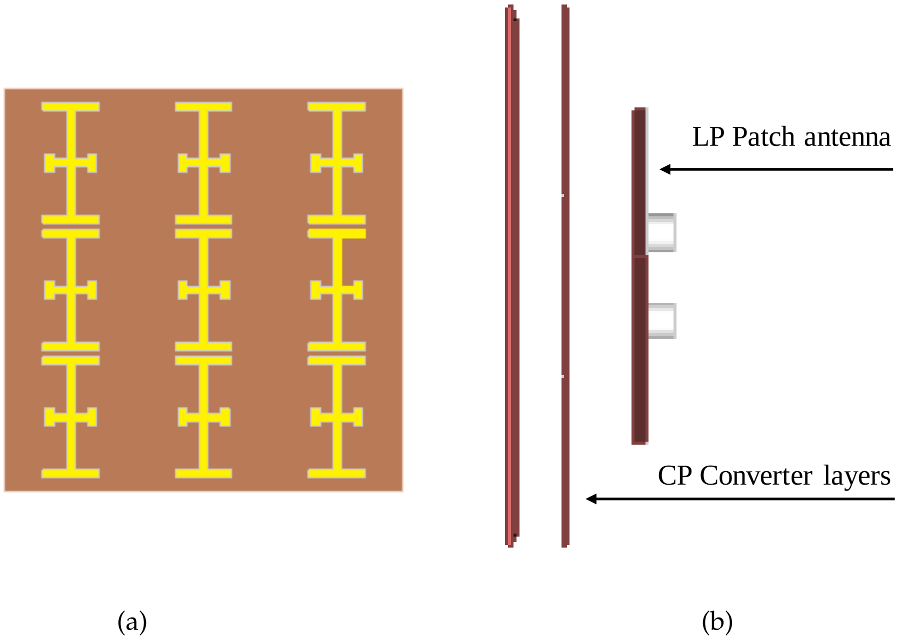

Figure 5.5: CP subarray structure (a) Top view. (b) Side view

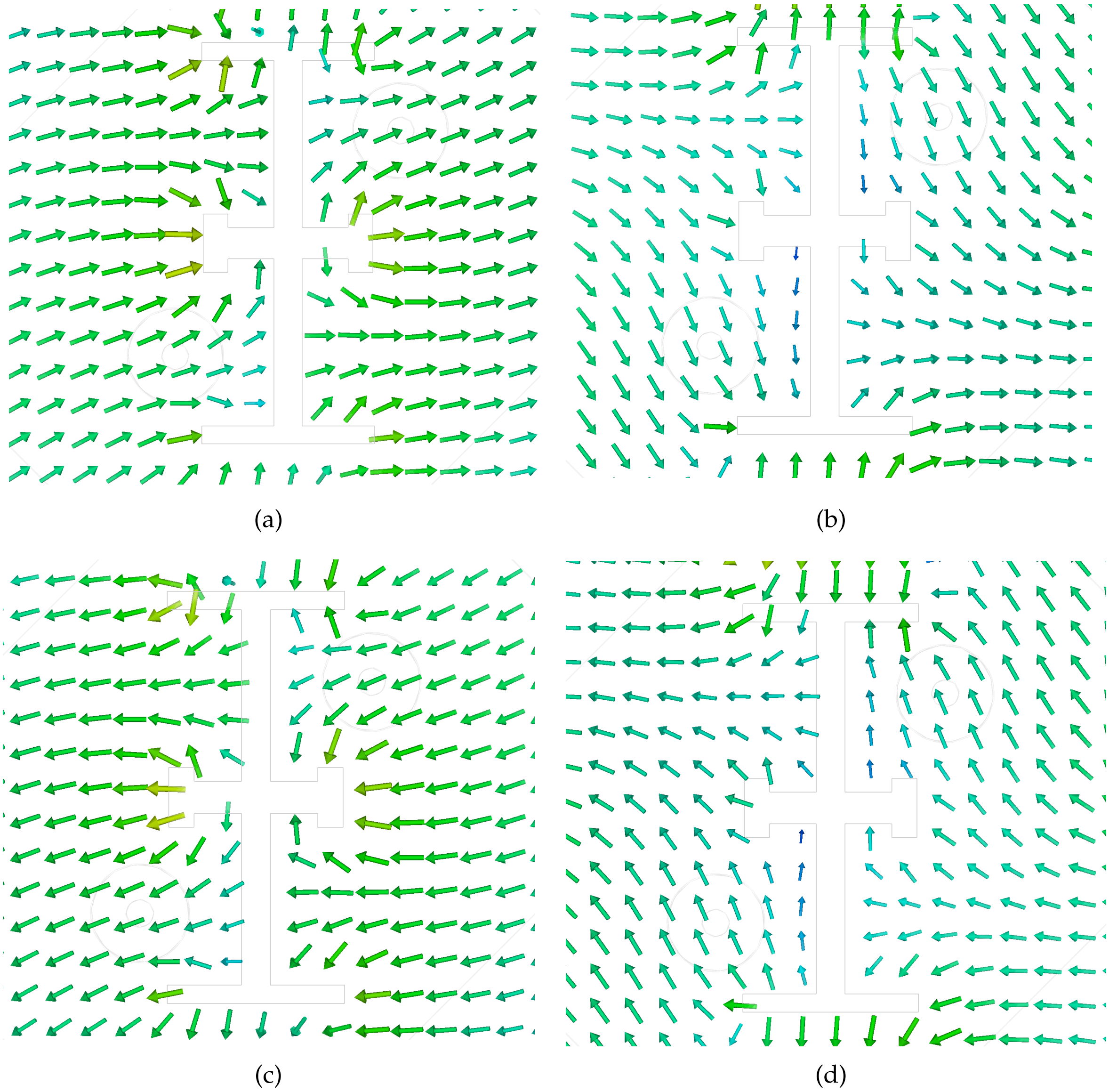
(a) (b) (c) (d)

Figure 5.6: Electric field distribution over subarray at 25 GHz (θ=0°, θ=90°, θ=180°, and θ=270°).

Table 5.2: Table of comparison

Refrence No	Frequency (GHz)	Gain (dBi)	AR %	η_a%	Area (λ_o^2)	Thickness (λ_o)	F/D
[63]	29	33.8	15.9	51.2	40	—	0.67
[64]	30	22.8	24.4	69.5	100	0.113	0.52
[65]	6	20.1	16.7	27	116	0.61	1
[66]	12	24.5	7.5	28.9	2.87	0.06	0.65
[67]	20.5	22	12	31.6	—	1.61	0.85
This work	28	30.6	23	34.24	218.5	0.6185	0.76

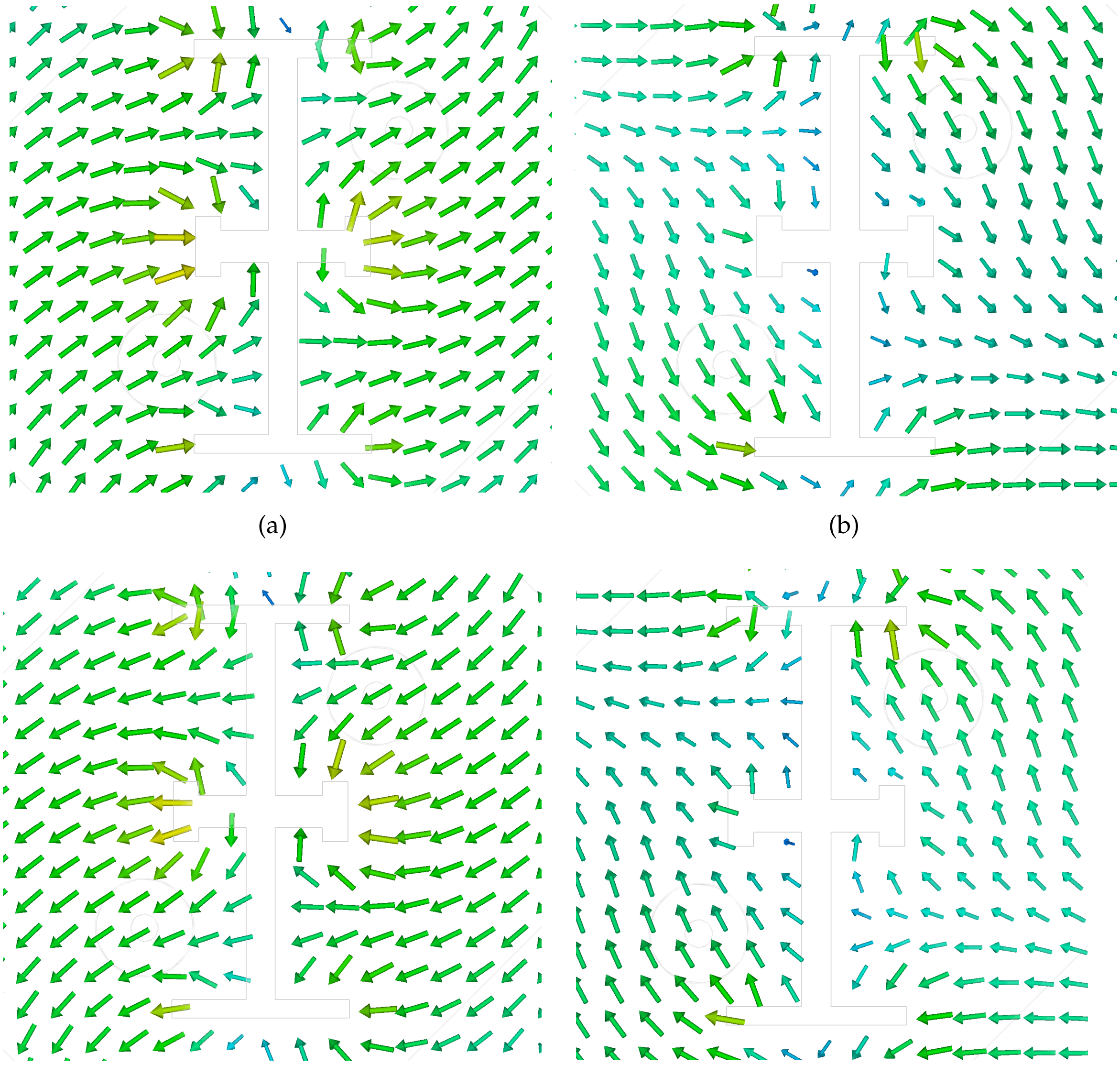

(a) (b)

(c) (d)

Figure 5.7: Electric field distribution over subarray at 28.5 GHz (θ=0°, θ=90°, θ=180°, and θ=270°).

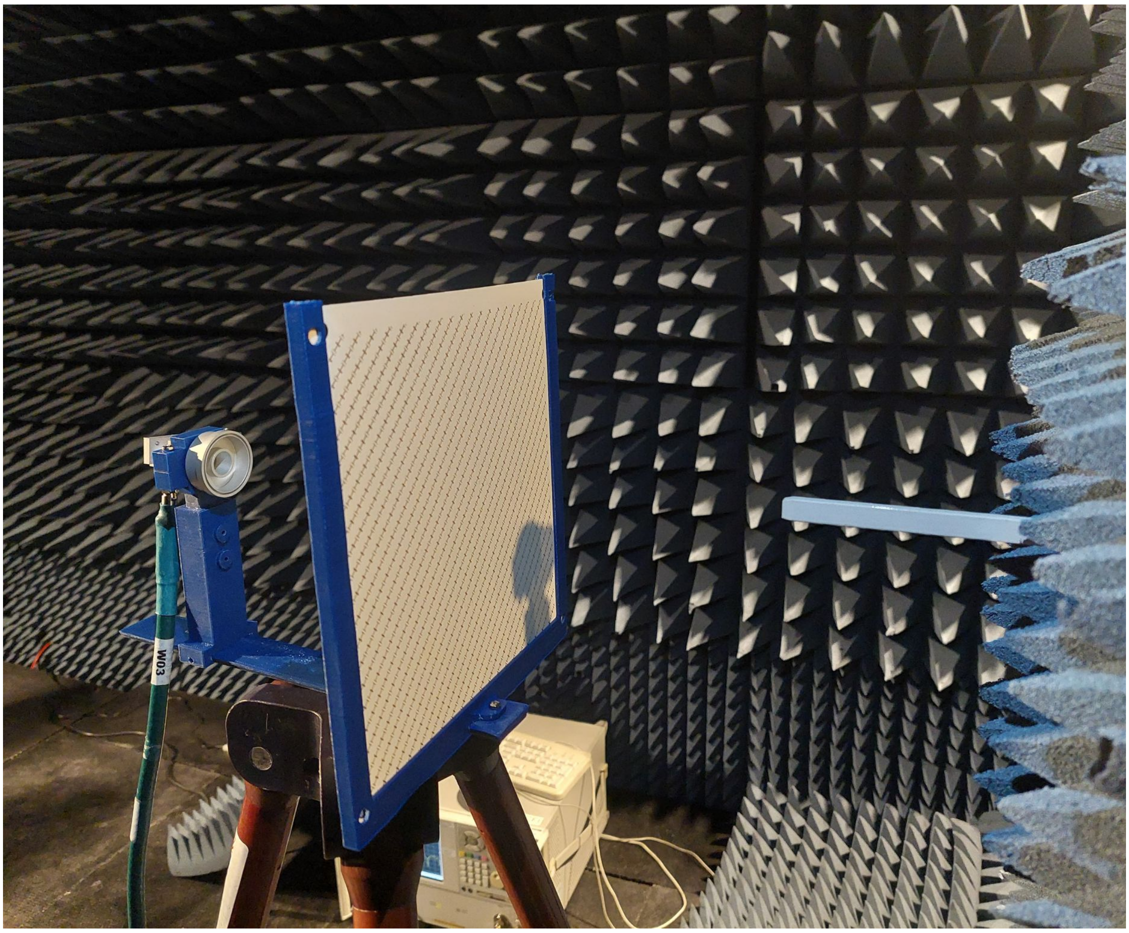

Figure 5.8: Circularly polarized transmit-array antenna measurement setup.

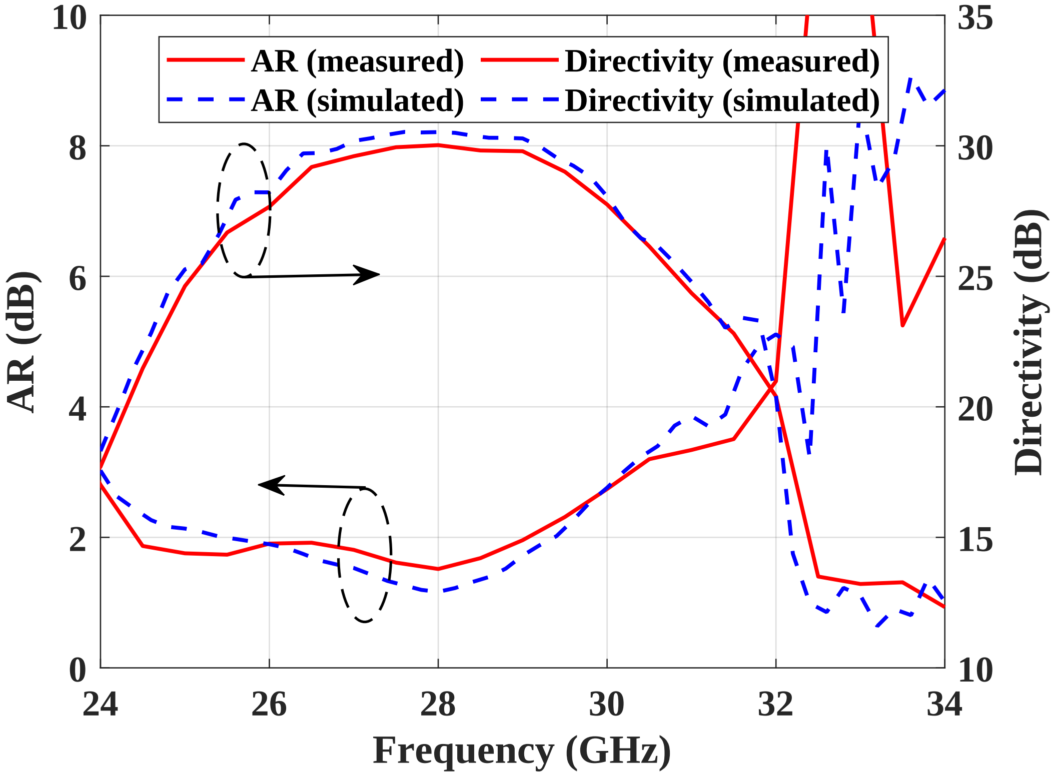

Figure 5.9: Simulated and measured CPTA antenna directivity and AR.

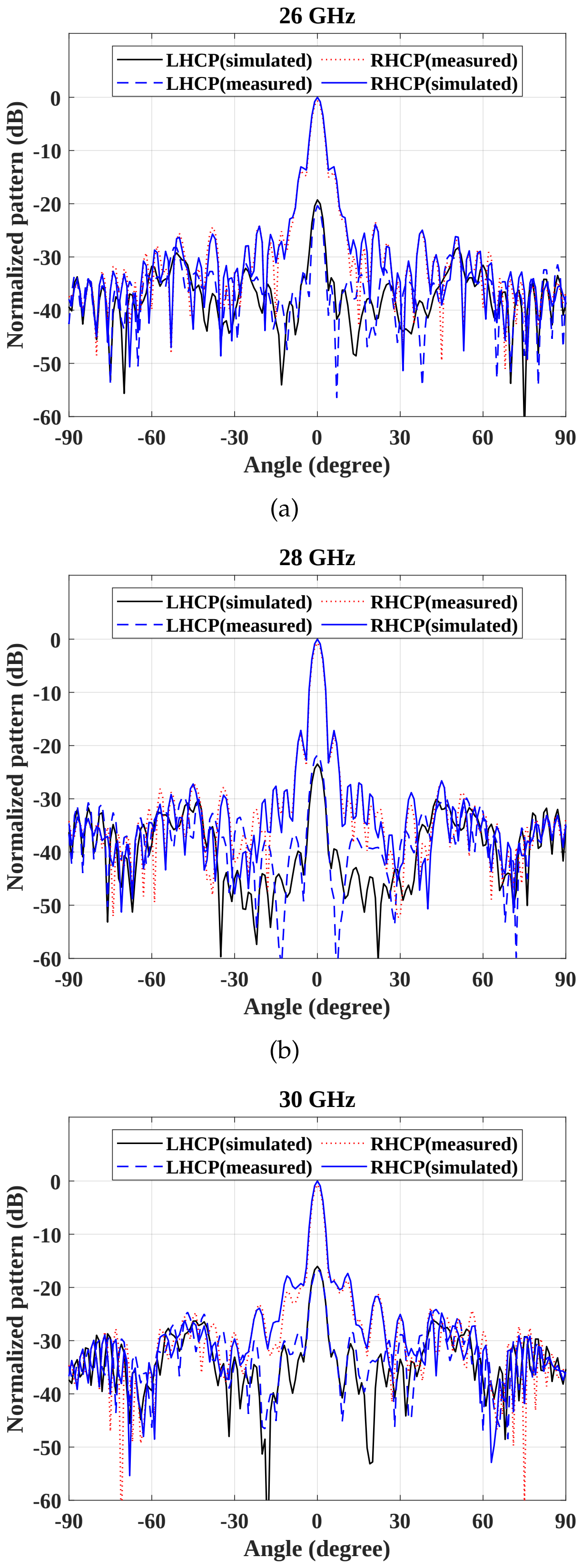

(a)

(b)

(c)

Figure 5.10: CPTA antenna radiation patterns at four different frequencies (ϕ=0°).

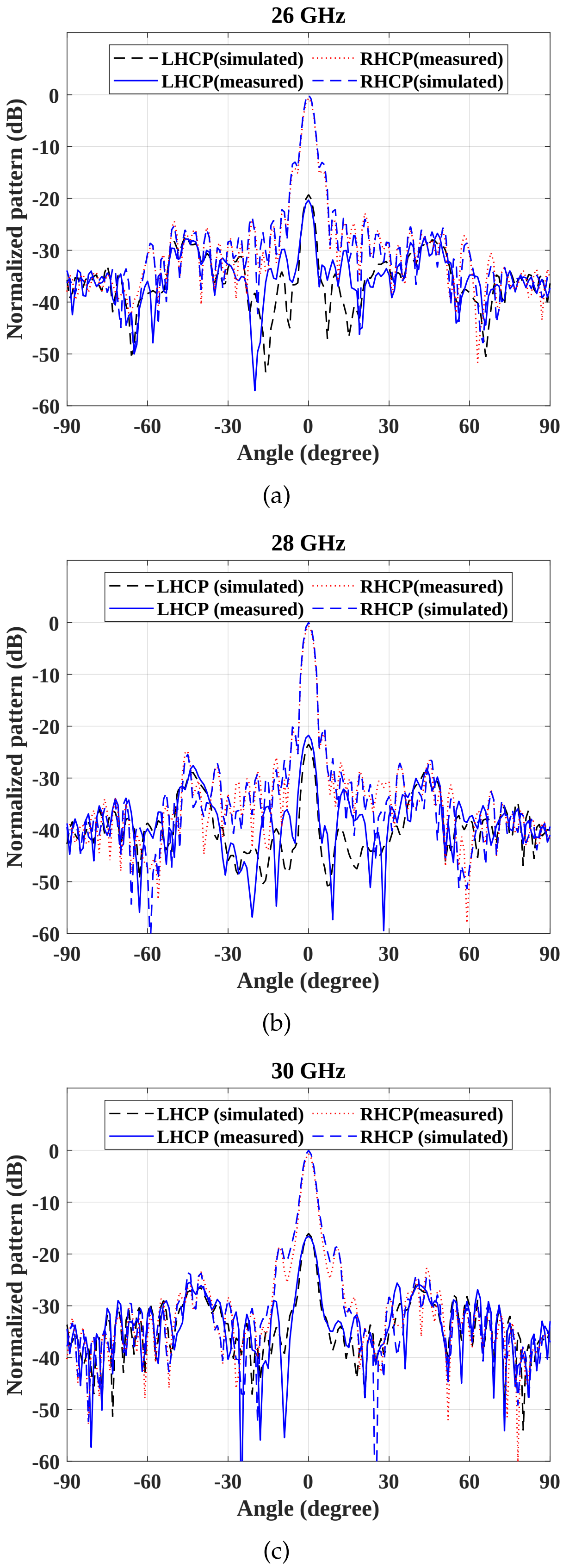

(a)

(b)

(c)

Figure 5.11: CPTA antenna radiation patterns at four different frequencies (ϕ=90°).

Chapter 6

Conclusion and Future Work

6.1 Conclusion

This work aims to design both linear and circular polarized TA antenna with high gain and wide bandwidth operating at the mm-wave band. To this end, the TA antenna design process starts by designing the individual element (UC). The first objective is to study and understand the capability and limitations of various reported TA antennas that operate in linear and circular polarization. The second objective is to examine methods to enhance LP-UC performances such as impedance bandwidth, gain, phase range, and radiation pattern in terms of beam direction, SLL, and cross-polarization. The third objective is to determine the potential effect of the feed antenna's radiation pattern on the aperture efficiency. The third objective is to assemble the proposed UC to design the whole transmit-array antenna. The fourth objective is to study methods to generate CP waves, in which CP UC has been designed. Finally, CP TA antenna is designed and examined. In chapter three, Antenna designers consider 5 G systems as an initial stage, in which high gain and great bandwidth techniques are required. Extensive research strategies that extend patch antenna bandwidth have been studied. Differential and capacitive feeding techniques extend the element bandwidth and suppress the cross-polarization. Then hybrid antenna is designed out of the patch antenna; the fabricated hybrid antenna result shows a wide-band and high gain. Since TA antenna illuminating source affects the TA antenna aperture efficiency, a conical horn is designed. The designed conical horn antenna radiation pattern model is $(\sec\theta)$, that field amplitude distribution should enhance the amplitude tapering efficiency. In chapter four, the design and preliminary results for UC, and the LPTA antenna are presented. The R/T UC are studied extensively. The UCs reflection coefficients are better than 10 dB, and isolations are greater than 30 dB for all the UCs for the frequency range 26 GHz to 31.5 GHz. Also, the UCs have phase frequency response that covers a 360° phase range. Moreover, a 3-bit quantization phase is achieved. As a result, the UC performance improved and became suitable for assembling a 2D arrays. The design methodology is validated, in which 18×18, 24×24, and 24×24 linearly polarized TA antennae are assembled and simulated at the mm-wave band (28 GHz). The aperture size and focal point distance effect are addressed and summarised. Then finally, a wide-band and high gain TA antenna was assembled and fabricated using 27×27 2D arrays. The TA antenna results are 17.9% 3-dB gain bandwidth; maximum gain is 31.14 dBi, SLL -28 dB, and cross-polarisation -27 dB. Chapter five investigates a wide-band circular polarized planar TA antenna with wide-band AR and high gain. This Jerusalem cross (JC) UC is considered the main block of the CP TA antenna. The designed UC supports the TA antenna by exceptional performances in terms of equality amplitude and phase of the orthogonal fields. The CPTA antenna was built using LP TA antenna and polarization converter in the final stage. The designed CPTA antenna in the final stage provides simulated matched bandwidth within a 3dB axial ratio of about 24% and a gain of 30.6 dBi at the centre frequency with a stable radiation pattern.

6.2 Future Work

This work is considered a research gateway for designing transmit-array antennas. Comprehensive research on several techniques to enhance an antenna's bandwidth and increase an antenna's gain will be continued. In terms of the antenna's bandwidth, the research will initially continue to find new methods to design broadband elements that can be used for path delay phase compensation. The research could be extended by:

- Designing a new element that has wider bandwidth and is small in size to decrease quantization error.

- Designing CP UC with more than two layers could increase AR bandwidth.
- The effect of the feeding antenna's radiation pattern on the TA antenna efficiency could be studied in more detail. The incidence field amplitude and phase have massive impact on the TA antenna efficiency, so feeding an antenna that reduces field tapering and minimizes incident field phase error is a future research area.
- For imaging applications, especially medical imaging, wideband, high gain, small size, and beam-steering antenna is in demand. The TA antenna could be the solution by decreasing the focal point distance using the folded techniques. Steering the TA antenna beam can be done using more than one feeding antenna or mechanically moving the feeding antenna.

Bibliography

[1] H. Kaouach, “Design and characterization of circularly polarized discrete lens antennas in 60-ghz band,” *IEEE Antennas and Wireless Propagation Letters*, vol. 15, pp. 1200–1203, 2015.

[2] B. Rahmati and H. Hassani, “High-efficient wideband slot transmitarray antenna,” *IEEE Transactions on Antennas and Propagation*, vol. 63, no. 11, pp. 5149–5155, 2015.

[3] A. H. Abdelrahman, A. Z. Elsherbeni, and F. Yang, “Transmitarray antenna design using cross-slot elements with no dielectric substrate,” *IEEE Antennas and Wireless Propagation Letters*, vol. 13, pp. 177–180, 2014.

[4] E. Hossain, M. Rasti, H. Tabassum, and A. Abdelnasser, “Evolution toward 5g multi-tier cellular wireless networks: An interference management perspective,” *IEEE Wireless Communications*, vol. 21, no. 3, pp. 118–127, 2014.

[5] A. Gohil, H. Modi, and S. K. Patel, “5g technology of mobile communication: A survey,” in *2013 international conference on intelligent systems and signal processing (ISSP)*. IEEE, 2013, pp. 288–292.

[6] T. S. Rappaport, S. Sun, R. Mayzus, H. Zhao, Y. Azar, K. Wang, G. N. Wong, J. K. Schulz, M. Samimi, and F. Gutierrez, “Millimeter wave mobile communications for 5g cellular: It will work!” *IEEE Access*, vol. 1, pp. 335–349, 2013.

[7] L. Yujiri, M. Shoucri, and P. Moffa, “Passive millimeter wave imaging,” *IEEE Microwave Magazine*, vol. 4, no. 3, pp. 39–50, Sep. 2003.

[8] E. Dahlman, S. Parkvall, D. Astély, and H. Tullberg, "Advanced antenna solutions for 5g wireless access," in *2014 48th Asilomar Conference on Signals, Systems and Computers*. IEEE, 2014, pp. 810–814.

[9] M. O. Bagheri, H. R. Hassani, and B. Rahmati, "Dual-band, dual-polarised metallic slot transmitarray antenna," *IET Microwaves, Antennas & Propagation*, vol. 11, no. 3, pp. 402–409, 2017.

[10] A. H. Abdelrahman, A. Z. Elsherbeni, and F. Yang, "High-gain and broadband transmitarray antenna using triple-layer spiral dipole elements," *IEEE Antennas and Wireless Propagation Letters*, vol. 13, pp. 1288–1291, 2014.

[11] B. Rahmati and H. Hassani, "High-efficient wideband slot transmitarray antenna," *IEEE Transactions on Antennas and Propagation*, vol. 63, no. 11, pp. 5149–5155, 2015.

[12] H. Kaouach, "Design and characterization of circularly polarized discrete lens antennas in 60 ghz band," *IEEE Antennas and Wireless Propagation Letters*, vol. 15, pp. 1200–1203, 2015.

[13] M. N. Jazi, M. R. Chaharmir, J. Shaker, and A. R. Sebak, "Broadband transmitarray antenna design using polarization-insensitive frequency selective surfaces," *IEEE Transactions on Antennas and Propagation*, vol. 64, no. 1, pp. 99–108, 2015.

[14] C. Jouanlanne, A. Clemente, M. Huchard, J. Keignart, C. Barbier, T. Le Nadan, and L. Petit, "Wideband linearly polarized transmitarray antenna for 60 ghz backhauling," *IEEE Transactions on Antennas and Propagation*, vol. 65, no. 3, pp. 1440–1445, 2017.

[15] Y. Niu, Y. Li, D. Jin, L. Su, and A. V. Vasilakos, "A survey of millimeter wave communications (mmwave) for 5g: opportunities and challenges," *Wireless networks*, vol. 21, no. 8, pp. 2657–2676, 2015.

[16] D. Liu, L. Wang, Y. Chen, M. Elkashlan, K.-K. Wong, R. Schober, and L. Hanzo, “User association in 5g networks: A survey and an outlook,” *IEEE Communications Surveys & Tutorials*, vol. 18, no. 2, pp. 1018–1044, 2016.

[17] J. A. Madrid, “A geometrical approach to time evolving wave fronts,” *Geophysical Journal International*, vol. 172, no. 3, pp. 1117–1122, 2008.

[18] P. Nayeri, F. Yang, and A. Z. Elsherbeni, *System Design and Aperture Efficiency Analysis*, 2018, pp. 49–78.

[19] C. Fan, W. Che, W. Yang, and S. He, “A novel pramc-based ultralow-profile transmitarray antenna by using ray tracing principle,” *IEEE Transactions on Antennas and Propagation*, vol. 65, no. 4, pp. 1779–1787, 2017.

[20] J. A. Encinar and J. A. Zornoza, “Broadband design of three-layer printed reflectarrays,” *IEEE Transactions on Antennas and Propagation*, vol. 51, no. 7, pp. 1662–1664, 2003.

[21] H. Nematollahi, J.-J. Laurin, J. Page, and J. A. Encinar, “Design of broadband transmitarray unit cells with comparative study of different numbers of layers,” *IEEE Transactions on Antennas and Propagation*, vol. 63, no. 4, pp. 1473–1481, 2015.

[22] A. H. Abdelrahman, A. Z. Elsherbeni, and F. Yang, “High-gain and broadband transmitarray antenna using triple-layer spiral dipole elements,” *IEEE Antennas and Wireless Propagation Letters*, vol. 13, pp. 1288–1291, 2014.

[23] H. Kaouach, L. Dussopt, J. Lantéri, R. Sauleau, and T. Koleck, “Linear and circular polarization transmit-arrays in v-band,” in *The 40th European Microwave Conference*. IEEE, 2010, pp. 1536–1539.

[24] K. Pham, N. T. Nguyen, A. Clemente, L. Di Palma, L. Le Coq, L. Dussopt, and R. Sauleau, “Design of wideband dual linearly polarized transmitarray antennas,” *IEEE Transactions on Antennas and Propagation*, vol. 64, no. 5, pp. 2022–2026, 2016.

[25] J. Huang and R. J. Pogorzelski, "A ka-band microstrip reflectarray with elements having variable rotation angles," *IEEE Transactions on Antennas and Propagation*, vol. 46, no. 5, pp. 650–656, 1998.

[26] J. Huang, "Microstrip reflectarray," *IEEE INt. Symp on Antennas and Propagation*, vol. 46, no. 5, pp. 612–615, 1991.

[27] D. M. Pozar, S. D. Targonski, and R. Pokuls, "A shaped-beam microstrip patch reflectarray," *IEEE Transactions on Antennas and Propagation*, vol. 47, no. 7, pp. 1167–1173, 1999.

[28] S. Sakurai, J. G. N. Rahmeier, T. Tomura, J. Hirokawa, and S. Gupta, "Millimeter-wave huygens' transmit arrays based on coupled metallic resonators," *IEEE Transactions on Antennas and Propagation*, vol. 69, no. 5, pp. 2686–2696, 2020.

[29] P. Mei, S. Zhang, and G. F. Pedersen, "A low-profile and beam-steerable transmitarray antenna: Design, fabrication, and measurement [antenna applications corner]," *IEEE Antennas and Propagation Magazine*, vol. 63, no. 5, pp. 88–101, 2021.

[30] L.-Z. Song, P.-Y. Qin, and Y. J. Guo, "A high-efficiency conformal transmitarray antenna employing dual-layer ultrathin huygens element," *IEEE Transactions on Antennas and Propagation*, vol. 69, no. 2, pp. 848–858, 2020.

[31] M. N. Jazi, M. R. Chaharmir, J. Shaker, and A. R. Sebak, "Broadband transmitarray antenna design using polarization-insensitive frequency selective surfaces," *IEEE Transactions on Antennas and Propagation*, vol. 64, no. 1, pp. 99–108, 2015.

[32] T. Liu, M. Li, F. Yang, and S. Xu, "Phase error analysis for reflectarray antennas based on study of quasi-periodic effect," in *2017 11th European Conference on Antennas and Propagation (EUCAP)*, 2017, pp. 3278–3281.

[33] M.-A. Milon, D. Cadoret, R. Gillard, and H. Legay, "'surrounded-element'approach for the simulation of reflectarray radiating cells," *IET Microwaves, Antennas & Propagation*, vol. 1, no. 2, pp. 289–293, 2007.

[34] M. A. Moharram and A. A. Kishk, "Optimum feeds for reflectarray antenna: synthesis and design," *IEEE transactions on antennas and propagation*, vol. 64, no. 2, pp. 469–483, 2015.

[35] W. L. Stutzman and G. A. Thiele, *Antenna theory and design*. John Wiley & Sons, 2012.

[36] P. Nayeri, A. Z. Elsherbeni, and F. Yang, "Radiation analysis approaches for reflectarray antennas [antenna designer's notebook]," *IEEE Antennas and Propagation Magazine*, vol. 55, no. 1, pp. 127–134, 2013.

[37] F. Y. Payam Nayeri and A. Z. Elsherbeni., *Reflectarray Antennas: Theory, Designs, and Applications*, ser. Antenna Theory and Design. Wiley, 2018. [Online]. Available: https://books.google.ca/books?id=xhZRA1K57wIC

[38] B. Y. Toh, R. Cahill, and V. F. Fusco, "Understanding and measuring circular polarization," *IEEE Transactions on Education*, vol. 46, no. 3, pp. 313–318, 2003.

[39] A. D. Nesic and D. A. Nesic, "Printed planar 8 × 8 array antenna with circular polarization for millimeter-wave application," *IEEE Antennas and Wireless Propagation Letters*, vol. 11, pp. 744–747, 2012.

[40] Q. Zhu, K. Ng, and C. H. Chan, "Printed circularly polarized spiral antenna array for millimeter-wave applications," *IEEE Transactions on Antennas and Propagation*, vol. 65, no. 2, pp. 636–643, 2017.

[41] T. Manabe, K. Sato, H. Masuzawa, K. Taira, T. Ihara, Y. Kasashima, and K. Yamaki, "Polarization dependence of multipath propagation and high-speed transmission characteristics of indoor millimeter-wave channel at 60 ghz," *IEEE Transactions on Vehicular Technology*, vol. 44, no. 2, pp. 268–274, 1995.

[42] C.-L. Mak, K. Luk, K. Lee, and Y. Chow, "Experimental study of a microstrip patch antenna with an l-shaped probe," *IEEE Transactions on antennas and propagation*, vol. 48, no. 5, pp. 777–783, 2000.

[43] Y. Ge, K. P. Esselle, and T. S. Bird, "E-shaped patch antennas for high-speed wireless networks," *IEEE Transactions on Antennas and Propagation*, vol. 52, no. 12, pp. 3213–3219, 2004.

[44] R. Chair, C.-L. Mak, K.-F. Lee, K.-M. Luk, and A. A. Kishk, "Miniature wide-band half u-slot and half e-shaped patch antennas," *IEEE transactions on antennas and propagation*, vol. 53, no. 8, pp. 2645–2652, 2005.

[45] Y. Wang, Y. Lu, G. Lu, W. Cao, and A. A. Kishk, "Broadband patch antenna with narrow width ground plane," in *2018 IEEE International Symposium on Antennas and Propagation & USNC/URSI National Radio Science Meeting*. IEEE, 2018, pp. 1735–1736.

[46] Y. He, C. Li, and J. Yang, "A low-profile dual-polarized stacked patch antenna for micro-base-station applications," in *2018 IEEE MTT-S International Wireless Symposium (IWS)*. IEEE, 2018, pp. 1–4.

[47] F. Zhang, F.-S. Zhang, C. Lin, and G. Zhao, "Broadband microstrip patch antenna array using stacked structure," in *2010 International Conference on Microwave and Millimeter Wave Technology*. IEEE, 2010, pp. 388–391.

[48] M. Asaadi and A. Sebak, "Gain and bandwidth enhancement of 2× 2 square dense dielectric patch antenna array using a holey superstrate," *IEEE Antennas and Wireless Propagation Letters*, vol. 16, pp. 1808–1811, 2017.

[49] L. C. Paul, M. S. Hosain, S. Sarker, M. H. Prio, M. Morshed, and A. K. Sarkar, "The effect of changing substrate material and thickness on the performance of inset feed microstrip patch antenna," *American Journal of Networks and Communications*, vol. 4, no. 3, pp. 54–58, 2015.

[50] P. Katehi and N. Alexopoulos, "On the effect of substrate thickness and permittivity on printed circuit dipole properties," *IEEE Transactions on Antennas and Propagation*, vol. 31, no. 1, pp. 34–39, 1983.

[51] S. Bhardwaj and Y. Rahmat-Samii, “Revisiting the generation of cross-polarization in rectangular patch antennas: A near-field approach,” *IEEE Antennas and Propagation Magazine*, vol. 56, no. 1, pp. 14–38, 2014.

[52] Z. Tong, A. Stelzer, and W. Menzel, “Improved expressions for calculating the impedance of differential feed rectangular microstrip patch antennas,” *IEEE microwave and wireless components letters*, vol. 22, no. 9, pp. 441–443, 2012.

[53] Y. P. Zhang and J. J. Wang, “Theory and analysis of differentially-driven microstrip antennas,” *IEEE Transactions on Antennas and Propagation*, vol. 54, no. 4, pp. 1092–1099, 2006.

[54] J.-D. Zhang, L. Zhu, Q.-S. Wu, N.-W. Liu, and W. Wu, “A compact microstrip-fed patch antenna with enhanced bandwidth and harmonic suppression,” *IEEE Transactions on Antennas and Propagation*, vol. 64, no. 12, pp. 5030–5037, 2016.

[55] N.-W. Liu, L. Zhu, W.-W. Choi, and X. Zhang, “A low-profile differential-fed patch antenna with bandwidth enhancement and sidelobe reduction under operation of tm 10 and tm 12 modes,” *IEEE Transactions on Antennas and Propagation*, vol. 66, no. 9, pp. 4854–4859, 2018.

[56] Z. Ahmed, M. M. Ahmed, and M. B. Ihsan, “A novel differential fed high gain patch antenna using resonant slot loading,” *Radioengineering*, vol. 27, no. 3, pp. 662–670, 2018.

[57] H. Jin, K.-S. Chin, W. Che, C.-C. Chang, H.-J. Li, and Q. Xue, “Differential-fed patch antenna arrays with low cross polarization and wide bandwidths,” *IEEE Antennas and Wireless Propagation Letters*, vol. 13, pp. 1069–1072, 2014.

[58] Q. Zhu, K. B. Ng, and C. H. Chan, “Complementary source based circularly polarized antenna arrays for millimeter-wave applications,” in *2014 IEEE International Workshop on Electromagnetics (iWEM)*. IEEE, 2014, pp. 260–261.

[59] M. Li and K.-M. Luk, “Low-cost wideband microstrip antenna array for 60-ghz applications,” *IEEE Transactions on Antennas and Propagation*, vol. 62, no. 6, pp. 3012–3018, 2014.

[60] H. Sun, Y.-X. Guo, and Z. Wang, “60-ghz circularly polarized u-slot patch antenna array on ltcc,” *IEEE Transactions on Antennas and Propagation*, vol. 61, no. 1, pp. 430–435, 2012.

[61] T. Wu, H. Su, L. Gan, H. Chen, J. Huang, and H. Zhang, “A compact and broadband microstrip stacked patch antenna with circular polarization for 2.45-ghz mobile rfid reader,” *IEEE Antennas and Wireless Propagation Letters*, vol. 12, pp. 623–626, 2013.

[62] F.-J. Huang, T.-C. Yo, C.-M. Lee, and C.-H. Luo, “Design of circular polarization antenna with harmonic suppression for rectenna application,” *IEEE Antennas and Wireless Propagation Letters*, vol. 11, pp. 592–595, 2012.

[63] F. Diaby, A. Clemente, K. T. Pham, R. Sauleau, and L. Dussopt, “Circularly polarized transmitarray antennas at ka-band,” *IEEE Antennas and Wireless Propagation Letters*, vol. 17, no. 7, pp. 1204–1208, 2018.

[64] L. Di Palma, A. Clemente, L. Dussopt, R. Sauleau, P. Potier, and P. Pouliguen, “Circularly polarized transmitarray with sequential rotation in ka-band,” *IEEE transactions on antennas and propagation*, vol. 63, no. 11, pp. 5118–5124, 2015.

[65] X. Zhong, L. Chen, Y. Shi, and X. Shi, “Design of multiple-polarization transmitarray antenna using rectangle ring slot elements,” *IEEE Antennas and Wireless Propagation Letters*, vol. 15, pp. 1803–1806, 2016.

[66] Y.-M. Cai, K. Li, W. Li, S. Gao, Y. Yin, L. Zhao, and W. Hu, “Dual-band circularly polarized transmitarray with single linearly polarized feed,” *IEEE Transactions on Antennas and Propagation*, vol. 68, no. 6, pp. 5015–5020, 2020.

[67] Z. H. Jiang, F. Wu, T. Yue, and W. Hong, "Wideband and low-profile integrated dual-circularly-polarized transmit-arrays enabled by antenna-filter-antenna phase shifting cells," *IEEE Transactions on Antennas and Propagation*, vol. 69, no. 11, pp. 7462–7475, 2021.

[68] C. Liu, A. Yan, C. Yu, and T. Xu, "Improvement on a 2× 2 elements high-gain circularly polarized antenna array," *International Journal of Antennas and Propagation*, vol. 2015, 2015.

[69] J. J. Pakan, "Antenna polarizer having two phase shifting medium," Apr. 4 1961, uS Patent 2,978,702.

[70] D. Lerner, "A wave polarization converter for circular polarization," *IEEE Transactions on Antennas and Propagation*, vol. 13, no. 1, pp. 3–7, 1965.

[71] A. d. C. Lima and E. A. Parker, "Fabry-perot approach to the design of double layer fss," *IEE Proceedings-Microwaves, Antennas and Propagation*, vol. 143, no. 2, pp. 157–162, 1996.

[72] E. Arnieri, F. Greco, L. Boccia, and G. Amendola, "A wide-angle scanning polarization converter based on jerusalem-cross frequency selective surface," in *2020 14th European Conference on Antennas and Propagation (EuCAP)*, 2020, pp. 1–5.

[73] S. M. A. M. H. Abadi and N. Behdad, "Wideband linear-to-circular polarization converters based on miniaturized-element frequency selective surfaces," *IEEE Transactions on Antennas and Propagation*, vol. 64, no. 2, pp. 525–534, 2015.

[74] M. Euler, V. Fusco, R. Dickie, R. Cahill, and J. Verheggen, "Sub-mm wet etched linear to circular polarization fss based polarization converters," *IEEE Transactions on Antennas and Propagation*, vol. 59, no. 8, pp. 3103–3106, 2011.

[75] M. Euler, V. Fusco, R. Cahill, and R. Dickie, "325 ghz single layer sub-millimeter wave fss based split slot ring linear to circular polarization convertor," *IEEE Transactions on Antennas and propagation*, vol. 58, no. 7, pp. 2457–2459, 2010.

[76] M.-A. Joyal and J.-J. Laurin, "Analysis and design of thin circular polarizers based on meander lines," *IEEE Transactions on Antennas and Propagation*, vol. 60, no. 6, pp. 3007–3011, 2012.

[77] P. Fei, Z. Shen, X. Wen, and F. Nian, "A single-layer circular polarizer based on hybrid meander line and loop configuration," *IEEE Transactions on Antennas and Propagation*, vol. 63, no. 10, pp. 4609–4614, 2015.

[78] J. D. Baena, S. B. Glybovski, J. P. del Risco, A. P. Slobozhanyuk, and P. A. Belov, "Broadband and thin linear-to-circular polarizers based on self-complementary zigzag metasurfaces," *IEEE Transactions on Antennas and Propagation*, vol. 65, no. 8, pp. 4124–4133, 2017.

[79] T. M. Hossain, H. Mirza, P. J. Soh, M. F. Jamlos, R. A. Sheikh, A. A. Al-Hadi, and P. Akkaraekthalin, "Broadband single-layered, single-sided flexible linear-to-circular polarizer using square loop array for s-band pico-satellites," *IEEE Access*, vol. 7, pp. 149 262–149 272, 2019.

[80] A. K. Fahad, C. Ruan, R. Nazir, M. Saleem, T. U. Haq, S. Ullah, and W. He, "Ultrathin metasheet for dual-wide-band linear to circular polarization conversion with wide-angle performance," *IEEE Access*, vol. 8, pp. 163 244–163 254, 2020.

[81] P. Naseri, S. A. Matos, J. R. Costa, C. A. Fernandes, and N. J. Fonseca, "Dual-band dual-linear-to-circular polarization converter in transmission mode application to k/ka-band satellite communications," *IEEE Transactions on Antennas and Propagation*, vol. 66, no. 12, pp. 7128–7137, 2018.

[82] E. Erfani, T. Denidni, S. Tatu, and M. Niroo-Jazi, "A broadband and high gain millimeter-wave hybrid dielectric resonator antenna," in *2016 17th International Symposium on Antenna Technology and Applied Electromagnetics (ANTEM)*, 2016, pp. 1–2.

[83] A. Elboushi and A. Sebak, "High-gain hybrid microstrip/conical horn antenna for mmw applications," *IEEE Antennas and Wireless Propagation Letters*, vol. 11, pp. 129–132, 2012.

[84] Y. Ge, Z. Sun, Z. Chen, and Y.-Y. Chen, "A high-gain wideband low-profile fabry–perot resonator antenna with a conical short horn," *IEEE Antennas and Wireless Propagation Letters*, vol. 15, pp. 1889–1892, 2016.

[85] Nasimuddin and K. P. Esselle, "A low-profile compact microwave antenna with high gain and wide bandwidth," *IEEE Transactions on Antennas and Propagation*, vol. 55, no. 6, pp. 1880–1883, 2007.

[86] V. G. Kasabegoudar and K. Vinoy, "Coplanar capacitively coupled probe fed microstrip antennas for wideband applications," *IEEE Transactions On antennas and propagation*, vol. 58, no. 10, pp. 3131–3138, 2010.

[87] L. Inclan-Sanchez, J.-L. Vazquez-Roy, and E. Rajo-Iglesias, "Proximity coupled microstrip patch antenna with reduced harmonic radiation," *IEEE Transactions on Antennas and Propagation*, vol. 57, no. 1, pp. 27–32, 2009.

[88] J. M. Gil, J. Monge, J. Rubio, and J. Zapata, "A cad-oriented method to analyze and design radiating structures based on bodies of revolution by using finite elements and generalized scattering matrix," *IEEE transactions on antennas and propagation*, vol. 54, no. 3, pp. 899–907, 2006.

[89] F. Xu and K. Wu, "Guided-wave and leakage characteristics of substrate integrated waveguide," *IEEE Transactions on microwave theory and techniques*, vol. 53, no. 1, pp. 66–73, 2005.

[90] K. Phalak and A. Sebak, "Surface integrated waveguide based triangular cavity backed t slot planar antenna at 60 ghz," in *2014 IEEE Antennas and Propagation Society International Symposium (APSURSI)*. IEEE, 2014, pp. 1495–1496.

[91] M. Alzidani, I. Afifi, M. Asaadi, and A. Sebak, “Ultra-wideband differential fed hybrid antenna with high-cross polarization discrimination for millimeter wave applications,” *IEEE Access*, vol. 8, pp. 80 673–80 683, 2020.

[92] F. Hyjazie and R. Paknys, “On the radiation from a large, open-ended waveguide,” *IEEE Antennas and Propagation Magazine*, vol. 44, no. 6, pp. 98–100, 2002.

List of Publications

Thesis Related Publications

Journal Papers

J1 M. Alzidani, I. Afifi, M. Asaadi and A. Sebak, "Ultra-Wideband Differential Fed Hybrid Antenna With High-Cross Polarization Discrimination for Millimeter Wave Applications," in IEEE Access, vol. 8, pp. 80673-80683, 2020, doi: 10.1109/ACCESS.2020.2988000.

J1 M. Alzidani, I. Afifi, and A. Sebak, "Design of Wideband Linearly Polarized 3-Bit Transmit-Array Antenna With Polarization Rotation Unit Cell," in IEEE Access, vol. 9, pp. 113393-113402, 2021, doi: 10.1109/ACCESS.2021.3093593.

Other Publications

Here is one jointly published papers during my PhD program that is not included in this thesis.

Conference Papers

J2 I. Afifi, M. Alzidani and A. Sebak, "Wideband printed ridge gap waveguide differential feeding aperture antenna for millimeter wave applications," 2019 IEEE International Symposium on Antennas and Propagation and USNC-URSI Radio Science Meeting, Atlanta, GA, USA, 2019, pp. 267-268, doi: 10.1109 /APUSNCURSINRSM. 2019. 8888584.